

LATERAL VIBRATION OF PIPELINES DURING J-LAY COUPLING OF SUSPENDED AND SEABED PIPELINES

BY
ZHECHEN HOU

Master of Science Thesis

LATERAL VIBRATION OF PIPELINES DURING J-LAY COUPLING OF SUSPENDED AND SEABED PIPELINES

in particular fulfillment of the requirements for the degree of

Master of Science
in Offshore Engineering

at the Delft University of Technology,
to be defended publicly on 18th Oct 2016

by

Zhechen HOU

Student number: 4402219

Thesis committee: Prof. Dr. A.V. Metrikine, Offshore Engineering (3ME), TU Delft
PhD Candidate Yang Qu, Offshore Engineering (3ME), TU Delft
Prof. Dr. ir. M. A. N. Hendriks, Faculty of Civil Engineering and Geosciences, TU Delft
Ass. Prof. Dr. ir. K. N. (Karel) van Dalen, Faculty of Civil Engineering and Geosciences, TU Delft



Copyright © 2016 by Z. HOU

An electronic version of this dissertation is available at

<http://repository.tudelft.nl/>.

ACKNOWLEDGEMENTS

After an intensive period of one year, today is the day: writing this note of thanks is the finishing touch on my thesis. Before proceeding to the main content, I would like to express my deepest gratitude to one and all, who directly and indirectly, have lent their hands in this venture.

Foremost, I would like to express my sincere gratitude to Prof. Dr. A.V. Metrikine and Mr. Yang Qu who introduced me to the area of structural dynamics and supported me with patient guidance, encouragement, and insightful comments throughout the whole period of the thesis project.

To my families and my closest friends, thanks for the continuous support and encouragement spiritually throughout my life, especially in times when they are sincerely needed.

*Zhechen HOU
Delft, Oct 2016*

ACRONYMS

VIV Vortex Induced Vibration	47
SCR Steel Catenary Riser	103
TDP Touch Down Point	30
TDZ Touch Down Zone	103
VCP Vessel Connection Point	55
IP Independence Principle	48
API American Petroleum Institute	81
DNV Det Norske Veritas	26
EOM Equation of motion	37
PDE Partial Differential Equations	37
ODE Ordinary Differential Equations	38
BLE Boundary layer end	108

CONTENTS

Acknowledgements	v
Acronyms	vii
List of Figures	xi
List of Tables	xv
1 Introduction	1
1.1 Background	1
1.2 Problem statement	3
1.2.1 Problem Description	3
1.2.2 Objectives	4
1.2.3 Assumptions	5
1.3 Thesis outline	8
2 Literature Study	9
2.1 Pipe-soil interaction model	9
2.1.1 Pipe-soil vertical interaction model	9
2.1.2 Pipe-soil lateral interaction model	11
2.2 VIV of suspended pipeline	15
2.2.1 Fluid flows past cylinder	15
3 Pipe-soil interaction model	25
3.1 Model Information	25
3.2 Model Description	37
3.3 Model Verification	41
3.4 Numerical results	42
4 Suspended pipeline model	47
4.1 Model Information	47
4.2 Model Description	53
4.3 Model Verification	59
4.4 Numerical results	60

5	Coupled pipeline model	65
5.1	Model Information	65
5.2	Model Description	67
5.3	Model Verification	73
5.4	Numerical results	74
6	Influence of TDZ	79
6.1	Model Information	79
6.2	Model Description	82
6.3	Numerical results	84
7	Influence of pipeline laying	87
7.1	Model Information	87
7.2	Model Description	90
7.3	Numerical results	98
8	Conclusion	103
8.1	Conclusion	103
8.2	Further study	104
A	Static laying configuration	105
A.1	Static initial configuration without current	106
A.2	Static initial configuration with current	110
B	VIV deduce	121
C	Numerical Solution	123
C.1	Newmark- β method	123
C.2	Jacobian Matrix	126
	References	130

LIST OF FIGURES

1.1 World energy consumption by sources (copyright from the Economist)	1
1.2 Illustration for S-lay (Left) and J-lay (Right) (Copyright from Saipem)	2
1.3 Illustration for laying process (Copyright from Zachary Westgate)	3
2.1 Schematic Illustration of SCR-seabed interaction in TDZ (Copyright from Elostá 2013)	10
2.2 soil model penetration modes (Copyright from Mark Randolph)	10
2.3 Soil model characteristics for different modes (Copyright from Mark Randolph)	11
2.4 Coulomb friction model (Copyright from Elostá 2013)	12
2.5 Lateral trilinear pipe-soil interaction model (Copyright from White 2008)	13
2.6 Illustration for trilinear model(Copyright from White 2008)	14
2.7 Regimes of flow around a smooth, circular cylinder in steady current	16
2.8 Staggered alternate vortex shedding – in-line and cross-flow response, J P Kenny (1993)	16
2.9 Relation between Strouhal number and Reynolds number (Source: MIT OPW)	17
2.10 Force components of lift and drag force	17
2.11 Relation between mean drag coefficients and Reynolds number	18
2.12 Relation between r.m.s of lift coefficients and Reynolds number	19
2.13 Schematic of the experimental arrangement	19
2.14 Cross-flow and in-line vibration amplitudes (A_Y and A_X) and response frequency f_Y as functions of reduced velocity. Dots (•) is only for cross-flow vibration results acquired by Khalak and Williamson in 1999, whereas Circles (◦) shows the later two degrees of freedom vibration including cross-flow and in-line results by Jauvtis and Willamson in 2003.	21
2.15 Regions of instability vortex shedding	22
3.1 Effective tension illustration	27
3.2 Static configuration of pipeline during laying(Copyright from Mark F. Randolph)	27
3.3 Rod model for axial pipe soil interaction	29
3.4 Illustration for typical force-displacement lateral friction response	33
3.5 Illustration for penetration of pipeline	34
3.6 Soil resistance calculation for time step n+1	35
3.7 Seabed beam model illustration	37
3.8 Finite difference element	38
3.9 Comparison between numerical and analytical results	42

3.10 Illustration for applied external displacement	43
3.11 Illustration for external displacement	44
3.12 Lateral vibration displacement for chosen nodes	44
3.13 Lateral vibration velocity for chosen nodes	45
3.14 Final shape	45
4.1 Attack angle of incident flow	49
4.2 Suspended beam model illustration	53
4.3 Finite difference element	54
4.4 20th mode shape in 2-D view	60
4.5 Envelope curve for lateral vibration ($U = 0.1952\text{m/s}$)	60
4.6 Displacement and spectra for lateral vibration (500 m)	61
4.7 Envelope curve for lateral vibration ($U = 0.1952\text{m/s}$)	62
4.8 Displacement and spectra for lateral vibration (500 m)	62
4.9 Modal shape examples	63
5.1 Coupled beam model illustration	66
5.2 Nodes division for overall model	69
5.3 20th mode shape in 2-D view	74
5.4 Envelope curve for coupled pipeline ($U = 0.1952\text{ m/s}$)	75
5.5 Displacement and spectra for lateral vibration of nodes	75
5.6 Envelope curve for coupled pipeline ($k_s = 6.95 \times 10^4\text{N/m}^2$)	76
5.7 Modal shape examples	78
6.1 Illustration for TDP movement at TDZ	80
6.2 Beam model illustration	82
6.3 Magnifying illustration for TDP movement	83
6.4 Soil force for adjacent nodes containing TDP	83
6.5 Envelope curve for coupled pipeline (With TDZ)	84
6.6 Lateral vibration of $L = 980\text{m}$	85
7.1 Beam model illustration including fictitious part (Top view)	91
7.2 Nodes division for beam model illustration including fictitious part (Top view)	92
7.3 Nodes division illustration for laying process (Top view)	97
7.4 Laying process illustration at varying time moments	99
7.5 Lateral displacement for nodes on suspended pipeline	100
7.6 Lateral displacement for nodes on fictitious pipeline	100
A.1 Illustration for beam & cable model (Copyright from Lenci)	106
A.2 Laying configuration for beam & cable model	110

A.3	Illustration for beam & cable model under currents	111
A.4	Force balance of suspended pipeline segment (Copyright from Wang Lizhong)	112
A.5	Calculation process illustration	116
A.6	Comparison between Lenci's model and the new model	117
A.7	Results for difference currents speed	119
A.8	Different current profile comparison	120
B.1	Fluid force for the pipeline segment (Copyright from Ogink)	121
C.1	Illustration for Newmark- β method	125

LIST OF TABLES

3.1	Model properties for seabed model	36
4.1	Model properties for suspended pipeline	52
4.2	First 20 eigen-frequencies of suspended pipeline	59

1

INTRODUCTION

1.1. BACKGROUND

Modern societies are becoming increasingly dependent on reliable and secure energy supplies to hold up economic growth and community prosperity. The worldwide primary energy consumption will definitely keep growing continuously in the future even though there is a certain degree of declination as the aftermath of financial crisis in some years. Various methods of acquiring energy from the nature have been developed along with the long development of human beings, including fossil fuels, hydroelectricity, renewable and nuclear energy. Among which, oil and gas remains the world's dominant fuel and thus still the engine of the world economy.

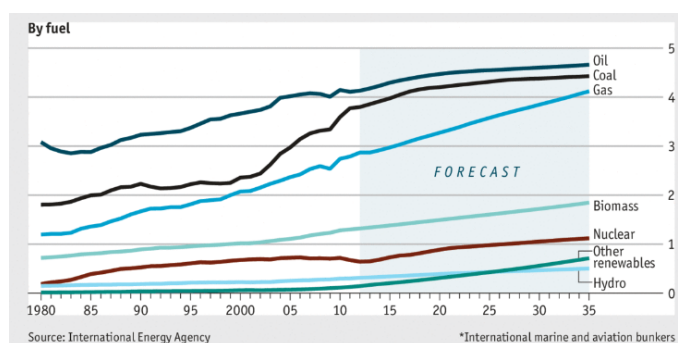


Figure 1.1: World energy consumption by sources (copyright from the Economist)

Currently, approximately 30 percent of world oil and gas production comes from offshore and it is expected to continue increasing in the future. Furthermore, advancements in technology have expanded

the industry to deeper water. Over the last few decades, offshore production has increased tremendously. The extraction of oil and gas from offshore area requires sub-sea pipelines to connect offshore facilities and transport these hydrocarbons to terminals, either onshore or offshore. Thus sub-sea pipelines are a significant component of offshore hydrocarbon developments.

Despite all kinds of pipe laying methods, a series of professional pipe-laying devices mounted on the vessel are used to lay pipelines into sub-sea area. The most frequently used methods are S-lay and J-lay method mainly according to the water depth.

The S-lay method is commonly used in all kinds of pipe laying projects with various water depth nowadays. While for extremely deep water, the departure angle of the pipe becomes so steep that required stinger length of S-lay vessels may not be feasible. Overcoming some of the obstacles in S-lay installation, J-lay operation has put less stress on the pipeline, that are laid into the sea water in an almost vertical position. Here, pipe is lifted via a tall tower on-board, and is inserted into the sea. Unlike double curvature obtained in S-lay, the pipeline only curves once in J-lay installation, appears in the shape of character "J" under the water[1].

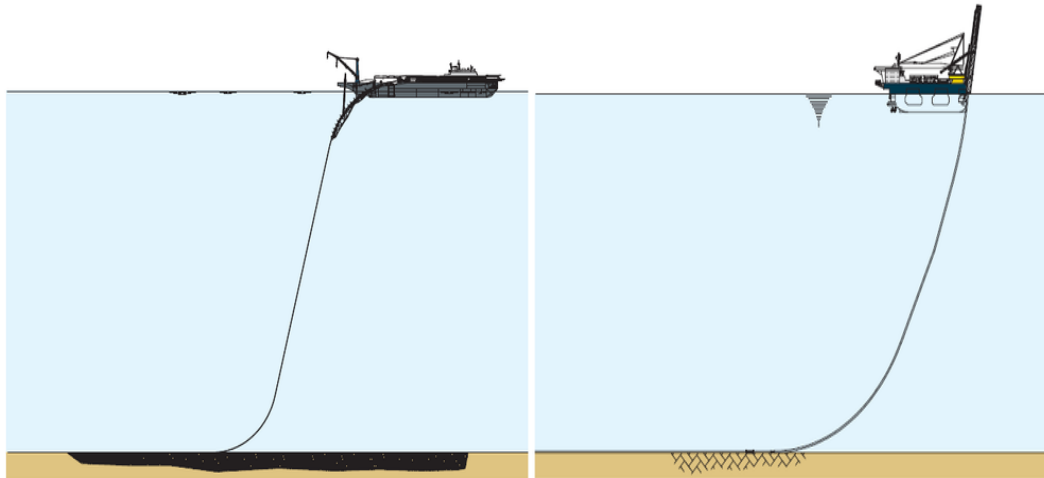


Figure 1.2: Illustration for S-lay (Left) and J-lay (Right) (Copyright from Saipem)

During pipe-laying process, complex pipelines design issues may appear, such as in-plane and out-of-plane vibration. The 'snake' bending in as-laid part of pipelines, is one of the unexpected consequences from pipeline motions, which require thorough consideration about the dynamics of pipelines during laying operation. In the past, more attention has been paid to the statics and dynamics of the suspended pipeline and pipe-soil interaction of seabed pipelines. These two parts are often analysed separately due to the sophistication for such kinds of problems.

This thesis mainly focuses on dynamic analysis for lateral vibration of pipelines comprising as-laid pipelines on seabed and suspended pipelines hanging from the laying vessel during J-lay process. For

the as-laid pipelines on seabed, a simplified dynamic model will be derived considering soil resistance based on pipe-soil interaction mechanism. Another separate dynamic model for the suspended pipeline will also be derived incorporating vortex induced vibration. After the separate models for both parts are determined and verified, they are further coupled together to analyse the relation between these parts, which in essence has simulated the static laying process. Furthermore, the dynamic laying process is also investigated into based on the above coupled model.

1.2. PROBLEM STATEMENT

1.2.1. PROBLEM DESCRIPTION

During the pipe laying process, suspended pipeline descends from a J-lay vessel in a nearly catenary configuration at a water depth of 910 m, connecting to the seabed pipeline as illustrated clearly in Fig.1.3.

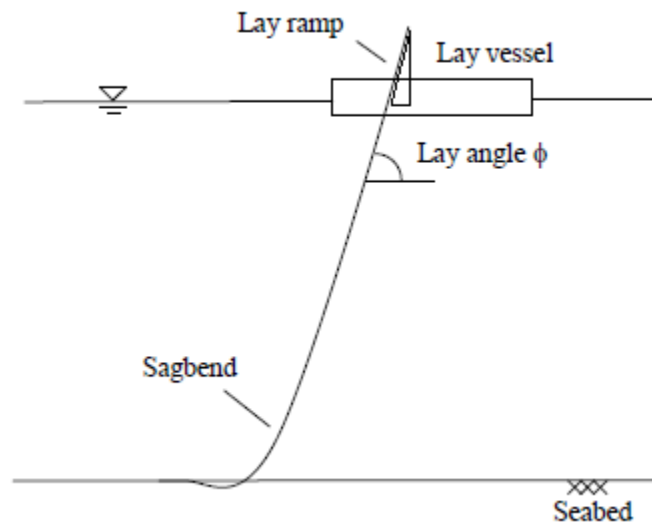


Figure 1.3: Illustration for laying process (Copyright from Zachary Westgate)

The suspended pipeline is connected to the laying vessel at a mean top laying angle of 80° , as shown in Fig.1.3. The outer diameter for the pipeline is 273 mm (10.75 inch) with a wall thickness of 20.6 mm (0.812 inch). During laying process, the total length of suspended pipelines can be calculated in the following chapter, while seabed pipelines are considered as a semi-infinite part. When building up the dynamic analysing model for the pipelines, the top-end is modelled as a fixed boundary, the infinite end on the seabed is modelled as fixed with a finite reasonable length long enough. The pipeline has a density of 7800 kg/m^3 for preliminary design intention. Soft clay is the main soil types for newly discovered deep

water field, which is also the main research interests of this thesis. For this kind of soil type, S_{u0} (mud line shear strength) typically ranges from 1.2 to 3.8 kPa at seabed level, and S_{ug} (shear strength gradient) ranges from 0.8 to 2.0 kPa/m [2] [3]. In the nonlinear soil model of this thesis, the value of S_{u0} and S_{ug} is chosen as 2.6 kPa and 1.25 kPa/m separately in the median range. The value of ρ_{soil} (saturated soil density) is 1500 kg/m^3 .

When the laying vessel is operating, the pipeline undergoes static force by its own weight and hydrostatic pressure and thus the suspended part will appear a modified catenary shape, or in other word the stiffened catenary as will be elaborated in Appendix A. In addition to the static load, the suspended pipeline is also loaded dynamically by waves, currents and vessel motions. The influence of currents will be considered in this essay, while the influence from waves and vessel motion is beyond the scope of this essay due to limited time. For the as-laid pipeline on seabed, an initial penetration length into the clay will be gradually reached due to its submerged self-weight. The pipe-soil interaction in as-laid pipeline provides resistance hindering the movements of seabed pipeline.

The coupling effects of pipeline, soil, currents in this research determines the vibration of pipeline system. Suspended pipeline begins to vibrate steadily under the influence of vortex induced vibration due to currents, which leads to the vibration of seabed pipeline. Also with the soil resistance, the seabed pipeline may arrive at a bending shape rather than its expected initial straight configuration. In this thesis, large displacement beyond limits result from lateral vibrations may jeopardize the integrity and safety of the system, thus it is essential to simulate and investigate into the dynamic laying process of the pipeline.

1.2.2. OBJECTIVES

The strategy for the research is to build up a simplified model simulating the out-of-plane vibration of pipeline in dynamic laying process, and to do subsequent analysing work. This thesis focuses on analysing the out-of-plane vibration of coupled pipeline system due to coupling effects of pipe-soil interaction in seabed pipeline, vortex induced vibration of suspended pipeline. This thesis also investigate into the influence of touch down zone and dynamic laying process on the probable bending configuration in seabed pipeline. The objectives of this thesis project can be summarized as:

- Build up analytical equation of motions for seabed pipeline and suspended pipeline.
- Simulate the lateral vibration of seabed pipeline capturing the essence of pipe-soil interaction.
- Simulate the VIV for suspended pipeline.
- Simulate the static laying process, namely the lateral vibration of coupled seabed and suspended pipeline system without length increment due to laying.
- Simulate the influence of touchdown zone on the bending configuration of the seabed pipeline.
- Simulate the dynamic laying process incorporating pipeline length increment, and investigate into its influence.

- Analyse acquired results and potential influential parameters.
- Propose effective solutions to minimize the lateral vibration.

1.2.3. ASSUMPTIONS

The dynamic analysis is an essential procedure for the lateral vibration of pipeline during laying process, which is also a rather difficult step to be modelled fully and precisely. Thus some reasonable assumptions and simplifications are proposed at the very beginning. The pipeline system comprising the seabed part and suspended part, and the dynamic behaviour of these two parts will be focused on the out-of-plane vibration only. The in-plane vibration is neglected. The initial static configuration of the suspended pipeline under effects of current flow is determined based on stiffened catenary assumption, which is calculated through numerical methods. After the initial static configuration of pipeline is set up, the lateral vibration of coupled pipeline system is analysed around this referential initial static configuration. Other assumptions that concern the properties of the pipeline, external dynamic forces, the boundary conditions and the numerical method that will be used to solve the equations of motion will be further discussed in detail as following.

Out-of-plane modelling

The laying speed of J-lay vessel is normally 50-150 m/hr , which is a rather small value compared to that of S-lay and reel-lay vessels. The pipeline laying process can thus be treated as an ideally continuous and steady movement. Throughout this research, the coupled pipeline system is considered to keep its initial static configuration in-plane under the effects of constant current flow. The dynamic motion of the pipeline model is vibrating at a small amplitude around the initial static configuration.

The main focus of this research is on the out-of-plane vibration for the pipeline system. Especially for the seabed pipeline, axial displacement is beyond the scope of this research and is assumed as no axial motion here. While the tension changing in seabed pipeline due to axial strain is the only concerned point in this research as will be explained in the tension calculation of Chapter 3.7. Situation may vary for the suspended pipeline part, due to the curved in-plane configuration. There are published papers support the point of view that if a curved beam model has uniform circular cross-section which is also doubly symmetric, the out-of plane vibration for the beam model can be seen as uncoupled with the in-plane vibration[4]. The amplitude of in-plane vibration for suspended pipeline due to vortex induced vibration is relatively small and in-plane vibration mainly results in the fatigue problem in engineering practice, which is beyond the scope of this research. Thus in-plane vibration of suspended part due to current flow will be neglected in this study. Moreover, if the radius of in-line curved beam becomes infinite, the curved beam model has transformed into a straight one. In this research, although the curved pipeline has a large bending angle from seabed to the sea level, but the water depth is deep enough, leading to a sufficient pipeline length. Consequently, the radius of curved beam model for suspended pipeline is large enough to make the assumption that the calculation of out-of-plane vibration part can be based on the calculation of a straight beam model.

Pipeline system properties

In this essay, the pipeline has a diameter of 0.273 m (10.75 inch), which is a rather small value compared to the length of laying pipeline, which can reach several kilometres. Besides, only lateral vibration is concerned in the essay and the torsion inside pipeline is beyond the scope of this research, which is neglected accordingly. Therefore the pipeline is considered as an Euler-Bernoulli beam.

The pipeline can be either air-filled or water-filled during laying process. The submerged weight of pipeline would also vary for these two methods. While for a deep water situation, the weight of water-filled pipeline may be too heavy for the laying vessel to carry. Thus in this study, air-filled pipeline is adopted during laying and the submerged weight is calculated accordingly.

Moreover, for the as-laid pipeline, the vertical initial penetration is only considered under the influence of its submerged weight and will stay at the same penetration level during the lateral vibration.

External forces

As current flows past a cylinder, vortex shedding may take place in the wake, which also occurs alternatively from both sides of the cylinder at a regular frequency, namely the shedding frequency. Current flow below the sea level can cause severe vortex-induced vibration if the shedding frequency, at which vortices are shed, is close to one of the eigen frequencies of the pipeline system. This process may induce in-line and cross-flow vibrations of circular structures. The magnitude of cross-flow direction VIV is much larger than that of in-line VIV. Currents induced VIV in the suspended pipeline will be transmitted into the seabed pipeline. The direction for currents in this essay is set as in-plane and horizontal as shown in Fig.1.3. Two kinds of current profile may be taken in this research, one is the uniform distribution which means the current speed is the same from sea level to seabed, the other one is the shear profile in which the current speed is zero at seabed and has maximum value at sea level.

When the pipeline vibrates in the water, the external forces exerted by the sea water on the as-laid will be modelled by the Morison equation, which is in this case equal to the summation of the drag force and the inertia force due to the accelerated water in the neighbourhood of the pipeline. While for the suspended pipeline, a wake oscillator model is adopted to simulate such interaction.

Boundary Conditions

In the construction procedures of simplified models within this research, the boundary conditions also plays an important role in modelling the vibration of pipeline. In the following chapters, the as-laid pipeline part and suspended pipeline part are first dealt with separately and then the coupled system of these two parts is analysed.

For seabed pipeline part, the pipeline is simplified as a semi-infinite beam. While seeking numerical solution through MATLAB, for convenience, this semi-infinite beam can be modelled as a beam with finite yet sufficient length. The boundary condition in this end can thus be treated as fixed. The boundary condition at the connection end with suspended pipeline, the boundary condition is also set as fixed boundary as in practice the slope angle is small. In order to model the lateral vibration transmitted from

the suspended part, the fixed boundary is also given an external displacement. Therefore the boundary end becomes fixed-sliding.

For the suspended pipeline part, the end connected to the vessel is considered as fixed since the lateral motion of laying vessel is not considered in this research. For the bottom end, the soil stiffness has only a scarce influence on the suspended part. It is the boundary phenomenon that really matters (Lenci et al). Thus, the assumption can be made that the bottom boundary end is fixed. In reality, the soil-pipe interaction process in touch down zone is really complex, which has strong nonlinear characteristics in both vertical and lateral direction. This is beyond the scope of this study.

For coupling of as-laid and suspended pipeline, the boundary conditions are both fixed and the interface conditions at the connection point are continuous, as will be explained in detail.

Methods for solving the equilibrium

For seabed pipeline, suspended pipeline and coupled pipeline system, the equations of motion will be given to describe their motions separately. In the calculation model, both VIV and pipe-soil interaction have strong non-linearity. Thus the solution is calculated in time domain in this essay. After equations of motion is given first, finite difference method is applied to discretise and simplify the equations of motion. Newmark- β method is used to solve the acquired ordinary differential equations. Given an initial input of the pipeline motion, the displacement, velocity and acceleration of the pipeline elements can be calculated step by step in time domain.

To sum up, main assumptions and simplifications are listed below:

- The pipeline is modelled as Euler-Bernoulli beam.
- Equations of motion for the beam is still in the elastic range during vibration
- Torsion and axial extension of the beam is neglected during dynamic laying modelling
- Out-of-plane vibration during laying process is focused, the coupling between in-plane and out-of-plane vibration is neglected.
- Vertical vibration of as-laid pipeline is neglected, and an initial penetration is assumed as static during the lateral vibration process.
- The pipe soil interaction model is used as an bi-linear soil model.
- Only the cross-flow vibration caused by VIV is concerned and in-line vibration is beyond the scope of this study
- The suspended pipeline model is fixed at both seabed and top end.
- The seabed pipeline model has finite sufficient length, is fixed at one end and fixed-sliding at the other end.
- The coupling pipeline is fixed at both boundary end.

- The setting of touchdown zone is simplified pre-defined to analyse its influence.
- Fictitious part is added into the coupled pipeline system to simulate the increasing length of pipeline during laying.s
- The lateral vibration of the pipeline are small with respect to the static configuration of the pipeline.
- Independence principle is considered as valid in large angle of inclination.
- The dynamic analysis of the pipeline system is analysed in time domain.

1.3. THESIS OUTLINE

The current thesis report comprises 7 chapters and is organized as follows:

Chapter 1 briefly explains a research background together with thesis problem description, objective, thesis outline and main assumptions.

Chapter 2 contains three basic fundamental areas of knowledge in the form of literature review: i) general information of laying process, ii) theory of pipe-soil interaction for as-laid pipeline, and iii) theory of vortex induced vibration due to current.

Chapter 3 presents derivation of equations of motion for as-laid pipeline and analysis of influential parameters.

Chapter 4 contains the equations of motion for suspended pipeline using wake-oscillator coupling model and the analysis of influential parameters.

Chapter 5 is a succeeding deduction from Chapter 3 and 4, depicting the coupling system of as-laid pipeline and suspended pipeline, which is mainly static laying process modelling without considering the increasing length of pipeline system.

Chapter 6 introduces the influence of touchdown zone on the vibration of seabed pipeline during laying process.

Chapter 7 builds up the dynamic laying model based on static laying process model in Chapter 5. The new model has compared the results and given qualitative analysis.

Chapter 8 is the conclusion summarizing the above chapters.

2

LITERATURE STUDY

2.1. PIPE-SOIL INTERACTION MODEL

During the pipe laying process, it is common practice to trench and bury the pipeline for maintaining stability and protection from trawl gear in shallow water. As the offshore oil and gas industry heads to deeper sea area, a more elegant way is to simply lay the pipelines on seabed for the consideration of trenching difficulty and economic costs. As the seabed plays the role of resistance component in analysing on-bottom pipeline movements thus properly depicting the process of pipe-soil interaction process is of vital importance.

Pipe-soil interaction resistance is more complex than simple friction but a highly non-linear response (Elosta et al 2013). The shallowly embedded pipeline-soil interaction model should incorporate both vertical and lateral responses to the external loading during pipeline laying process.

In recent decades, there are several typical experiments carried out and the corresponding models built up, the hysteretic non-linear model depicting vertical response of pipe-soil interaction (Randolph et al 2009), and the gradually improved lateral response modelling by bilinear model (Classical Coulomb friction approach), trilinear model (Wagner et al 1989, Brennodden et al 1989, White and Cheuk 2008) and plasticity-based macro-element model (Zhang et al 2002).

2.1.1. PIPE-SOIL VERTICAL INTERACTION MODEL

Advanced non-linear pipe-soil interaction models have been developed and validated by recent laboratory and field experiments and the following theoretical simulation work with acceptable accuracy (Randolph et al 2009). In Randolph's non-linear pipe-soil vertical interaction model, the essence of soil stiffness changing with the magnitude of pipeline penetration and cyclic motions is emphasized.

The model first uses the pipeline diameter, soil shear strength varying with depth and soil density

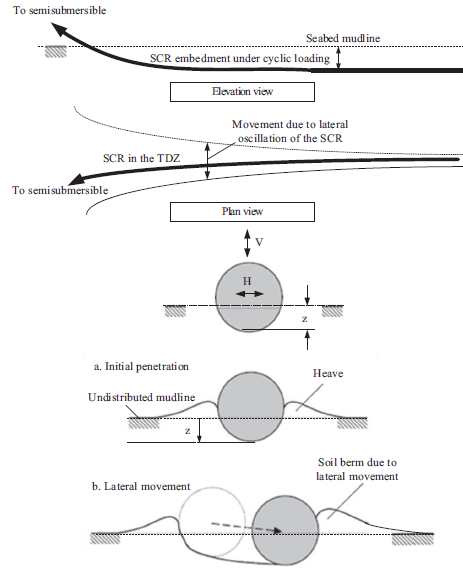


Figure 2.1: Schematic Illustration of SCR-seabed interaction in TDZ (Copyright from Elostá 2013)

as its input data, then considered additional parameters to include vertical interaction features like pipe embedment, cyclic loading motion, and soil suction effect. Consequently, the vertical soil resistance on seabed is depicted by four different penetration modes, which are Not-in-Contact, Initial Penetration, Uplift and Re-penetration. The process of which is illustrated in Fig.2.2.

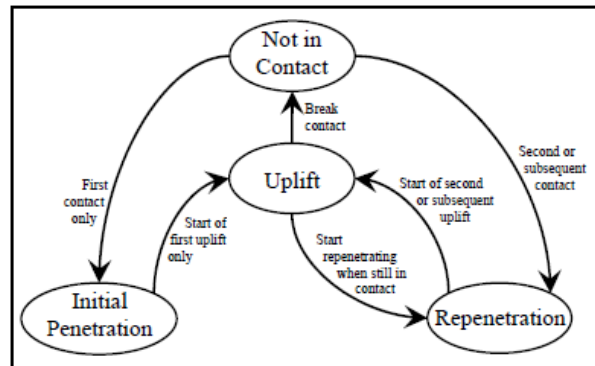


Figure 2.2: soil model penetration modes (Copyright from Mark Randolph)

Along with four penetration modes, corresponding depictive functions are used for these modes and the function parameters are updated every time with increasing penetration under cyclic load in vertical

plane. The following Fig.2.3 makes the penetration process clearer.

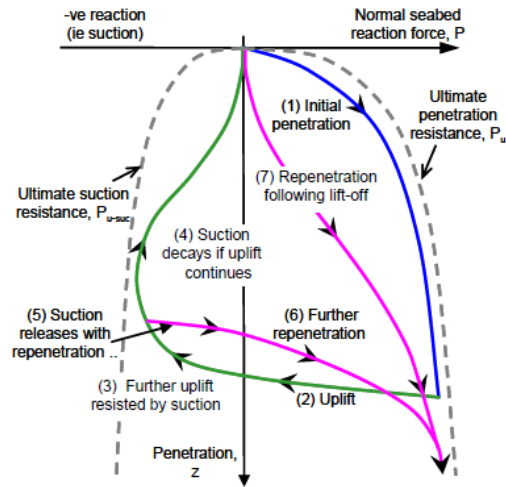


Figure 2.3: Soil model characteristics for different modes (Copyright from Mark Randolph)

Randolph's model is proved still to be clear and effective for practical engineering use, although no consideration is made for the softening effects of soil because of remolding process.

2.1.2. PIPE-SOIL LATERAL INTERACTION MODEL

Decades ago in industry practice, lateral soil resistance was estimated with a Coulomb friction model calculating the lateral resistance by effective submerged pipeline vertical force (submerged pipeline weight minus hydrodynamic lift force) and a simple soil friction coefficient only depending on soil type.

Wagner in 1987 had improved the pipe-soil interaction model taking the soil strength information and loading history effects into consideration. Afterwards Brennodden et al 1989 further improved the interaction model incorporating the variation of pipe penetration due to arbitrary loading conditions. Furthermore Bruton et al 2006 has defined four stage of pipe-soil interaction and mentioned the building of soil berms occurs with cyclic lateral loading. White and Cheuk 2007 developed an approach for elaborating the growth of lateral soil resistance resulting from monotonic and cyclic model response due to berm resistance. Besides, the most sophisticated pipe-soil interaction model is plasticity based macro element model using a framework of work hardening plasticity to create models for the generalized response of a pipe resting on soil under combined V-H (Vertical-Horizontal) loading.

Coulomb friction model (Bi-linear lateral resistance model)

The Coulomb friction model [5] can be illustrated clearly in Fig.2.4, lateral soil resistance in this bilinear model is calculated as :

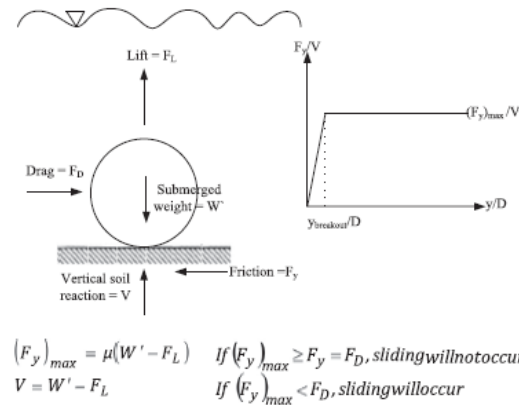


Figure 2.4: Coulomb friction model (Copyright from Elostia 2013)

$$(F_y)_{max} = \mu V \quad \text{with } V = W_s - F_L \quad (2.1)$$

Namely the simple model only depends on the effective submerged pipeline weight and soil type. Conventional industry practice for pipeline design with this model is to mimic the pipe-soil interaction by applying spring slider elements at intervals along the pipeline. The relation of lateral resistance and displacement for this bi-linear elastic modelling can be seen in Fig.2.4.

The resistance and displacement curve shows that the linear part of lateral friction force is given by $F = -k_s A y$ and has reached a maximum of μV in breakout displacement $y_{breakout}$, where $y_{breakout} = \mu V / k_s A$ as a result.

Two-component model

Pipe-soil resistance is far more complicated than Coulomb friction model, to improve this process emphasizing on loading history and pipe penetration, Wagner developed a two component model by estimating the lateral soil resistance with sliding resistance and soil passive resistance after analyzing experiment test data. The first component mimicking the sliding resistance of the pipe along a flat soil surface depends on the effective submerged pipeline weight. The second component, considering soil resistance caused by passive failure of soil wedge in front of the partially embedded pipeline, depends on the pipe penetration and soil strength.

This improved model has the general form of:

$$F_H = F_F + F_R \quad (2.2)$$

Where F_H is the total lateral soil resistance, F_F is the sliding resistance and F_R is the lateral passive soil resistance term.

This equation can also be specified further in sand model and clay model,

$$F_H = \mu V + \beta \gamma A \quad (\text{sand model})$$

Where μ is the soil sliding resistance coefficient, V is the effective submerged pipeline weight, β is the empirical soil passive resistance coefficient, γ is the effective weight of sand and A is the pipe-soil lateral contact area.

$$F_H = \mu V + \beta c \frac{A}{D} \quad (\text{clay model})$$

Where c is the remolded undrained shear strength for the clay, D is the pipe diameter. In this two-component model, Brennodden et al 1989 further developed an improved calculation approach for F_R using an energy based method rather than the empirically estimation as stated above.

Tri-linear lateral resistance model

Beyond the simple bilinear friction model and the two-component model, a more sophisticated trilinear lateral pipe-soil interaction model had been developed by Bruton et al 2006. The model was further improved by including detailed calculation for berm resistance due to soil accumulation in front of the pipeline (White and Cheuk 2008). As illustrated in Fig.2.5, the trilinear model mimic the lateral soil response using independent values of pipe-soil breakout resistance, and residual resistance. The pipe laying process leads to a larger penetration than the initial penetration caused by effective submerged weight of pipeline alone in the touch down zone. Thus there will appear over-penetration of the pipeline in touch down zone compared to the already laid pipeline far away.

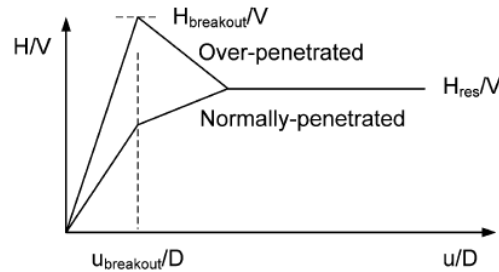


Figure 2.5: Lateral trilinear pipe-soil interaction model (Copyright from White 2008)

Bruton has analysed the experimental results and draw the conclusion that normalized dimensionless breakout resistance, $h_{breakout} = H_{breakout}/Ds_u$ depends on the current normalized vertical load, $v = V/Ds_u$, the initial embedment depth, w_{init}/D , and the dimensionless ratio of soil strength to weight, $s_u/\gamma'D$. The following expression is used to depict the model well:

$$h_{breakout} = \mu v + \frac{3}{\sqrt{s_u/\gamma'D}} \frac{w_{init}}{D} \quad \text{with } \mu = 0.2 \quad (2.3)$$

For this tri-linear model, the lateral pipe-soil resistance has reached a constant value after breakout. The defined dimensionless residual resistance, $h_{residual} = H_{residual}/Ds_u$ depends on the dimensionless soil strength weight ratio, $s_u/\gamma'D$. The expression of residual resistance is:

$$\frac{h_{residual}}{v} = 1 - 0.65 \left[1 - \exp\left(-\frac{1}{2} \frac{s_u}{\gamma'D}\right) \right] \quad (2.4)$$

The occurrence of such breakout resistance is within less than 1/2 diameter for lateral pipe displacement, while residual resistance first occurs within 3 to 5 diameters. Thus lateral resistance is governed by residual resistance when large lateral displacement of the pipeline appears due to external excitations.

Actually the residual resistance is slightly increasing when the pipeline move laterally because a berm of soil has built up in front of the pipe. Especially during cycle loading, soil berms at the extremities of pipeline displacement range will cause an additional resistance during subsequent larger cycles. Thus an improved model has been developed by White and Cheuk elaborating the influence of soil berms. The improved model is illustrated as:

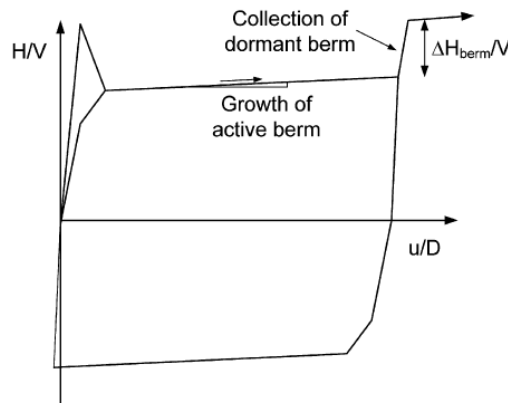


Figure 2.6: Illustration for trilinear model(Copyright from White 2008)

The berm resistance is added to the residual resistance in a trilinear model stated above, and can be predicted as,

$$h_{berm} = \left(\frac{H_{berm}}{Ds_u} \right) = \left(\alpha \lambda v^\beta \frac{u}{D} \right)^\delta \quad (2.5)$$

Where $\alpha = 0.015$ and $\beta = 2.3$ as simulated value for embedment of a rough pipe, for $w/D < 0.5$, λ is related to the actual shape of the berm and the value of which is assumed as 1 here, δ is assumed to be 0.5.

2.2. VIV OF SUSPENDED PIPELINE

The coupling effects of structures and fluids has been studied dating back to the start of offshore subjects. The suspended pipeline in deep water may experience the dynamic coupling force of wave and currents. General theory about flow passes cylinder will be explained in detail here.

2.2.1. FLUID FLOWS PAST CYLINDER

When a real fluid flows past a bluff body, such as a cylinder, various form of flow can be developed. The Reynold number is used to characterize different types of flow, which is defined as:

$$Re = \frac{VD}{\nu}$$

Where V is velocity of flow, D is the diameter of a cylinder and ν is the kinematic viscosity of the fluid. The flow regimes changes a lot when the characteristic Reynold number of the flow changes, as shown in Fig.2.7.

For a very small value of Re , the flow pasts around the cylinder without separation. At the Re value of about 40, vortex first appears and the vortex street remains laminar. It will keeps its form in spanwise direction until the Re value goes beyond 200. The wake is completely turbulent for $Re > 300$, and the regime for $300 < Re < 3 \times 10^5$ is known as the sub-critical flow regime.

The vortices appears in the wake of the cylinder and the wake will become gradually unstable while increasing the value of Reynolds number. The phenomenon that vortices repeatedly form and are typically alternately shed into the flow from each side of the cylinder, is referred as vortex shedding. The vortex shedding phenomenon shown in Fig.2.8 in is common to all the flow regimes with the property of $Re > 40$, as shown from Fig.2.7. An alternative vortex shedding from both side of the cylinder forms one period for vortex shedding. Here also comes the meaning of shedding frequency at which the vortices are shed at pairs.

$$f_s = \frac{St}{D} V \quad (2.6)$$

Where f_s is the shedding frequency, D is the diameter of a cylinder and V is flow speed. St is the Strouhal number which has a relation with Reynolds number. The relation is verified by series of experiments and is depicted in Fig.2.9. The Strouhal number is intrinsically a dimensionless number describing oscillating flow mechanisms. Moreover, it is strongly influenced by the surface roughness and cross-section shape of the bluff bodies, also by the turbulence and effects of shear for incoming flow. Wall proximity is also an important influential factor. In Fig.2.9, the most interesting phenomenon is that St is practically constant and equal to 0.2 in the sub-critical flow regime ($300 < Re < 3 \times 10^5$). In which regime, the shedding frequency has a linear relation with the flow velocity for a determined cylinder diameter. While for $Re > 3 \times 10^5$ the Strouhal number increases a little bit for rough surface bodies and dramatically for smooth surface bodies. Thus the vortices and fluctuations are no longer regular and its frequency becomes harder to define.

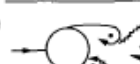
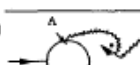
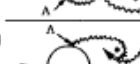
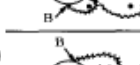
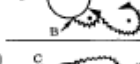
a)		No separation. Creeping flow	$Re < 5$
b)		A fixed pair of symmetric vortices	$5 < Re < 40$
c)		Laminar vortex street	$40 < Re < 200$
d)		Transition to turbulence in the wake	$200 < Re < 300$
e)		Wake completely turbulent. A: Laminar boundary layer separation	$300 < Re < 3 \times 10^5$ Subcritical
f)		A: Laminar boundary layer separation B: Turbulent boundary layer separation; but boundary layer laminar	$3 \times 10^5 < Re < 3.5 \times 10^5$ Critical (Lower transition)
g)		B: Turbulent boundary layer separation; the boundary layer partly laminar partly turbulent	$3.5 \times 10^5 < Re < 1.5 \times 10^6$ Supercritical
h)		C: Boundary layer com- pletely turbulent at one side	$1.5 \times 10^6 < Re < 4 \times 10^6$ Upper transition
ii)		C: Boundary layer com- pletely turbulent at two sides	$4 \times 10^6 < Re$ Transcritical

Figure 2.7: Regimes of flow around a smooth, circular cylinder in steady current

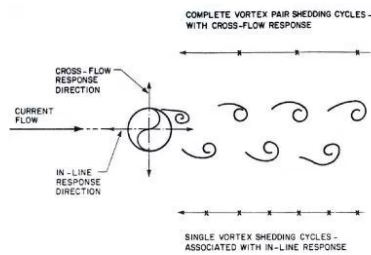


Figure 2.8: Staggered alternate vortex shedding – in-line and cross-flow response, J P Kenny (1993)

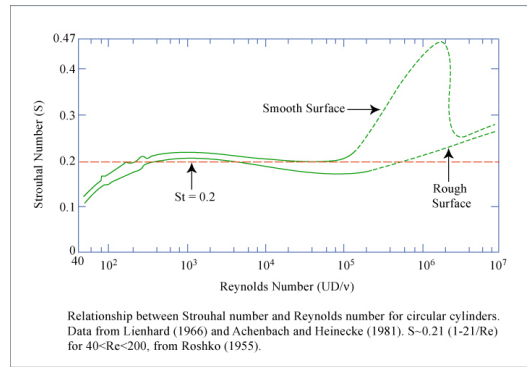


Figure 2.9: Relation between Strouhal number and Reynolds number (Source: MIT OPW)

FLOW FORCES ON THE CYLINDER

The above-mentioned section discussed different flow forms cross a circular cylinder related to the Reynolds number. The flow is commonly featured with vortex shedding except for very small Reynolds number ($Re < 40$) which is really out of interest for engineering use. Thus this section will discuss about the forces induced by these vortices.

As a consequence of the vortex-shedding phenomenon, vortices are (alternately) shed behind the cylinder thus a cyclic pressure variation will occur in the wake. At the location where the vortex is closest to the cylinder the local velocities in the wake will be highest and the local corresponding pressures will be lowest. This mechanism leads to a resulting force directed toward the vortex. The force component in the flow direction is called the drag force. The force component perpendicular to the flow direction is called lift force as shown in Fig. 2.10. The pressure distribution around the cylinder undergoes a periodic

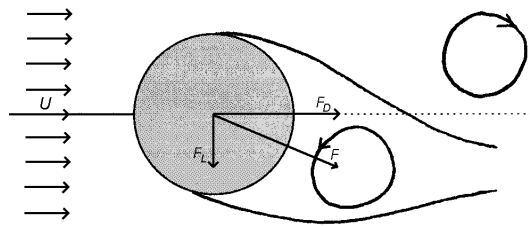


Figure 2.10: Force components of lift and drag force

change as the shedding process progresses, resulting in a periodic variation in the force components on the cylinder. The shedding frequency has been defined already, and there is also a clear relation between lift force frequency and drag force frequency. The frequency of lift force is the same as the frequency for vortex shedding (in pairs) frequency f_s . While the frequency for drag force is twice the frequency of vortex shedding f_s defined above. Lift and drag force can be expressed as a relation of non-dimensional

coefficients C_L and C_D separately in the form of Eq.(2.7).

$$\overline{F}_D = \frac{1}{2}\rho DV^2\overline{C}_D \quad (2.7a)$$

$$\overline{F}_L = \frac{1}{2}\rho DV^2\overline{C}_L \quad (2.7b)$$

where the overline in drag and lift coefficients means the average value. What is more, the mean drag and lift coefficient can also be shown as a function of Reynolds number as the following picture shown in Fig.2.11 and Fig.2.12.

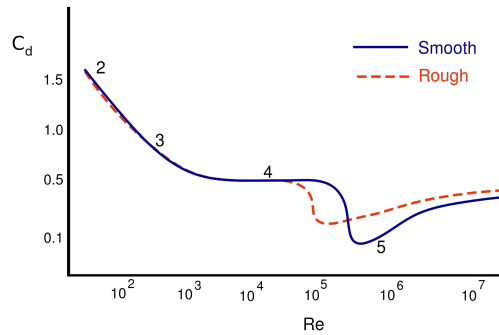


Figure 2.11: Relation between mean drag coefficients and Reynolds number

The relation between mean drag coefficients and Reynolds number shown in Fig.2.11 contains the functions for stationary cylinder with rough and smooth surface. As seen from Fig.2.11, C_D decreases monotonously with Re at the very beginning until Re reaches the value of about 300. Continuously, C_D is assumed as a basically constant value, roughly 1.2, throughout the sub-critical Re range ($300 < Re < 3 \times 10^5$), the value of which is always used in most cases. When Re reaches the value of 3×10^5 , there is a dramatic fall in C_D , the drag coefficient decreases abruptly and is assumed as a much lower value, about 0.25, in the supercritical Re range, $3.5 \times 10^5 < Re < 1.5 \times 10^6$ (Fig. 2.11). The phenomenon of this fall is called the drag crisis.

With the same purpose, the Root Mean Square value (RMS) of the lift force coefficients is often used to quantify the lift force. The RMS lift coefficient for a stationary cylinder is shown in Fig.2.12.

VIV FOR OSCILLATING CYLINDER

In the previous section, drag and lift forces for a stationary cylinder are explained in general. For actual situation, the cylinder undergoing environmental loading may oscillate in the water, namely the vortex induced vibration. The maximum magnitude for the VIV of cylinder can reach about 1 diameter of the cylinder, when the shedding frequency is close to the the natural frequency of the cylinder. This phenomenon is also called the lock-in phenomenon which is mainly decided by the environmental loading and the intrinsic characteristic of the cylinder.

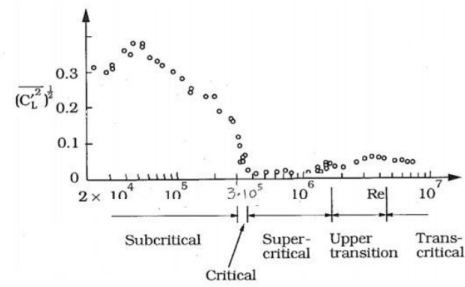


Figure 2.12: Relation between r.m.s of lift coefficients and Reynolds number

A typical experiment studying into the vortex induced vibration of a free cylinder was conducted by Khalak and Williamson. The experiment shows the results about a cylinder moving freely in a crossflow direction under steady current flow. An illustration is shown in Fig.2.13.

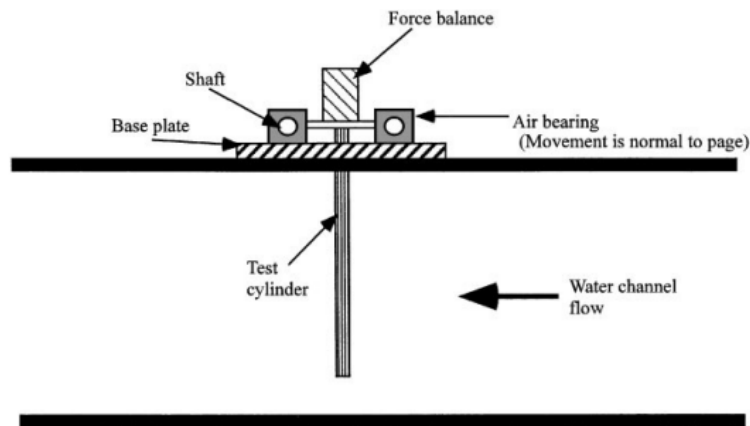


Figure 2.13: Schematic of the experimental arrangement

The experiments acquired the results for steady state response of the cylinder, which contain information about the reduced velocity for currents, maximum cylinder vibration amplitude, cylinder vibration frequency and shedding frequency. The experiment is repeated for different steady flow velocities and thus with different reduced velocity. In VIV, the current which causes the vibrations is important, because the speed of the current will determine the frequency of the vibration. The value of the velocities setting in the experiment is conducted both in increasing and decreasing trend, in order to capture the characteristic of hysteretic effects.

Later the such experiments are repeated by Jauvtis and Williamson including both cross-flow and in-line direction vibration for the cylinder, namely a two degree of freedom vibration for the cylinder. The

results of both experiments are shown in Fig.2.14.

Dots (•) is cross-flow vibration results acquired by Khalak and Williamson in 1999, whereas Circles (◦) shows the later two degrees of freedom vibration results by Jauvtis and Williamson in 2003.

In Fig.2.14, the upper one shows the relation between reduced velocity and maximum amplitude of cross-flow, in-line cylinder vibration. While the lower one shows the relation between the reduced velocity and cylinder vibration frequency. The results are also shown in dimensionless parameters, A_y is the ratio of actual cross-flow vibration amplitude and cylinder diameter. The same situation also applies to A_x which is for the in-line vibration. The frequency response f_y of the cylinder is the ratio of natural frequency of the system.

Moreover, the reduced velocity is considered in finding the expected velocity range and is defined as:

$$V_n = \frac{V}{Df_n} \quad (2.8)$$

Where f_n is the n-th natural frequency of the experimental cylinder. The response of a flexible cylinder in a uniform steady flow is characterised by three regions of instability (Fig.??).

These regions are defined by empirical rules (Wooton et al.,1972)

- The first region of in-line vibration instability occurs in the range of about $1.2 \leq U_r \leq 2.5$, the maximum response amplitude, at about $U_r = 1.9$, is associated with symmetric vortex shedding.
- The second region of in-line vibration instability occurs in the range of about $2.7 \leq U_r \leq 3.8$, the maximum response amplitude, at about $U_r = 2.6$, is associated with asymmetric vortex shedding.
- The third region of cross-flow vibration instability occurs in the range of about $4.8 \leq U_r \leq 8.0$, the maximum response amplitude, at about $U_r = 5$ to 6, is associated with asymmetric vortex shedding.

While taking both view of Fig.2.14 and Fig.2.15, some similarities can be found clearly. Compared with the maximum amplitude of cross-flow vibration, the maximum in-line flow amplitude is relatively small and is less significant unless the fatigue problem for pipelines is investigated into, which is beyond the scope of this research. Thus for the main research proposal of lateral vibration in this essay, only the cross-flow vibrations is concerned.

Another important deduction should be stated here:

$$V_n = \frac{V}{Df_n} = \frac{f_s D}{St} \cdot \frac{1}{Df_n} = \frac{1}{St} \frac{f_s}{f_n}$$

Where as already defined above, the value of Strouhal number St is considered as constant equalling to 0.2. Further more, when the shedding frequency approaches vibration frequency of the cylinder during actual resonance phenomenon, a typical value of reduced velocity $V_n \approx 5$ can be derived. Thus, once the natural oscillation frequency of a structure such as risers is known, one can determine V_n and use it as a rough estimation to predict a danger from resonant vortex-induced oscillations.

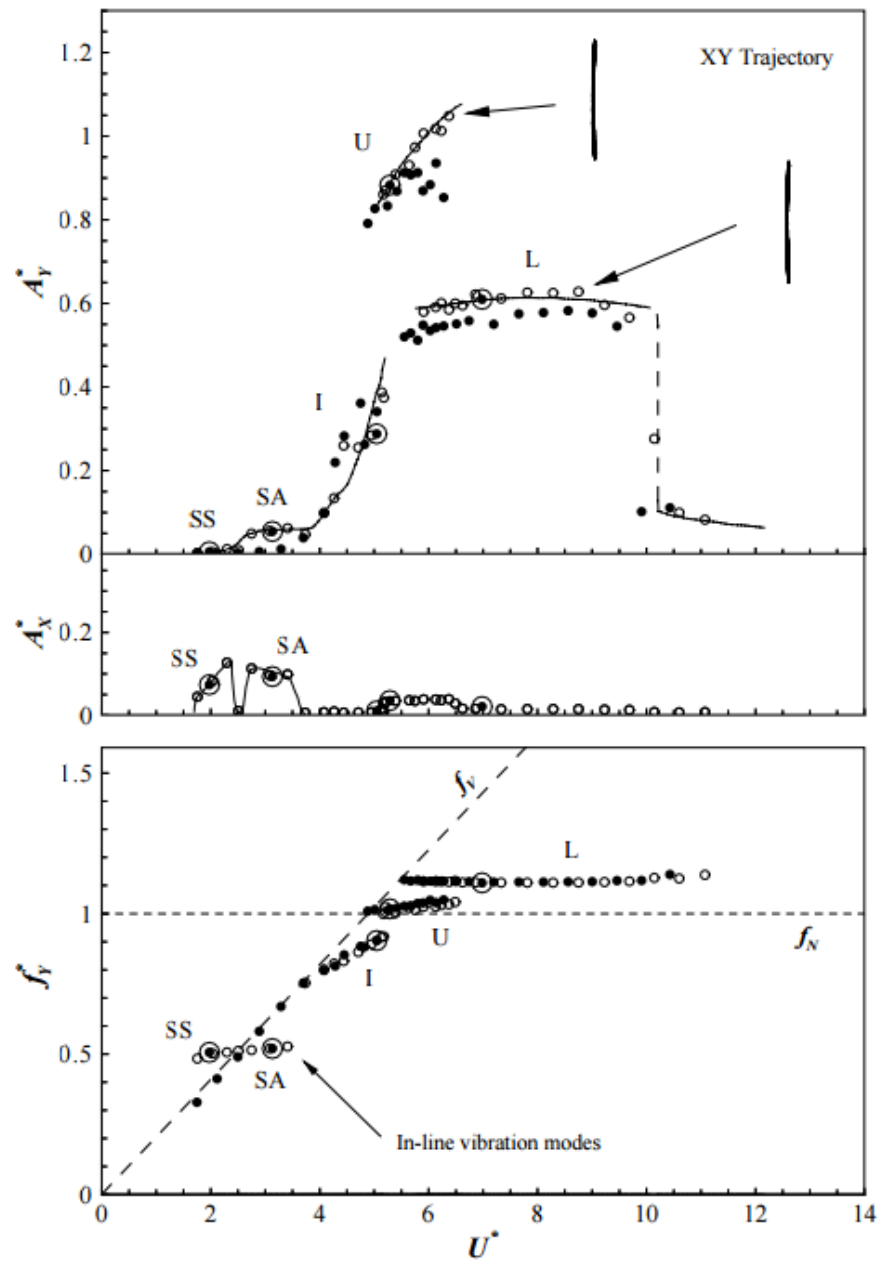


Figure 2.14: Cross-flow and in-line vibration amplitudes (A_Y and A_X) and response frequency f_Y as functions of reduced velocity. Dots (\bullet) is only for cross-flow vibration results acquired by Khalak and Williamson in 1999, whereas Circles (\circ) shows the later two degrees of freedom vibration including cross-flow and in-line results by Jauvtis and Williamson in 2003.

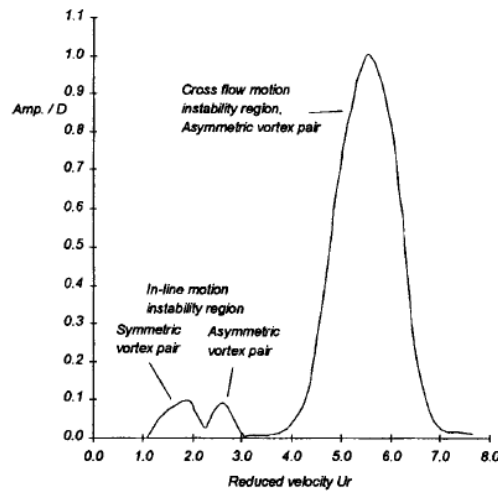


Figure 2.15: Regions of instability vortex shedding

Now investigating back into the experimental results in Fig.2.14, typical phenomena mainly focusing on cross-flow vibrations are concluded as following:

- When the value of reduced velocity $V_n < 3$, the vibration amplitude is relatively small. VIV can be considered as non-existence. Still, vortex shedding frequency can be calculated using Strouhal principal as 2.6 which is the same situation as a stationary cylinder.
- Once the reduced velocity V_n approaches the value of 5, vortex induced vibration may occur. The shedding frequency begin to exceed the control of Strouhal principal and reached a constant value, which equals to the natural frequency of the structure despite the increasing of V_n . This phenomenon is called lock-in or synchronization of shedding frequency.
- When the lock-in regions extends during the range $4 < V_n < 11$, three types of vibration modes are classified, namely the initial branch(I), the upper branch(U) and the lower branch(L). The vibration frequency increases slowly within the upper branch while remains constant within the lower branch.
- When the value of $V_n > 11$, the shedding frequency unlocks from the vibration frequency, the value of shedding frequency begin to comply with the Stouhal frequency again. When the value of $V_n > 14$, VIV is no longer observed.

With the typical phenomena observed from the experiments, the fluid forces on oscillating cylinder must be investigated. Still, the focus of fluid forces contains drag and lift forces in this condition. In the case that the amplitude of vibration is very small, the coefficients for drag and lift force can be seen as the

same as that for a rigid stationary cylinder. While for the cylinder in vortex induced vibration case, the amplitude of the vibration is relatively large enough to take significant effects on the wake patterns, and further on the drag and lift coefficients.

Take the drag coefficients as an example when the VIV synchronization happens. The modified drag coefficients is dependent on the amplitude of cylinder vibration. The following relations was given by Sarpkaya(1981) for in-line vibrations illustrating in Fig.2.15.

$$C_d = C_{d0} + (0.12 + 3.80 \frac{Ay(x)}{D}) \quad \text{first instability region} \quad (2.9a)$$

$$C_d = C_{d0} + (0.08 + 2.66 \frac{Ay(x)}{D}) \quad \text{second instability region} \quad (2.9b)$$

where $y(x)$ is the mode shape and A is the magnitude of the modal response. For cross-flow vibrations in the third instability region, DNV(1991) had suggested the following empirical equation.

$$C_d = C_{d0} (1 + \frac{0.9Ay(x)}{D}) \quad (2.10)$$

The fluctuating drag components increase the total load by a factor of 2 to 3. Also in the experiment performed by Khalak and Williamson, both drag and lift coefficients in cylinder vibration case have large difference compared to the stationary case, therefore reasonable fluid forces modelling must be taken into account. Currently, for numerical modelling and analysing the VIV of cylinder, a testified wake oscillator model is chosen by solving coupling equations of structural motions and fluid flow.

The wake oscillator models put into the fluid forces into equations of motion for the cylinder by a nonlinear oscillator equation representing the fluid forces. The nonlinear equations are often described by a Van der Pol equations as will be elaborated later.

3

PIPE-SOIL INTERACTION MODEL

As stated in section 1.2.1, the pipeline system during J-lay process comprises the seabed part and suspended part. This chapter presents a simplified model for simulating the lateral vibration of pipeline on seabed separately. The chosen pipe-soil interaction pattern is incorporated and testified in this model, as the most influential factor for seabed pipeline. After the simplified simulation model is settled, the phenomenon appeared for the vibration of beam model is observed and analysed.

3.1. MODEL INFORMATION

During laying process, the pipeline on seabed is increasing its length as the laying vessel working continuously. The length of seabed pipeline can be very large from the initial laid point to the touchdown point. When the seabed pipeline is only taken into consideration, it can be seen as a semi-infinite length tensioned Euler-Bernoulli beam with suitable boundary conditions. While for the numerically calculation simplicity, the seabed pipeline is considered as a beam with sufficient length at which boundary end the pipeline is undisturbed and can be considered as a fixed boundary. The assumptions for this model is described previously in section 1.2.3.

Vertical penetration

The focus of this research is on the lateral vibration of the pipeline system during laying process. The vertical motion of the pipeline is neglected considering the coupling effects of vertical and lateral vibration is small. Thus the vertical motion is neglected and the vertical penetration is assumed as a constant value during the lateral vibration process. This constant value for vertical penetration length is defined as initial embedment, which is equalling to the penetration of pipeline invert (the bottom of pipeline) below mean seabed level. During the actual industrial practice, this value is highly unpredictable due to too

many influential factors existed in reality. The complicated dynamic forces due to laying performance is one of the large influential factor. Laying rate, laying vessel type and the curvature of suspended pipeline catenary approaching seabed will also arouse changes in the value of embedment. The recommended results acquired in lab tests are also highly influenced by subsequent consolidation-induced settlement.

A design equation is proposed by D.Bruton [6] under the basis of limited data. The equation connects the normalised initial pipeline penetration (z_{init}/D) and the normalised vertical load resulting from effective pipe weight ($V/DS_{u_{invert}}$) and soil sensitivity (S_t), which is the ratio of intact to remolded shear strength.

$$\frac{z_{init}}{D} = \frac{S_t}{45} v^2 = \frac{S_t}{45} \left(\frac{V}{DS_{u_{invert}}} \right)^2 \quad (3.1)$$

For the reason of limited research and no robust analysis in this area, thus in this research, the soil strength at the invert ($V/DS_{u_{invert}}$) is used as a representative value rather than using the exact values related to varying penetration depth. Detailed data used in the equation is concluded in Tab. 3.1.

Tension in the beam

The axial force in this beam model is really an influential parameter for the lateral vibration of the model. Thus it is highly necessary to clarifying the properties and magnitude of the axial force in on-bottom horizontal pipeline.

The meaning for effective tension in submerged pipeline is explained here beforehand. For a submerged pipeline without a closed surface, the concept of effective axial force is used to clarify the axial force should be used to calculate the behaviour of the pipeline (Fyrileiv and Collberg, 2005) [7]. As seen in Fig. 3.1, the unclosed section with an axial force, N , and the external pressure, p_e , can be replaced by a section where the external pressure acts over a closed surface and gives the resulting force equal to the weight of the displaced water, namely the buoyancy of the pipe section (middle figure), and an axial force equal to $N + p_e A_e$.

A similar deduce can be exerted also on the case of internal pressure. Afterwards, the effective axial force can be expressed as the combination of true wall stress of the section and the internal and eternal pressure as in Eq.3.2.

$$S = N - p_i A_i + p_e A_e \quad (3.2)$$

For the as-laid pipeline on seabed, when the pipe temperature and internal pressure are the same as the time when pipelines were laid, the effective axial force S (in the horizontal direction) is equalling to the effective laying tension H as given in Det Norske Veritas (DNV) code[8]. The effective laying tension is further investigated in the following description.

$$S = H \quad (3.3)$$

During the pipe laying process of J-lay, it is also worth mentioning that the vertical force per unit

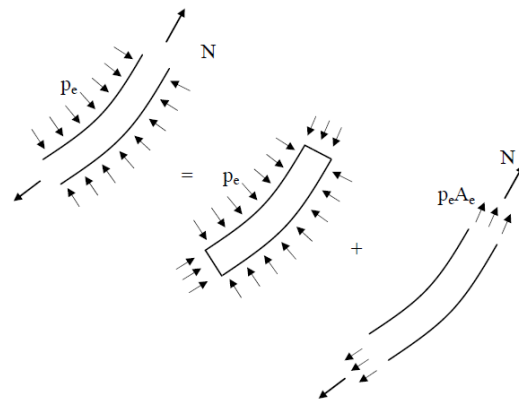


Figure 3.1: Effective tension illustration

length between the pipeline and the soil in the vicinity of the touch down point will exceed the submerged self-weight of the pipeline. While such change of vertical force is beyond the scope of this research will not be discussed here. Lest there is no current flows and the laying process is not considered, the horizontal force in the pipeline is kept constant through the suspended part of the pipeline and the on-bottom part of the pipeline as given above. The configuration is illustrated in Fig.3.2. The horizontal tension defined here is the same as the meaning of effective laying tension stated in Eq.3.3.

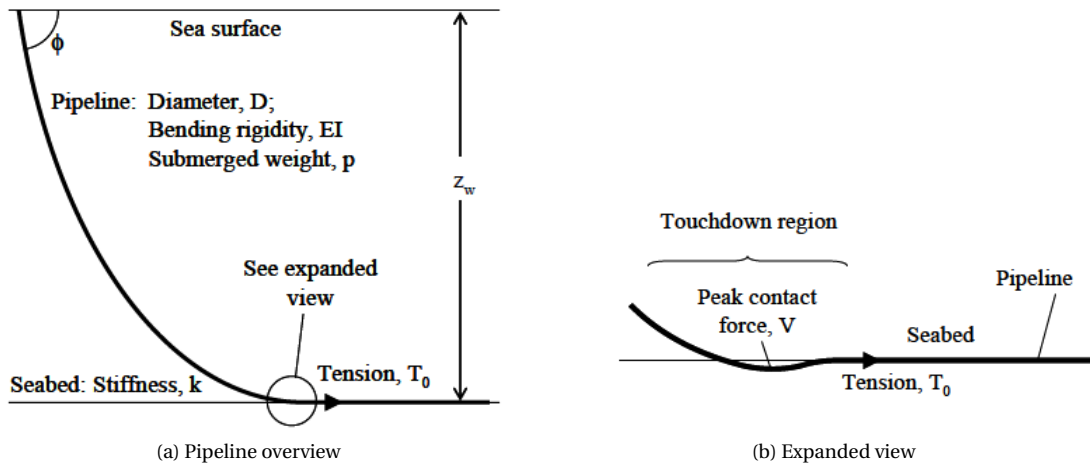


Figure 3.2: Static configuration of pipeline during laying(Copyright from Mark F. Randolph)

The horizontal tension can be quantitatively calculated during the derivation for initial laying configuration of pipeline during J-lay. For a simple catenary assumption for the initial configuration, the horizontal tension can be expressed in terms of water depth, z_w , hang-off angle, ϕ , and the pipeline unit

submerged weight, W' , as Eq.3.4. This force can also be a reference to the horizontal tension which laying vessel should provide.

$$\frac{T_0}{W' z_w} = \frac{\cos \phi}{1 - \cos \phi} W' \quad (3.4)$$

A pure catenary shape for the initial configuration is just a far too simplified model to describe the correct laying static configuration for the whole pipeline system. The reason for choosing a simple catenary assumption is that, for large parts of pipeline, the bending (namely the second derivative of the angle) of suspended pipeline is relatively small and thus be neglected. A catenary assumption is valid here. While in the contact region of suspended pipeline and soil near the touch down point, the bending is influential and the pipeline behaves more like a beam. In the J-lay process for deep water situation, a more accurate analytical calculation method using boundary-layer assumption is described by Lenci and Callegari [9]. While this method has not considered the influence of current flows, in this essay, a more detailed calculation method is proposed for the initial static configuration both considering the boundary layer phenomenon and current flow as in the appendix. During this derivation process, horizontal laying tension at the connection touchdown point is also solved.

To make it more clear, the characteristic length, λ , for the boundary layer is defined as Eq.3.5. Extra attention should be paid here that the given definition of characteristic length is just an experiential equation used for quick examinations. The actual value varies according to a variety of factors depending on particular situation when the pipeline is laid.

$$\lambda = \sqrt{\frac{EI}{T_0}} \quad (3.5)$$

The idea of using the above-mentioned assumption for the tension in seabed pipeline is fairly controversial as per the laying process is incorporated. During the pipeline laying operation, tension in seabed pipeline has a changing value rather than a constant value as that in the lower end of suspended pipeline in Eq.3.3. The reason results from the axial interaction between seabed pipeline and soil. After sufficient time, the tension may be released when the axial relative length between pipeline and soil decreases. Since the aim of this research is focusing on the period during laying process, thus the tension changing due to axial pipe soil interaction should be considered here.

In this research, the main focus is simulating the lateral vibration of pipelines in laying process. The axial tension along the seabed pipelines can not be simply assumed as the same as the tension in the TDP calculated from the suspended part, the calculation process is deduced in Appendix A in detail. After investigating into the problem, axial soil force can be seen as axially distributed spring along the seabed pipeline. The stiffness of equivalent spring is determined by the soil properties and is calculated by empirical equation in this research. Also the axial force is concerned with the axial strain of the pipeline rather than the lateral bending any more. To conclude, tension in the seabed pipeline during laying process is considered as a semi-infinite rod on elastic foundation subjected to static tension on the other end as shown in Fig.3.3. The dynamic axial tension distribution may vary from the static axial tension

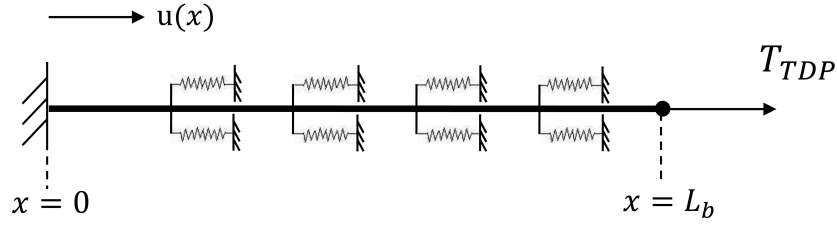


Figure 3.3: Rod model for axial pipe soil interaction

distribution to some extent due to plenty of factors in the dynamic laying process. But this has beyond the scope of the essay, the focus of which is still the lateral vibration of the pipeline and the axial condition of the pipeline will be considered the same during the research. Thus the static axial tension results calculated will be used in the dynamic analysis of the lateral vibration. In this new distributed tension calculation model, the static axial tension results is concerned largely with the axial strain of the rod due to the tension on the right end. It should be noticed that the tension here is referred as the true wall tension since it is concerned with the exact strain in the pipeline. Thus the effective tension calculated from the suspended part should be transformed into true wall tension using Eq.3.2.

The equation of motion for the rod is:

$$\frac{\partial^2 u}{\partial t^2} - c^2 \frac{\partial^2 u}{\partial x^2} + \omega_0^2 u = 0, \quad \omega_0 = \sqrt{\frac{k_d}{\rho A}} \quad c = \sqrt{\frac{E}{\rho}} \quad (3.6)$$

Thus the static equation of equilibrium for the rod model in Fig.3.3 is:

$$-c^2 \frac{\partial^2 u}{\partial x^2} + \omega_0^2 u = 0, \quad \omega_0 = \sqrt{\frac{k_d}{\rho A}} \quad c = \sqrt{\frac{E}{\rho}} \quad (3.7)$$

The general solution for Eq.3.7 is easy to find in the form of $u(x) = C_1 \exp(\lambda_1 x) + C_2 \exp(\lambda_2 x)$, substituted into Eq.3.7, the following relationship can be derived:

$$\sum_{i=1}^2 C_i (\lambda_i^2 - \beta^2) \exp(\lambda_i x) = 0 \quad (3.8)$$

Equation 3.8 must be always satisfied to guarantee that there is a solution for Eq.3.7. Thus the only way to do this is letting $\lambda_i^2 = \beta^2$, which can be written in another way as $\lambda_1 = \beta$ and $\lambda_2 = -\beta$. Here, $\beta^2 = \omega_0^2 / c^2$. Then the general solution can be further simplified as $u(x) = C_1 \exp(\beta x) + C_2 \exp(-\beta x)$. To solve the general solution, there are still two constants unknowns C_1 and C_2 to be derived. This can be done by

introducing the boundary conditions for the rod model as the following.

The boundary condition in left end ($x = 0$) of the rod model is shown as Eq.3.9.

$$u(x) = 0 \quad (3.9)$$

The boundary condition in right end ($x = L_b$), L_b is the length of rod model, is given in Eq.3.10.

$$EA\beta [C_1 \exp(\beta x) - C_2 \exp(-\beta x)] = T_{true} \quad (3.10)$$

Notice that in Eq.3.10, T_{true} can be transformed from the effective tension T_{eff} calculated from connection point (Touch Down Point (TDP)) between the suspended pipeline and seabed pipeline. The transformation equation is the same as that in Eq.3.2.

After substituting the general solutions of rod model into boundary conditions, C_1 and C_2 are found as

$$C_1 = -C_2 = \frac{T_{true}}{2EA\beta \cosh(\beta L_b)} \quad (3.11)$$

Since all the unknown variables are deduced above, the general solution can be finally simplified as

$$u(x) = \frac{T_{true}}{EA\beta \cosh(\beta L_b)} \sinh(\beta x) \quad (3.12)$$

With the above deduce process, the static axial strain $u(x)$ of the rod model under constant tension T_{true} is derived. Thus the axial tension which is directly concerned with axial strain can be derived accordingly.

$$T(x) = EA \frac{\partial u(x)}{\partial x} = \frac{T_{true}}{\cosh(\beta L_b)} \cosh(\beta x) \quad (3.13)$$

The derivative of tension part is also concerned in the following equation of motion for the seabed pipeline model, thus is also given here previously as,

$$T'(x) = \frac{\beta T_{true}}{\cosh(\beta L_b)} \sinh(\beta x) \quad (3.14)$$

The axial tension and corresponding first order derivative along the pipeline length have been deduced through the above process. After the initial configuration of suspended pipeline is set up, the axial force of the connection point (TDP) can be determined and the seabed pipeline tension can be calculated next as given in the above process.

Damping in the pipeline

Damping in an oscillatory system is a description used to represent the energy dissipated in the oscillation. The energy loss will restrict or prevent its oscillations. In a large structure system, damping may take effects through different mechanisms such as,

- Viscous effects (dashpot, shock absorber)
- External friction (slippage in structure joints)
- Internal friction (characteristic of the material type)
- Structural nonlinearity (plasticity, gaps)

Thus in actual case, damping is rather difficult to model precisely because of too many triggering mechanisms. In the numerical model, the values of damping are often based on the empirical values from dynamic tests. The damping value is a mathematical approximation because of its difficulty to quantify. For convenience, modal damping ratios (ζ_n) are usually used as a percent of critical damping correspondent to the n -th modal shape response in linear elastic materials. For the typical steel material, the material damping due to internal friction in pipelines is usually small and has a representative value of 0.5% if no other information is available. This value is considered to be very conservative [10].

For simplification in this research, only material damping is considered here in the pipeline model. An effective method is proposed here to determine the damping matrix with acceptable precision, which in other words is the proportional damping matrix shown in the following.

From the micro perspective, as stated by Clough [11], if it is assumed that damping stresses are developed in proportion to the strain velocity, a uniaxial stress strain relation of the form

$$\sigma = E[\epsilon + a_1 \dot{\epsilon}] \quad (3.15)$$

may be adopted where E is Young's modulus and a_1 is a damping coefficient. Then the Euler-Bernoulli hypothesis that plane section remain plane leads to the relation

$$M(x, t) = EI(x)[v''(x, t) + a_1 \dot{v}''(x, t)] \quad (3.16)$$

Thus for the formulations of the partial equations of motion for beam model including internal friction types of damping represented by Eq.3.15 and Eq.3.16 can be derived in the following section.

Here, the determination for the value of stiffness proportionality factor a_1 results from the concept of Rayleigh damping model, which is usually adopted for the estimation of system damping. This expression for global damping matrix is a linear combination of the global mass and global stiffness matrices as shown in Eq.3.17.

$$C = a_0 M + a_1 K \quad (3.17)$$

The equation is intrinsically orthogonal with the eigenvectors of the system and thus the relation of modal damping ratio ζ at frequency ω for Eq.3.18 is given. With two given values of modal damping ratio ζ_n at two specified frequencies ω_n , the damping coefficients a_1 can be derived.

$$\zeta_n = \frac{1}{2} \left(\frac{a_0}{\omega_n} + a_1 \omega_n \right) \quad (3.18)$$

While after running several numerical model of the beam model in this research, the mass proportional damping matrix only takes little influence compared to the stiffness proportional damping matrix. Thus for simplicity, the stiffness proportional damping model is adopted. In the numerical beam model, the dominating vibration frequency remains unknown and changes a lot under different situation. The stiffness proportional Rayleigh damping model here may leads to very large value of damping input, which influence the validity of data acquired. For the purpose of qualitatively analysing the problem, an estimation value of coefficient a_1 used here is given as 0.02 through engineering experience[12].

3

External force on the model

The pipeline on the seabed is mainly environmentally loaded by surrounding water and seabed soil. The vertical direction force is out of consideration here. Only lateral direction force resulting from pipe-soil interaction and pipe-fluid interaction is concerned here.

The surrounding sea water in the seabed is considered as still for the seabed pipeline analysis model. The sea water will definitely exerting the static fluid force and dynamic fluid force on the pipeline during vibration. The static fluid force results in a combination of the submerged weight of the pipeline, external and internal pressure, buoyancy force for the pipeline, which only contributing to in-plane condition of the pipeline and thus will not be thoroughly explained here. The fluid will exerting dynamic fluid force in a combination form of drag force, inertia force and Froude-Krilov force due to the lateral motions of the pipeline. In this research, the expression is depicted using the Morison's equation

$$F = \underbrace{\rho V \dot{u}}_a + \underbrace{\rho C_a V (\dot{u} - \dot{v})}_b + \underbrace{\frac{1}{2} \rho C_d A (u - v) |u - v|}_c \quad (3.19)$$

where the total force comprises three parts:

- a : Froude-Krylov force,
- b : Hydrodynamic mass force
- c : Drag force

and note that the added mass coefficient C_a is related to the inertia coefficient C_m as $C_m = 1 + C_a$. Here u means the instantaneous flow velocity of the surrounding fluid and v is the oscillating velocity of the pipeline itself. Since the surrounding water is considered as still in lateral direction for this model, thus the Morison's equation used in the model can be simplified as

$$F = -\rho C_a V \dot{v} - \frac{1}{2} \rho C_d A v |v| \quad (3.20)$$

The pipe-soil interaction force during the pipeline vibration is explained here. The soil resistance force is always having an opposite direction to the motion direction of the pipeline, or in other word, the soil resistance force is always hindering the motion of pipeline through energy dissipation. A simplified

soil resistance model yet with acceptable accuracy on the soil properties must be reasonably chosen, which is of vital importance to the characteristic lateral vibration of pipeline.

The soil resistance force also contains three parts with reference to the directions of motion for pipeline, namely the axial resistance, vertical resistance and lateral resistance. The vertical direction force is considered as constant after the initial penetration of the pipeline into seabed. The axial resistance is beyond the scope of this essay and is thus neglected. For the soil resistance in lateral direction, a Coulomb friction 'bilinear' model is adopted in this research as shown in Fig.2.4.

In this pipe-soil interaction model, the seabed friction has a maximum value μV , where μ is the friction coefficients related to soil types and V is the seabed contact reaction force in the normal direction to the seabed plane. The resistance force direction is always opposite to the motion of pipeline. In the actual case, every nodes of the beam model for the pipeline will experience specific motion history, the motion of which is intrinsically a cyclic motion. For a 1 DOF system with sinusoidal displacement example, this relation between the soil resistance force and displacement history can be illustrated as Fig.3.4.

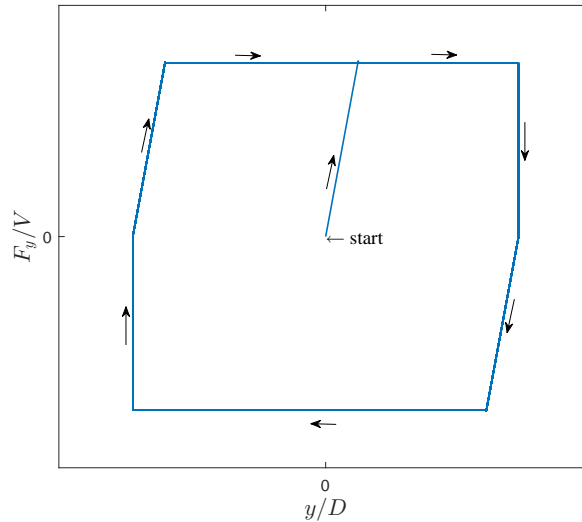


Figure 3.4: Illustration for typical force-displacement lateral friction response

In this friction model, the transition from a friction force of 0 to $+\mu V$ happens in a linear variation over the deflection range of $y_{breakout}$. Here $y_{breakout}$ is given by $y_{breakout} = \mu V / k_s A'$. Where A' is the contact area and k_s is the shear stiffness for soil based on the specified soil shear strength properties. According to the rule of thumb, shear stiffness is assumed as equalling to the $20/D'$ times the undrained shear strength of soil at a penetration depth of $0.5D'$, where D' is the contact diameter of the penetrating object as shown in Fig.3.5. Thus the shear stiffness is given by $k_s = (20/D')[s_{u0} + s_{ug}(D'/2)]$. Higher values of shear stiffness lead to the linear increasing part occurs over a shorter distance, and vice versa.

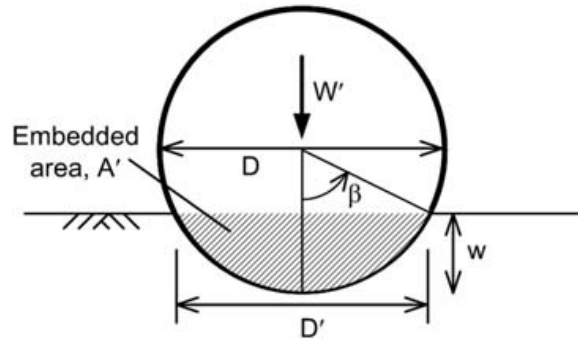
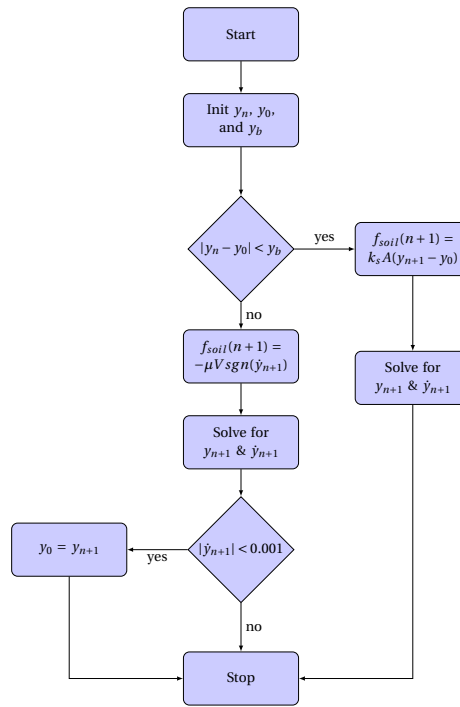


Figure 3.5: Illustration for penetration of pipeline

During the actual vibration of pipeline, the motion will definitely not be like a regular harmonic motion. Thus the soil resistance model illustrated in Fig.3.4 is an ideal situation and need improvement in reality. With all the necessary conditions given in this section, the equations of motion for the beam model can be set up in the following section and the equations will be solved in time domain through Newmark- β method below. For each segment of the pipeline represented by node when using finite difference method, the time domain solution for the vibration can be acquired in time domain. At each time step for the solution, soil resistance force in the equation of motion for the beam model will certainly change according to its own displacement history and motion status. A flow chart for the judgement of pipeline is illustrated here as Fig.3.6. An important assumption here is that the pipeline segment is considered as static when the velocity of which is smaller than (0.001m/s).

As illustrated in Fig.3.6, the flow chart is depicting the numerical calculation steps for the soil resistance force during the pipeline vibration process in one time step. The pipeline segments may vibrate irregularly due to the complex environment loading in practice. The soil resistance model in Fig.3.4 is actually resulting in a stick-slip phenomenon in the beam model. In the stick stage, namely the displacement is within the range of defined $y_{breakout}$, the soil resistance force is linearly increasing. While in the slip stage, the soil resistance is a constant value. The initial lateral displacement y_0 is given as a reference. When the pipeline begin to vibrate, the motion is calculated by time step. For the time step $n + 1$, standards are established for the judgements of whether the pipeline segments is in the stick or slip stage. Different stage results in different soil resistance force calculation. As shown in Fig.3.6, if the absolute difference value between lateral displacement in time step n and the initial reference value y_0 is smaller than the value of $y_{breakout}$, then the pipeline segment is in the stick stage, and is in the slip stage on the contrary. While in the slip stage, the reference value for pipeline segments should be reassigned if the velocity of which is smaller than a defined value, namely 0.001m/s. The reassigned value is the displacement of current position for the pipeline segment.

Figure 3.6: Soil resistance calculation for time step $n+1$ **Boundary conditions**

The beam model in this part is proposed mainly focusing on pipeline vibration under the influence of pipe-soil interaction. This pipeline model can be seen as a beam model with infinite length on one end and connects to the suspended part on the other end.

Pipeline system comprising suspended pipeline part and on-bottom pipeline part are splitted at the touch down point, making the characteristic of each part clearer. Further research will be investigated into for the influence that whether the vortex-induced vibration of suspended pipeline part will effect the seabed part pipeline largely through the connecting point (touch down point). The displacement is continuous in the touch down point connecting these two pipeline parts. Thus for the beam model at the touch down point, an external displacement is given to model the influence of suspended pipeline. The displacement is postulated as a harmonic one δ for simplicity and following parameter study.

The boundary conditions at the touch down point are given by:

$$y(L, t) = \delta \quad (3.21a)$$

$$y'(L_b, t) = 0 \quad (3.21b)$$

The vibration energy for seabed pipeline has the only input transmitted from the vortex induced vibration

Pipeline Properties				
E	D_o	t	ρ_{pipe}	φ
Young's modulus	Outer diameter	Wall thickness	Pipeline density	Laying angle
2.07·10 ¹¹ N/m ²	273 mm	20.6 mm	7850 kg/m ³	80 deg
Soil Properties				
ρ_{clay}	S_{u0}	S_{ug}	S_t	μ
Clay density	Shear strength	Shear gradient	Soil sensitivity	Friction coeff.
1500 kg/m ³	2600 Pa	1250 Pa/m	1	0.2
Water Properties				
ρ_{sea}	d	C_a	C_d	
Water density	Water depth	Added mass	Drag coefficient	
1025 kg/m ³	910 m	1.0	1.25	

Table 3.1: Model properties for seabed model

of suspended pipeline. Meanwhile, seabed pipeline undergoes damping effects like soil resistance, fluid damping effects together with material damping as stated before. Thus after a sufficient finite length, input energy from suspended pipeline will be exhausted out. The soil resistance force is rather a highly non-linear force and is highly dependent on the actual motion status of the pipeline itself. It is very hard to linearise the soil force and derive an analytical solution for an acceptable length of the beam model. Thus after several numerical results examined, an acceptable pipeline length L_b can be settled.

For this boundary transformed from an infinite length boundary end, it is rather clear that this end can be seen as a fixed end. Thus the boundary conditions at this end can be concluded as:

$$y(0, t) = 0 \quad (3.22a)$$

$$y'(0, t) = 0 \quad (3.22b)$$

With the necessary information stated above, the equations of motion for the beam model can be derived in the following section. The specific data used in this model is concluded as Tab.3.1.

3.2. MODEL DESCRIPTION

After the solid theoretical background is laid in Sec.3.1, the illustration in Fig.3.7 and equation of motions for this beam model will be elaborated in this part. Notice that the beam model is for the seabed pipeline part only. δ means the harmonic displacement given at this boundary end.

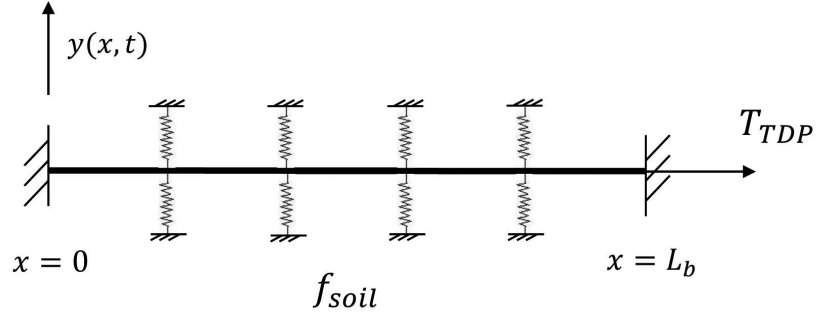


Figure 3.7: Seabed beam model illustration

In order to analyse the dynamic response for the beam model, the governing Equation of motion (EOM) for which is concluded as Eq.3.23.

$$\frac{\partial^2}{\partial x^2} \left[EI(x) \left(\frac{\partial^2 y(x, t)}{\partial x^2} + a_1 \frac{\partial^3 y(x, t)}{\partial x^2 \partial t} \right) \right] - \frac{\partial}{\partial x} \left[T_b(x) \frac{\partial y(x, t)}{\partial x} \right] + \rho A \frac{\partial^2 y(x, t)}{\partial t^2} = f_{ext} \quad (3.23)$$

Where y is the lateral displacement for the beam model, $T_b(x)$ is the tension along on-bottom pipeline length, ρA is the mass of the pipeline in unit length. At the left side of Eq.3.23, $f_{ext} = f_{water} + f_{soil}$, where f_{water} comprises the drag and lift force shown in Eq.3.24, and f_{soil} consists of soil resistance in two stages as stated in the soil resistance part shown as Eq.3.25. The boundary conditions is already stated in Eq.3.21 and Eq.3.22.

$$f_{water} = f_{inertia} + f_{drag} = -\rho C_a \frac{\pi}{4} D_0^2 \ddot{y}(x, t) - \frac{1}{2} \rho C_d D_0 \dot{y}(x, t) |\dot{y}(x, t)| \quad (3.24)$$

$$f_{soil} = \begin{cases} k_s A' y(x, t) & \text{Stick stage} \\ \mu V & \text{Slip stage} \end{cases} \quad (3.25)$$

After the equations of motions for the beam model is settled, the next step is to correctly solve the partial differential equations with given initial status of the beam. The lateral displacement $y(x, t)$ contains both information of time and space. Since the Partial Differential Equations (PDE) contains two variables and is highly nonlinear in this case including soil force and fluid force. The analytical solution for it will

become a nearly impossible task to accomplish, which is not included in this research. Thus for the numerical solution, this beam model is divided into N_b elements, which has a length of $h = L_b/N_b$ and are represented by node. The magnitude of h will influence the accuracy of numerical solution for discrete nodes on the beam model. The element division is shown as Fig.3.8.

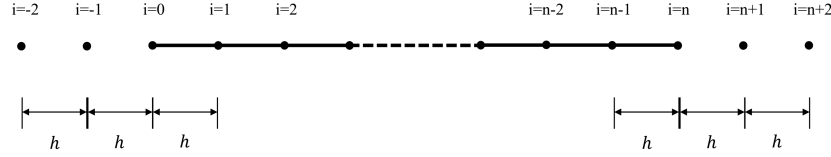


Figure 3.8: Finite difference element

The PDE will be simplified using PDE in space. The higher order terms of the partial differential equation in space will be reduced, making the PDE turn into an Ordinary Differential Equations (ODE). Central finite difference method is used here as shown in Eq.3.26.

$$y'_i \approx \frac{y_{i+1} - y_{i-1}}{2h} \quad (3.26a)$$

$$y''_i \approx \frac{y_{i+1} - 2y_i + y_{i-1}}{h^2} \quad (3.26b)$$

$$y'''_i \approx \frac{y_{i+2} - 2y_{i+1} + 2y_{i-1} - y_{i-2}}{2h^3} \quad (3.26c)$$

$$y''''_i \approx \frac{y_{i+2} - 4y_{i+1} + 6y_i - 4y_{i-1} + y_{i-2}}{h^4} \quad (3.26d)$$

As stated in Sec.3.1, the tension in beam model is varying along the seabed pipeline and the properties of the beam model remains the same throughout the entire pipeline length. Namely the variables EI are constant values, while T is not. After substituting the approximation for derivatives of space into the governing differential equations and the boundary conditions, the following simplified equations can be written finally. The deduction process of which is well explained here.

$$\begin{aligned} & \rho A \ddot{y}_i + EI \left(\frac{y_{i+2} - 4y_{i+1} + 6y_i - 4y_{i-1} + y_{i-2}}{h^4} \right) - T_b(i) \left(\frac{y_{i+1} - 2y_i + y_{i-1}}{h^2} \right) \\ & + a_1 EI \left(\frac{\dot{y}_{i+2} - 4\dot{y}_{i+1} + 6\dot{y}_i - 4\dot{y}_{i-1} + \dot{y}_{i-2}}{h^4} \right) - T'_b(i) \frac{y_{i+1} - y_{i-1}}{2h} = f_{water_i} + f_{soil_i} \end{aligned} \quad (3.27)$$

The equation can be further simplified as Eq.3.28 after sorting out the terms in Eq.3.27.

$$\begin{aligned} & \rho A \ddot{y}_i + (A_k y_{i+2} - B_k y_{i+1} + C_k y_i - B_k y_{i-1} + A_k y_{i-2}) \\ & + (A_c \dot{y}_{i+2} - B_c \dot{y}_{i+1} + C_c \dot{y}_i - B_c \dot{y}_{i-1} + A_c \dot{y}_{i-2}) = f_{water_i} + f_{soil_i} \end{aligned} \quad (3.28)$$

Where the coefficients in Eq.3.28 is expanded here.

$$\begin{aligned} A_k &= \frac{EI}{h^4} & B_{k_i} &= \frac{4EI}{h^4} + \frac{T_i}{h^2} + \frac{T'_i}{2h} & C_{k_i} &= \frac{6EI}{h^4} + \frac{2T_i}{h^2} & D_{k_i} &= \frac{4EI}{h^4} + \frac{T_i}{h^2} - \frac{T'_i}{2h} \\ A_c &= \frac{a_1 EI}{h^4} & B_c &= \frac{4a_1 EI}{h^4} & C_c &= \frac{6a_1 EI}{h^4} \end{aligned} \quad (3.29)$$

Notice that in Eq.3.28, the displacements for y_{-2} and y_{-1} do not exist when it comes to node $i = 0$. The same situation happens for nodes y_{n+1} and y_{n+2} when it comes to node $i = n$ as shown in Fig.3.8. In order to solve this problem, boundary conditions for this beam model must be introduced here.

Thus for boundary end in Eq.3.22, the following equation is derived:

$$y_0 = 0 \quad (3.30a)$$

$$y'_0 = \frac{y_1 - y_{-1}}{2h} = 0 \quad (3.30b)$$

For the boundary end in Eq.3.21, the following equation is derived:

$$y_n = \delta \quad (3.31a)$$

$$y'_n = \frac{y_{n+1} - y_{n-1}}{2h} = 0 \quad (3.31b)$$

From the boundary conditions given, it is clear that node $i = 0$ and node $i = n$ is already known. Then the focus is on node $i = 1$ and $i = n - 1$, the governing differential equations for these two nodes are written separately.

For node $i = 1$, the governing differential equations is written as

$$\begin{aligned} \rho A \ddot{y}_1 + (A_k y_3 - B_{k1} y_2 + C_{k1} y_1 - D_{k1} k y_0 + A_k y_{-1}) \\ + (A_c \dot{y}_3 - B_c \dot{y}_2 + C_c \dot{y}_1 - B_c \dot{y}_0 + A_c \dot{y}_{-1}) = f_{water1} + f_{soil1} \end{aligned} \quad (3.32)$$

Eq.3.32 can be further simplified as Eq.3.33 using the boundary condition in Eq.3.30.

$$\rho A \ddot{y}_1 + ((A_k + C_{k1}) y_1 - B_{k1} y_2 + A_k y_3) + ((A_c + C_c) \dot{y}_1 - B_c \dot{y}_2 + A_c \dot{y}_3) = f_{water1} + f_{soil1} \quad (3.33)$$

For node $i = n - 1$, the governing differential equations is written as

$$\begin{aligned} \rho A \ddot{y}_{n-1} + (A_k y_{n+1} - B_{k_{n-1}} y_n + C_{k_{n-1}} y_{n-1} - D_{k_{n-1}} k y_{n-2} + A_k y_{n-3}) \\ + (A_c \dot{y}_{n+1} - B_c \dot{y}_n + C_c \dot{y}_{n-1} - B_c \dot{y}_{n-2} + A_c \dot{y}_{n-3}) = f_{water_{n-1}} + f_{soil_{n-1}} \end{aligned} \quad (3.34)$$

Eq.3.32 can be further simplified as Eq.3.35 using the boundary condition in Eq.3.31.

$$\begin{aligned} \rho A \ddot{y}_1 + ((A_k + C_{k_{n-1}}) y_{n-1} - D_{k_{n-1}} y_{n-2} + A_k y_{n-3}) + ((A_c + C_c) \dot{y}_{n-1} - B_c \dot{y}_{n-2} + A_c \dot{y}_{n-3}) \\ - (B_{k_{n-1}}) \delta - B_c \dot{\delta} = f_{water_{n-1}} + f_{soil_{n-1}} \end{aligned} \quad (3.35)$$

Besides the nodes at the boundary end, for ordinary nodes $i = 2, 3, \dots, n-2$, inside the beam model, the governing differential equations are written as Eq.3.28.

Since all the PDE are written out, the matrix form for these equations can thus be concluded for the sake of simplicity.

$$M \cdot \ddot{Y} + C \cdot \dot{Y} + K \cdot Y = F \quad (3.36)$$

Where terms Y , \dot{Y} and \ddot{Y} are the displacement, velocity and the acceleration for the nodes on beam model respectively. Detailed composition is shown as Eq.3.37.

$$Y = \begin{bmatrix} y_1 \\ y_2 \\ \vdots \\ y_{n-2} \\ y_{n-1} \end{bmatrix} \quad \dot{Y} = \begin{bmatrix} \dot{y}_1 \\ \dot{y}_2 \\ \vdots \\ \dot{y}_{n-2} \\ \dot{y}_{n-1} \end{bmatrix} \quad \ddot{Y} = \begin{bmatrix} \ddot{y}_1 \\ \ddot{y}_2 \\ \vdots \\ \ddot{y}_{n-2} \\ \ddot{y}_{n-1} \end{bmatrix} \quad (3.37)$$

Where term F represents a summation of all kinds of equivalent force stated above. In this beam model, the F includes the assembly force matrix resulting from water, soil and the external displacement δ in node n as shown in Eq.3.35. It should be pointed out that the water inducing force consists of two parts, drag and inertia force in this example stated in Eq.3.24. The inertia force is always considered as hydrodynamic mass force and is only related to the acceleration of beam elements itself. Thus the inertia force is often written into the mass matrix as the added mass. Thus for simplicity, the water force here is only the drag force only.

$$\begin{aligned} F &= F_{drag} + F_{soil} + F_{node_n} \\ &= \begin{bmatrix} -\frac{1}{2}\rho C_d D_0 \dot{y}_1 |\dot{y}_1| \\ -\frac{1}{2}\rho C_d D_0 \dot{y}_2 |\dot{y}_2| \\ \vdots \\ -\frac{1}{2}\rho C_d D_0 \dot{y}_{n-2} |\dot{y}_{n-2}| \\ -\frac{1}{2}\rho C_d D_0 \dot{y}_{n-1} |\dot{y}_{n-1}| \end{bmatrix} + \begin{bmatrix} -f_{soil_1} \\ -f_{soil_2} \\ \vdots \\ -f_{soil_{n-2}} \\ -f_{soil_{n-1}} \end{bmatrix} + \begin{bmatrix} 0 \\ 0 \\ \vdots \\ -A_k \\ B_{k_{n-1}} \end{bmatrix} \cdot \delta + \begin{bmatrix} 0 \\ 0 \\ \vdots \\ -A_c \\ B_c \end{bmatrix} \cdot \dot{\delta} \end{aligned} \quad (3.38)$$

As stated above, the added mass is always included in the mass matrix. Here, symbol m_a is used to represent the added mass, which equals to $\rho C_a \frac{\pi}{4} D_0^2$. The mass matrix here is a $(n-1) \times (n-1)$ diagonal matrix as shown in Eq.3.39.

$$M = (\rho A + m_a) \begin{bmatrix} 1 & & & & \\ & 1 & & & \\ & & \ddots & & \\ & & & 1 & \\ & & & & 1 \end{bmatrix} \quad (3.39)$$

The analytical solution used in this research for natural frequency of beams under tensile axial loads is referred to A.Bokaian 1990[13]. In his research, analytical solutions for the natural frequencies and mode shapes are concluded, which are for uniform beam models with various boundary conditions and is loaded by constant tension along the beam. Thus a quick yet simple estimation can be examined. The beam model modelling the on-bottom pipeline proposed in this chapter is intrinsically a clamped-pinned beam model as that in the thesis of A.Bokaian. Thus with given parameters for the beam model here, a quick estimation can be exerted following the solution procedures given in the essay.

The equivalent stiffness matrix and mass matrix for the numerical calculation of the beam model is given in Eq.3.39 and Eq.3.40. Then the numerical solution for the natural frequencies of the beam model can be calculated here, which is under the assumption of an undamped free vibration beam. The characteristic equation is in the form of Eq.3.42.

$$|[K] - \omega^2 [M]| = 0 \quad (3.42)$$

The result for the comparison of these two methods is illustrated in Fig.3.9. In this verification example, the beam model has a length of 100 m and the other properties are the same as defined before. The first to the twentieth natural frequency of the beam model are given in the figure. The results calculated from both analytical and numerical method have little difference, which is within negligible error range. Thus the numerical beam model here can be seen as trustworthy and acceptable in the following parts.

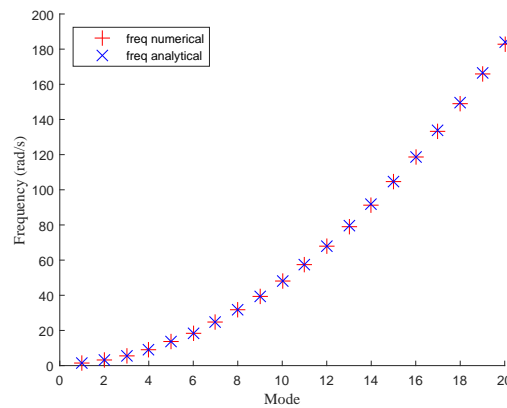


Figure 3.9: Comparison between numerical and analytical results

3.4. NUMERICAL RESULTS

After the solid groundwork has been laid in previous sections, numerical results for the vibration of beam model will be presented in this section with reasonable inputs. The main aim of this section is to investigate into the validity of the beam model, and to find out whether the pipe soil interaction model can

perform well or not in the simulation.

Thus, here a beam model of length 100 m, with the given external displacement on the right boundary δ . The input of δ is initially a harmonic function and the amplitude of which decays gradually to zero. This setting mechanism is specifically designed to check i) how the beam model reacts to the given external displacement ii) if the soil resistance can keep the bending shape of beam model supposing the input energy is dissipate out eventually.

For the external given displacement δ , the amplitude is set as $\zeta_\delta = 0.25\text{m}$ and the frequency is given as $\omega_\delta = \pi\text{rad/s}$. Thus the period $T_\delta = 2\pi/\omega_\delta$ can be acquired. There are in total 16 oscillations of δ for this simulation. From time t_{start} , δ begins to decay exponentially, which approaching 0.1% of initial amplitude in time of t_{decay} . This setting is shown as:

$$\delta = \begin{cases} \zeta \cdot (\cos(\omega t) - 1) & \text{if } 0 \leq t \leq 0.5T_\delta; \\ 2\zeta \cdot \cos(\omega t) & \text{if } 0.5T_\delta < t \leq t_{start}; \\ 2 \cdot e^{\alpha_\delta(t-t_{start})} \cos(\omega t) & \text{if } t_{start} < t \leq 16T. \end{cases} \quad (3.43)$$

Where $\alpha_\delta = -\ln(0.001)/t_{decay}$, this setting is to guarantee the amplitude of external displacement will becomes the ratio 0.001 of the initial amplitude in time period of t_{decay} . The first two equation is to make sure the external displacement is applied to the beam smoothly without impact, namely a sudden increase of velocity into the beam end. To be more clear, the setting of δ is shown as Fig.3.10.

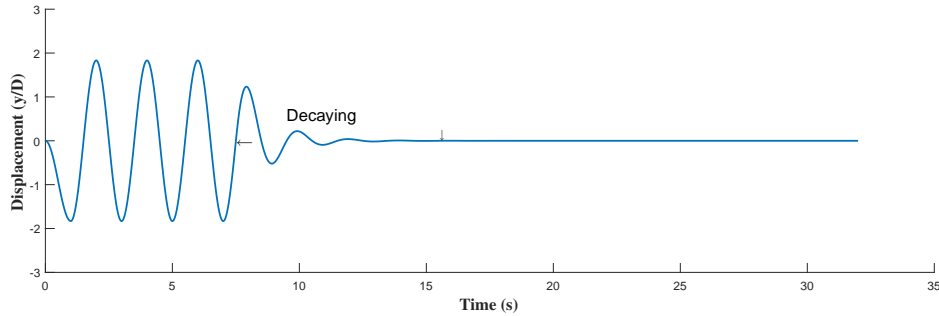


Figure 3.10: Illustration for applied external displacement

After applying the specified external displacement δ to the right fixed boundary of the beam model as shown in Fig.3.7, the whole vibration process can be solved step by step given the initial conditions of the beam model as already elaborated in previous sections. The results are recorded as well. Thus after the simulation ends, the results of beam vibration can be analysed. The lateral displacement of the beam model can be shown in the figure of 3-D view as Fig.3.11.

In the dimension includes pipeline length, simulation time from zero moment to end and the lateral displacement of the beam model. When the boundary end is applied with external displacement at the pipeline length of 100 m, the beam model begin to vibrate, causing the whole beam model to vibrate.

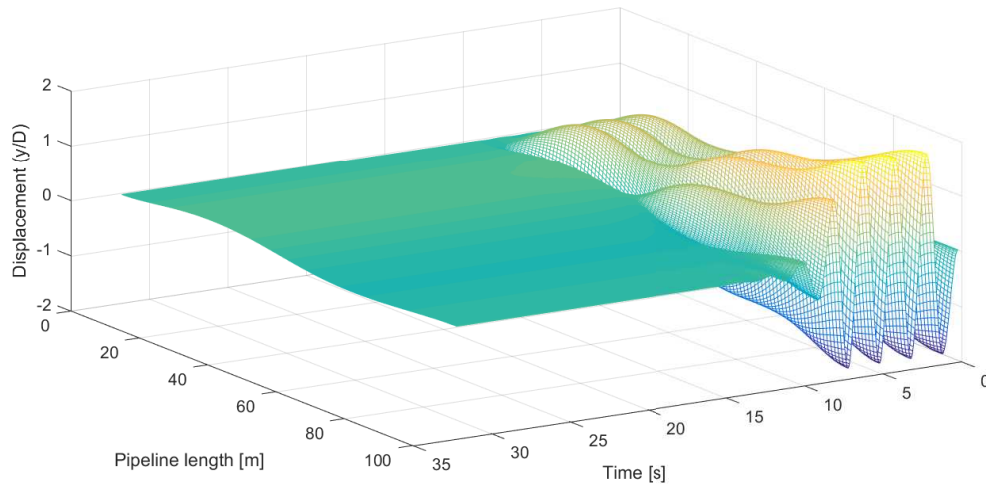


Figure 3.11: Illustration for external displacement

As can be seen that, the transmitted wave from the pipeline length at 100 m to the 0 m, has aroused the vibration of the entire beam. After the amplitude of the external displacement starts to decay and becomes zero, under the interaction of pipe and soil, further movements of the beam is resisted and can be finally kept in a bending shape at the time end.

To be more specific, three nodes locate at the $L = 25$ m, $L = 50$ m and $L = 75$ m separately are selected for their motions during the simulation. The displacement and velocity information for these nodes throughout the simulation are plotted in Fig.3.12 and Fig.3.13 accordingly.

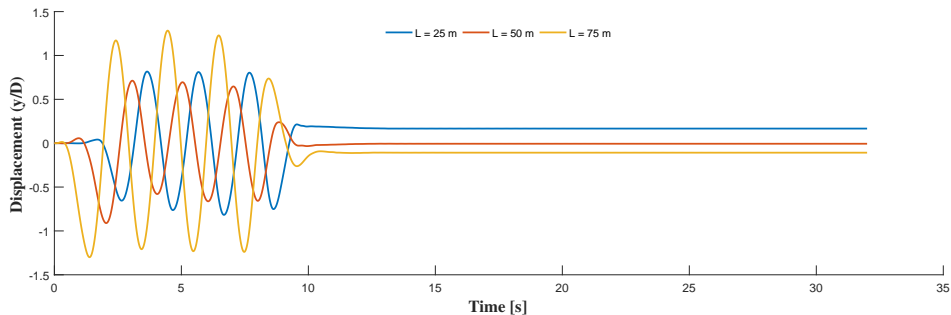


Figure 3.12: Lateral vibration displacement for chosen nodes

Fig.3.12 represents lateral displacement of these three nodes related to the simulation time. Initially, these three nodes all vibrate regularly at different amplitudes. Along with the decaying process of δ , the

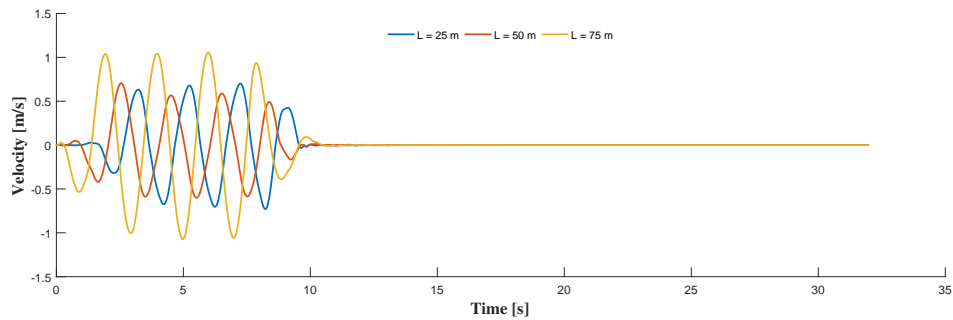


Figure 3.13: Lateral vibration velocity for chosen nodes

amplitudes for these three nodes are decreasing as well until they are kept at a constant displacement from initially balance place under the influence of soil resistance. While Fig.3.13 is the velocity information of these nodes, notice that, the velocity becomes zero at last due to the energy dissipation of both soil resistance and hydrodynamic resistance. The combination of these two figures has shown that at last the beam model becomes static yet with a bending shape like 'snake' under the effects of soil.

To be more clear, the final shape at the end of this simulation is shown specifically as Fig.3.14.

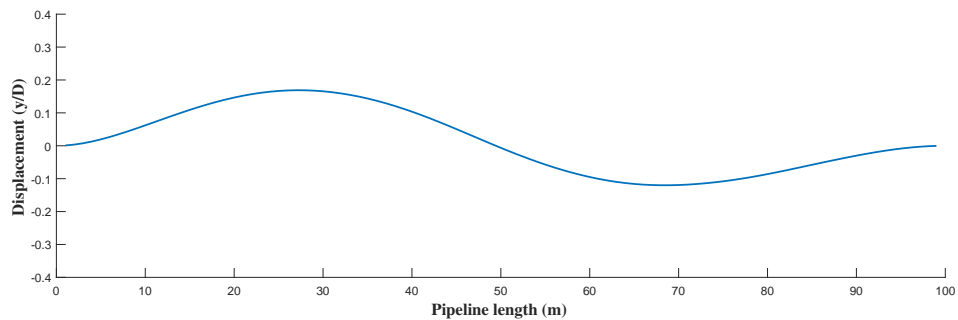


Figure 3.14: Final shape

From these results acquired, conclusion can be drawn that this separate simulation model for seabed pipelines is effective to correctly modelling the pipe soil interaction. This model will be added to the coupled pipeline system later.

4

SUSPENDED PIPELINE MODEL

This chapter presents a simplified model for simulating the lateral vibration of suspended pipeline, which connecting the laying vessel and seabed pipelines. Under the influence of currents, the suspended pipeline may experience Vortex Induced Vibration (VIV). Larger amplitude of cross-flow vibration occurs compared to that of in-line vibration. The vibration in suspended part is transmitted to the seabed pipeline in the form of wave, and arouse its vibration as well. The assumptions for this model is described previously in section 1.2.3. The main focus of this chapter is correctly building up a descriptive model for the VIV of suspended pipeline. Some simulations will also be exerted with different key parameters. In Sec.4.1, some basic theoretical support for this model has been explained. The elaboration steps for the numerical model have been built up in Sec.4.2. At last, some verification and results have been recorded in the Sec.4.4.

4.1. MODEL INFORMATION

Sea state is really complicated during laying process, thus the suspended pipeline may undergo various sources of external environmental loading coupling with the vessel motions and seabed pipeline resistance. Vessel motions will not be considered here in research work. This model is focusing on the lateral vibration of suspended pipeline under the effects of VIV due to uniform flow. While only taking the suspended pipeline into consideration, the pipeline can be seen as a tensioned straight Euler-Bernoulli beam with suitable boundary condition on both ends. Detailed model information will be elaborated as following.

Environmental loading on the model

As already stated in Sec.1.2.1, the in-plane horizontal steady current is assumed as the only environmental loading for the suspended part. The illustration is shown in Fig.1.3.

Experiments for VIV have shown the phenomena that the cross-flow vibration of the cylinder is much larger than the in-line vibration. The in-line vibration is the main cause for the fatigue problem of the suspended pipelines, such as risers. This problem is beyond the scope for this research work. Another reason is that current is the main exciting source for the VIV of the pipeline. For deep sea laying process, the effects of waves will not be taken into consideration here. Thus for the research interests of lateral vibration for the suspended pipeline, a uniform in-plane currents plays the only role of the environmental loading.

This uniform current will results in two kinds of forces. The first kind is the lift force which is the reason for cross-flow vibration of the pipeline. The force will be simulated using a coupling equation of wake oscillator model, that will be explained with detail later. The other kind of forces is the in-line hydrodynamic force expressed approximately by the Morison equation as Eq.3.19. Since the current is uniform here and the in-plane motion is not considered here, the Morison equation is simplified as Eq.4.1.

$$F = \frac{1}{2} \rho C_d A u |u| \quad (4.1)$$

Where u means the uniform current speed. From the equation, there is only drag force due to the current left. The in-plane drag force here will contribute to the static in-plane configuration.

It must be clarified in this section that the initial configuration for suspended pipeline is in a bending shape, as can be shown in Fig.1.3, which is also known as a stiffened catenary explained in the next section. This means that a certain length of suspended pipeline will be placed at an attack angle of the incident flow although with the assumption of uniform in-plane current, as shown in Fig.4.1. The resulting fluid force, including the following VIV lift force and drag force, may change related to the inclination angle of the pipeline segment.

Many results from various researches on VIV of a flexibly mounted rigid cylinder are usually for the cases when the incident flow direction is normal to the axial axis of the cylinder. Thus some adjustments should be made here. One hypothesis is made here that the VIV in inclined cylinders are alike with the perpendicularly incident case, as long as the normal components of the incident flow is considered. This is called the Independence Principle (IP). The so-called independence principle shown in experiments is usually used and described by Eq.4.2.

$$U_n = U \cdot \sin(\theta) \quad (4.2)$$

Where θ is the attack angle of the incident flow with the suspended pipeline segment, U is the incident current speed, and U_n is the current velocity component normal to the pipeline segment. The lift force calculation for VIV model can be based on the new current speed for each segment with different inclination angle. In this case, some literature also reported that the vortex shedding frequency is close to the value which is calculated from the Strouhal equation in Eq.2.9. For the calculation of drag force here, C_D is kept as the same as that in the normal incident current case. In this essay, the inclination angle of pipeline segment results in the same value of attack angle for incident current flow.

Finally, it should also be taken care that the independence principle is only theoretically accepted in

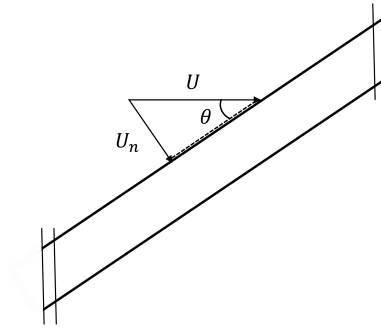


Figure 4.1: Attack angle of incident flow

the sub-critical range of Re as in Fig.2.7, which is suitable for the case in this research. While also in some cases, indicating that the independence principle may not be able to work well for large inclination angles. Results have shown that the influence of the axial component of incident flow can not be neglected for large inclination angles. Since there is no solid consensus toward this problem, the IP is assumed to be valid in this research for simplicity.

Static configuration

Before continue the analysis for out-of-plane motions for the suspended pipelines, one fundamental basis should be pointed out clearly that the in-plane configuration of this suspended part is the corner stone for following analysis. It should be elaborated first. In-plane static configuration is determined due to the coupling effects of submerged weight for the pipeline, strong drag force due to uniform currents [14], boundary layer phenomenon when approaching the seabed and the characteristics of pipeline properties. In the general assumption in Sec.1.2.3, the in-plane vibration will not be discussed here. Once the static configuration is solved, it will be assumed that the bending shape is constant during the out-of-plane vibration of suspended pipeline both in static and dynamic laying process.

For J-lay process in deep sea conditions, main part of the suspended pipelines are usually considered as catenary shaped. While only in the contacting zone with the seabed, the minor part of suspended pipelines is considered as beam due to the boundary layer phenomenon. The phenomenon shows that the boundary condition of the seabed end is crucial to the initial shape of suspended pipeline. It is also pivotal to the shear force and bending moment in the contact zone of suspended pipeline with the seabed.

The deduction steps for the configuration is well explained and analysed in Appendix.A. After the in-plane static configuration is settled, the suspended pipeline can be considered as vibrating around the static place in out-of-plane direction. This in-plane space information can be recorded for three-dimensional illustration of the beam. Moreover, the tension in the beam for simulating the suspended pipeline is also determined. In which, the tension is increasing from the seabed to the top end because

of the increasing submerged weight with growing pipeline length. The horizontal tension in the TDP for the seabed pipeline model can be determined from this model as well.

Moreover, the in-plane and out-of-plane vibrations for a plane curved beam are coupled for most cases. In this research, the Euler-Bernoulli beam is assumed to simulate the lateral vibration of the pipeline here. Thus the transverse shear deformation and the rotatory inertia are not taken into account in this model. What is more, the suspended pipeline has a uniform circular cross-section along the pipeline length from seabed end to vessel end. Also, the cross-section for suspended pipeline can also be seen as doubly symmetric, which means the shear centre and the centroid is at the same point. With these conditions, the out-of plane vibration for the pipeline can be seen as uncoupled with the in-plane vibration[4]. Furthermore as stated in 1.2.3, for deep water pipeline the radius of in-line curved pipeline becomes very large, the curved beam model has transformed into a straight one. This means the lateral vibration of suspended pipeline in this research can be seen as independent from the in-plane static configuration. The lateral vibration for pipeline beam model can be considered as a straight beam with equivalent length. The equations of motion for which are built up at Sec.4.2.

4

Boundary conditions

The suspended pipeline part connects seabed pipelines at the TDP and the laying vessel at the sea level. The boundary conditions for these two ends are elaborated in this section.

When the laying vessel is in operation, the configuration of suspended pipeline is considered as a constant shape as the initial configuration as stated above. With reference to practical J-lay process, the connection between suspended pipeline and the vessel is restricted in lateral relative displacement and slope angle, thus the boundary condition of which can be seen as clamped.

The local coordinates system is used here along the suspended pipeline length. The origin point is settled at the TDP at the seabed. The suspended pipeline length is assumed as L_s here. Thus the boundary conditions at the suspended pipeline end point at the vessel are concluded:

$$y(L_s, t) = 0 \quad (4.3a)$$

$$y'(L_s, t) = 0 \quad (4.3b)$$

The other boundary end of suspended pipeline is connected to the seabed pipeline at the TDP, thus some reference can be made here with Eq.3.21. Similarly, fixed boundary is adopted here. This is also for the simplicity of the verification of the VIV part only. Because in the overall pipeline system, the connection point in TDP of these two pipeline parts is continuous. Thus for the purpose of verifying the validation of the separate model, this boundary condition is acceptable. The boundary conditions here are given by:

$$y(0, t) = 0 \quad (4.4a)$$

$$y'(0, t) = 0 \quad (4.4b)$$

Based on the statement of boundary condition above, the equations of motion for the beam model can be derived in Sec.4.2.

Wake oscillator model

As stated in the literature review of Sec.2.2, the drag force and lift force for a stationary rigid cylinder can be expressed through the estimation for drag and lift coefficient. But when the experimental cylinders undergoing uniform incident flow are permitted to oscillate with the flow, where VIV may occur under certain circumstances, the lift and drag force are heavily influenced by the coupling of cylinder motion and the oscillating wake behind the cylinder. The cross-flow and in-line force may experience the magnification effects. Some empirical equations are concluded through experimental results. While for most cases, the wake oscillator model is used for simulating the coupling effects of cylinder vibration and wake of flow in time domain.

Plenty of wake oscillator models have been developed through years, these models are intrinsically phenomenological models for the purpose of simulating the VIV phenomena acquired in experiments.[15] When the experimental cylinder are not fixed, the flow pattern and the motion of cylinder will influence each other until the coupling mechanism reaches a steady state. VIV may occur when the shedding frequency of the flow approaches the natural frequency of the cylinder, under the condition of which lock-in or synchronization may occur. This will effectively increase the amplitude of the cylinder vibration since there is an energy transfer from the flow to cylinder. Focusing on the cross-flow direction, lift force will also grows effectively until the steady state has been arrived. In steady state, the energy input and dissipation have reached a balance. This is the self-excitation and self-limiting mechanism between wake oscillation and cylinder vibration.

In this essay, a Van der Pol type wake oscillator is used to modelling this phenomenon. The coupling of wake oscillation with the cylinder is through common terms in coupling equations for cylinder and for the wake as shown in Sec.4.2. The equation for Van der Pol type oscillator used in this research is expressed as:

$$\ddot{q} + \epsilon\omega_s(q^2 - 1)\dot{q} + \omega_s^2 q = f \quad (4.5)$$

Where q is the dimensionless wake variable associated with the expression for fluctuating lift force coefficient of the structure. ϵ is the tuning coefficient, ω_s is the shedding frequency for the flow with specific velocity, f is the forcing term coupling with the structure variable in the future, which models the effects of cylinder vibration on the wake patterns. Some basic idea about this Van der Pol type wake oscillator model is explained here. Eq.4.5 has provided a stable quasi-harmonic oscillation of finite amplitude $q_0 = 2$ at the frequency of ω_s [16]. The damping term $\epsilon\omega_s(q^2 - 1)\dot{q}$ in this expression plays the role of modelling the self-exciting and self-limiting mechanism of the VIV phenomenological model. In detail, the negative part give the increasing trend of q and the positive part limit its growth. For an explanation case, the forcing term is given as $f = A\cos(\omega_f t)$. Where A is the another tuning coefficient here and ω_f is the frequency for this harmonic force.

After several numerical models have been performed, some comments about this Van der Pol type wake oscillator model are concluded here due to observed results:

- With larger value for tuning coefficient ϵ , the wake variable arrives at its steady state faster and the nonlinear phenomenon becomes clearer.
- The magnitude of ϵ controls the damping magnitude, thus the value for wake variable may get smaller with larger value of ϵ in forced condition
- Parameter A in this expression is used to control the lock-in range for VIV phenomenological model. Larger A results in a wider synchronization range as shown in Fig.2.14, which means the lock-in between shedding frequency and vibration frequency becomes easier. Larger A also leads to a larger value of q in steady state.

The specific data used in this model is concluded as Tab.4.1.

Pipeline Properties				
E	D_o	t	ρ_{pipe}	L
Young's modulus	Outer diameter	Wall thickness	Pipeline density	Suspend Length
$2.07 \cdot 10^{11} \text{ N/m}^2$	273 mm	20.6 mm	7850 kg/m^3	1102 m
Water Properties				
U	C_a	C_{D0}	C_{L0}	St
Current speed	Added mass	Mean Drag coeff.	Mean Lift coeff.	Strouhal number
0.1952 m/s	1.0	1.1856	0.3842	0.1932
Tuning Coefficients				
A	ϵ	A	ϵ	θ
$\theta \leq 45^\circ$	$\theta \leq 45^\circ$	$\theta > 45^\circ$	$\theta > 45^\circ$	Inclination angle
4	0.05	1	0.1	-

Table 4.1: Model properties for suspended pipeline

4.2. MODEL DESCRIPTION

After the necessary information and some simplifications provided in Sec.4.1, the problem for lateral vibration of this suspended pipeline in J-lay process can be illustrated as Fig.4.2.

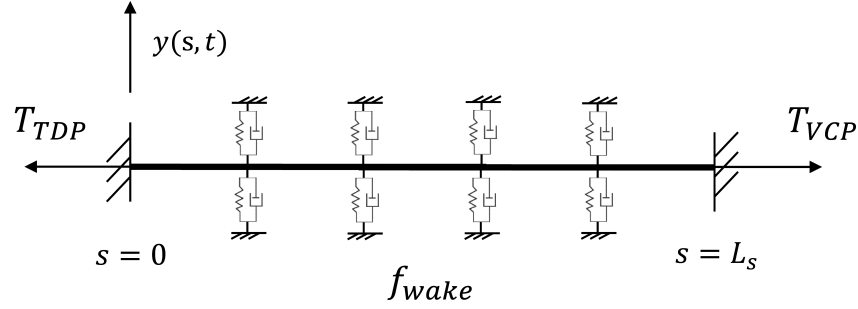


Figure 4.2: Suspended beam model illustration

Notice that the beam model is for the suspended pipeline part only and is assumed as a straight beam for lateral motions. The length of straight beam is equal to the length of suspended pipeline itself. The tension in this model is changing from the bottom to the upper end. The determination of tension force is determined from the initial configuration for J-lay suspended pipeline, as deduced in Appendix A.

As stated earlier, the research focuses on the lateral vibration of the pipeline model resulting from VIV. The governing differential equation for the suspended pipeline is concluded as Eq.4.6.

$$\frac{\partial^2}{\partial s^2} \left[EI(s) \left(\frac{\partial^2 y(s,t)}{\partial s^2} + a_1 \frac{\partial^3 y(s,t)}{\partial s^2 \partial t} \right) \right] - \frac{\partial}{\partial s} \left[T(s) \frac{\partial y(s,t)}{\partial s} \right] + (m + m_a) \frac{\partial^2 y(s,t)}{\partial t^2} = f_q \quad (4.6)$$

Where y is the lateral displacement for the beam model, $T(s)$ is the tension along the suspended pipeline length, m is the mass of the pipeline in unit length and m_a is the hydrodynamic added mass. At the left side of Eq.4.6, f_q means the coupling force from wake variable, and can be expressed as

$$f_q = \frac{1}{2} \rho DV(s)^2 C_{VY}(s)$$

Where C_{VY} is the cross-flow force coefficient and is written as:

$$\begin{aligned} C_{VY} &= (C_{VD} \sin \beta + C_{VL} \cos \beta) \frac{U^2}{V(s)^2} \\ &= \left(C_{D0} \sin \beta + \frac{C_{L0} q}{2} \cos \beta \right) \frac{U^2}{V(s)^2} \end{aligned}$$

The definition of C_{VL} is referred to the essay of Faccinetti 2004 [16] and is proportional to the wake variable q as

$$C_{VL} = \frac{C_{L0}q}{2}$$

Here C_{L0} is a lift force coefficient supposing the beam model is stationary. C_{VD} is assumed as equalling to the mean drag coefficient C_{D0} as that for a stationary cylinder as a function of Reynolds number. The detailed deduce for coupling process of wake and the beam model can be referred in Appendix B. In which, expressions of $\sin \beta$, $\cos \beta$ and U are also defined and explained.

The cross-flow lift force is modelled using a Van der Pol type wake oscillator.

$$\frac{\partial^2 q(s, t)}{\partial t^2} + \epsilon \omega_s(s) (q^2(s, t) - 1) \frac{\partial q(s, t)}{\partial t} + \omega_s^2(s) q(s, t) = \frac{A}{D} \left(\frac{\partial^2 y(s, t)}{\partial t^2} \right) \quad (4.7)$$

Where q is the wake variable, ϵ and A in Eq.4.7 are the tuning coefficients. Above all, Eq.4.6 and Eq.4.7 include two variable, namely the beam model displacement and the wake variable, the coupling equations are used to model the interaction between the beam model motions and the cross-flow lift force of coupling system. Since the coupling equations of motion for the beam model of suspended pipeline are settled, the next step should be seeking solutions for such descriptive equations in time domain. Numerical solutions would be the only approach for these coupling equations due to strong nonlinearity.

The displacement variable $y(s, t)$ is the partial derivative of both space and time while the wake variable q only contains derivative of time. Before seeking numerical solutions for the equations, some simplifications on the variable should be prepared. Thus the beam model is previously divided into N_s elements which contains $N_s + 1$ nodes. Note that the bending beam here is considered as a straight beam and the local coordinates in the beam model is along the suspended pipeline. Hence, the length model of the beam model is equivalent to that of the suspended pipeline length. The approach for element division is the same as that in Chapter. 3. The element division can be shown in Fig.4.3, and each element has a length of $h = L_s / N_s$

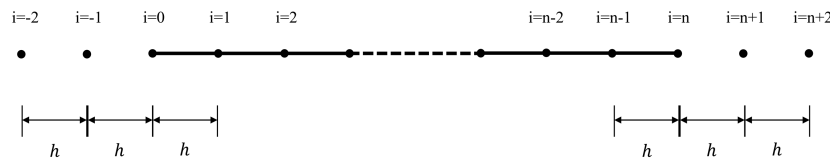


Figure 4.3: Finite difference element

The partial derivative of $y(s, t)$ in space is simplified using the central difference method as already defined in Eq.3.26. These simplification equations are an estimation for the derivative with truncation error of order h^2 , which is acceptable in this calculation with enough precision. After the simplification,

the partial derivative of displacement is reduced from fourth order to zeroth order, namely the displacement itself. The partial differential equation, containing multiple variables of space and time, can be simplified into ordinary differential equations which deals with only time variable. To continue, the coupling equations can be solved using Newmark's method here with reasonable given initial values for both parameters of displacement and wake variable.

In the process of simplifying the equations of motion for beam model in Eq.4.6, it should be noted that the beam model has uniform along the length, thus has constant bending constants EI . While for the tension term $T(s)$ in the beam model, the value of which is not constant any more. With the coupling influence of submerged weight, drag force and the horizontal laying tension in the suspended pipeline, the tension in suspended pipeline is changing from the bottom TDP to the upper Vessel Connection Point (VCP). The detailed tension information is determined by the calculating process for the initial configuration of the suspended pipeline. The same situation happens for the first order derivative of the tension force. Thus Eq.4.6 can be written as the following expression,

$$EIy''''(s, t) + a_1EI\dot{y}''''(s, t) - T(s)y'' - T'(s)y'(s, t) + (m + m_a)\ddot{y}(s, t) = f_q \quad (4.8)$$

After substituting the approximation for derivatives of space into the simplified governing differential equation in Eq.4.8 and the boundary conditions provided above, the deduction process for final simplified equation is well explained here.

$$(m + m_a)\ddot{y}_i + EI\left(\frac{y_{i+2} - 4y_{i+1} + 6y_i - 4y_{i-1} + y_{i-2}}{h^4}\right) - T(i)\left(\frac{y_{i+1} - 2y_i + y_{i-1}}{h^2}\right) + a_1EI\left(\frac{\dot{y}_{i+2} - 4\dot{y}_{i+1} + 6\dot{y}_i - 4\dot{y}_{i-1} + \dot{y}_{i-2}}{h^4}\right) - T'(i)\frac{y_{i+1} - y_{i-1}}{2h} = f_q \quad (4.9)$$

The equation can be further simplified as Eq.4.10 after sorting out the terms in Eq.4.9.

$$(m + m_a)\ddot{y}_i + (A_k y_{i+2} - B_{ki} y_{i+1} + C_{ki} y_i - D_{ki} y_{i-1} + A_k y_{i-2}) + (A_c \dot{y}_{i+2} - B_c \dot{y}_{i+1} + C_c \dot{y}_i - B_c \dot{y}_{i-1} + A_c \dot{y}_{i-2}) = f_q \quad (4.10)$$

Where the coefficients in Eq.4.2 is expanded here.

$$A_k = \frac{EI}{h^4} \quad B_{ki} = \frac{4EI}{h^4} + \frac{T_i}{h^2} + \frac{T'_i}{2h} \quad C_{ki} = \frac{6EI}{h^4} + \frac{2T_i}{h^2} \quad D_{ki} = \frac{4EI}{h^4} + \frac{T_i}{h^2} - \frac{T'_i}{2h}$$

$$A_c = \frac{a_1EI}{h^4} \quad B_c = \frac{4a_1EI}{h^4} \quad C_c = \frac{6a_1EI}{h^4}$$

It should be emphasized in Eq.4.2 that, coefficients B_{ki} , C_{ki} and D_{ki} are changing with nodes, while the other coefficients are constant values. The reason comes that the tension in the beam model is changing as stated above, as well as the gradient for changing tension, the influence of which are expressed through these varying coefficients. The value of these tension term in nodes are acquired in the Appendix A.

The relation remains unquestionable in the inner nodes for the beam model, but for the boundary

nodes $i = 0, i = 1, i = n - 1$ and $i = n$ in Fig.4.3, the displacement for fictitious nodes $i = -2, i = -1, i = n + 1$ and $i = n + 2$ are needed in order to fulfill the requirement of Eq.4.10. This problem can be solved using the boundary conditions provided above. Relations for displacements of these four fictitious nodes can be substituted through the simplification of four boundary conditions in Eq.4.3 and Eq.4.4.

For boundary end in Eq.4.3, the following equation is derived:

$$y_0 = 0 \quad (4.11a)$$

$$y'_0 = \frac{y_1 - y_{-1}}{2h} = 0 \quad (4.11b)$$

For the boundary end in Eq.4.4, the following equation is derived:

$$y_n = 0 \quad (4.12a)$$

$$y'_n = \frac{y_{n+1} - y_{n-1}}{2h} = 0 \quad (4.12b)$$

From the boundary conditions given, it is clear that displacements for node $i = 0$ and node $i = n$ are already known. Then the focus is on node $i = 1$ and $i = n - 1$, the governing differential equations for these two nodes are written separately.

For node $i = 1$:

$$\begin{aligned} (m + m_a) \ddot{y}_1 + (A_k y_3 - B_{k1} y_2 + C_{k1} y_1 - D_{k1} k y_0 + A_{k1} y_{-1}) \\ + (A_c \dot{y}_3 - B_c \dot{y}_2 + C_c \dot{y}_1 - B_c \dot{y}_0 + A_c \dot{y}_{-1}) = f_q \end{aligned} \quad (4.13)$$

Eq.4.13 can be further simplified as Eq.4.14 using the boundary condition in Eq.4.11.

$$(m + m_a) \ddot{y}_1 + (A_k + C_k) y_1 - B_k y_2 + A_k y_3 + ((A_c + C_c) \dot{y}_1 - B_c \dot{y}_2 + A_c \dot{y}_3) = f_q \quad (4.14)$$

For node $i = n - 1$:

$$\begin{aligned} (m + m_a) \ddot{y}_{n-1} + (A_k y_{n+1} - B_{k_{n-1}} y_n + C_{k_{n-1}} y_{n-1} - D_{k_{n-1}} k y_{n-2} + A_{k_{n-1}} y_{n-3}) \\ + (A_c \dot{y}_{n+1} - B_c \dot{y}_n + C_c \dot{y}_{n-1} - B_c \dot{y}_{n-2} + A_c \dot{y}_{n-3}) = f_q \end{aligned} \quad (4.15)$$

Eq.4.15 can be further simplified as Eq.4.16 using the boundary condition in Eq.4.12.

$$(m + m_a) \ddot{y}_1 + ((A_k + C_{k_{n-1}}) y_{n-1} - D_{k_{n-1}} y_{n-2} + A_k y_{n-3}) + ((A_c + C_c) \dot{y}_{n-1} - B_c \dot{y}_{n-2} + A_c \dot{y}_{n-3}) = f_q \quad (4.16)$$

Besides the nodes at the boundary end, for inner nodes $i = 2, 3, \dots, n - 2$, of the beam model, the governing differential equations are written as Eq.4.10.

Since all the partial difference equations are written out, the matrix form for these equations can thus

be concluded for the sake of simplicity.

$$M \cdot \ddot{Y} + C \cdot \dot{Y} + K \cdot Y = F \quad (4.17)$$

Where terms Y , \dot{Y} and \ddot{Y} are the displacement, velocity and the acceleration for the nodes on beam model respectively. Detailed composition is shown as Eq.4.18.

$$Y = \begin{bmatrix} y_1 \\ y_2 \\ \vdots \\ y_{n-2} \\ y_{n-1} \end{bmatrix} \quad \dot{Y} = \begin{bmatrix} \dot{y}_1 \\ \dot{y}_2 \\ \vdots \\ \dot{y}_{n-2} \\ \dot{y}_{n-1} \end{bmatrix} \quad \ddot{Y} = \begin{bmatrix} \ddot{y}_1 \\ \ddot{y}_2 \\ \vdots \\ \ddot{y}_{n-2} \\ \ddot{y}_{n-1} \end{bmatrix} \quad (4.18)$$

In Eq.4.19, term F represents a summation of all kinds of equivalent force stated above. In this beam model, the F includes the assembly force matrix resulting from the coupling effects of wake variable q . Also, the variable V represents the current velocity perpendicular to the beam model, which has varying value for different nodes. The reason comes from the facts that the suspended pipeline has changing in-plane bending angle. Thus the uniform current will interact the pipeline at a varying angle. The current speed at each nodes of the beam model is different after normalization as stated in the previous section. In the numerical calculation process in Newmark's method, the wake variable in the force term here is always considered as an external force term and will be solved together in each time step.

$$F = \begin{bmatrix} \frac{1}{2} \rho D V_1^2 C_{V Y_1} \\ \frac{1}{2} \rho D V_2^2 C_{V Y_2} \\ \vdots \\ \frac{1}{2} \rho D V_{n-2}^2 C_{V Y_{n-2}} \\ \frac{1}{2} \rho D V_{n-1}^2 C_{V Y_{n-1}} \end{bmatrix} \quad (4.19)$$

As stated above, the added mass is always included in the mass matrix. Here, symbol m_a is used to represent the added mass, which equals to $\rho C_a \frac{\pi}{4} D_0^2$. The mass matrix here is a $(n-1) \times (n-1)$ diagonal matrix as shown in Eq.4.20.

$$M = (m + m_a) \begin{bmatrix} 1 & & & & \\ & 1 & & & \\ & & \ddots & & \\ & & & 1 & \\ & & & & 1 \end{bmatrix} \quad (4.20)$$

The equivalent stiffness matrix together with the equivalent damping matrix for the beam model are concluded as following Eq.4.21 and Eq.4.22. The coefficients $A_k, B_{k_i}, C_{k_i}, D_{k_i}, A_c, B_c, C_c$ in the equivalent stiff-

Freq. ord.	1	2	3	4	5	6	7	8	9	10
ω (rad/s)	0.158	0.262	0.374	0.490	0.610	0.732	0.857	0.985	1.116	1.249
Freq. ord.	11	12	13	14	15	16	17	18	19	20
ω (rad/s)	1.386	1.526	1.669	1.815	1.965	2.119	2.276	2.436	2.601	2.769

Table 4.2: First 20 eigen-frequencies of suspended pipeline

Principle as stated in Sec.4.1.

The initial coupling equations for beam model and wake variable are in continuous form as Eq.4.6 and Eq.4.7, and now have been transformed into truncated nodes form as Eq.4.10 and Eq.4.23. The coupling equations contains 2 unknown variable of displacement $y_i(t)$ and wake variable $q_i(t)$ at each nodes in the beam model, both of which are a function of only time now. The remaining problem turns into solving the ordinary differential equations as a function of time. The second order partial derivative of time is the highest order for these equations. These ordinary equations can be solved using Newmark's method together with the mathematical tool for solving nonlinear equations in Matlab. After reasonable initial conditions are given, the solution will be given as per time step.

4.3. MODEL VERIFICATION

After the setting up of the numerical beam model, a quick check of the eigen-frequencies for this beam model can be exerted before carrying on the numerical solution. Since the tension in suspended pipeline model is changing, the analytical solution for eigen-frequencies will be much too complicated. Thus the numerical solution will become the only approach. The results get from numerical solution will be checked whether the results will be in the acceptable region or not for typical offshore pipelines.

The equivalent stiffness matrix and mass matrix for the numerical calculation of the beam model is given in Eq.4.20 and Eq.4.21. Then the numerical solution for the natural frequencies of the beam model can be calculated here with a proper number of elements for the beam discreteness given above, which is under the assumption of an undamped free vibration beam. The characteristic equation is in the form of Eq.4.24.

$$|[K] - \omega^2 [M]| = 0 \quad (4.24)$$

The first 20 eigen-frequencies acquired through numerical solutions are concluded in Tab.4.2. It should be noticed here that the results of natural frequencies here is based on the initial configuration of suspended pipelines under the current speed of U as given in Tab.4.1. The results is quite convincing for typical offshore pipelines in actual projects. Along with the natural frequencies from numerical solutions, the first 20 mode shapes are also acquired. It should be noticed that the amplitude of modal shape for the whole pipeline is decreasing from TDP at seabed to the vessel connection point at sea level, which is clearer in a 2 dimensional view of lateral vibration mode along the pipeline length as an example shown

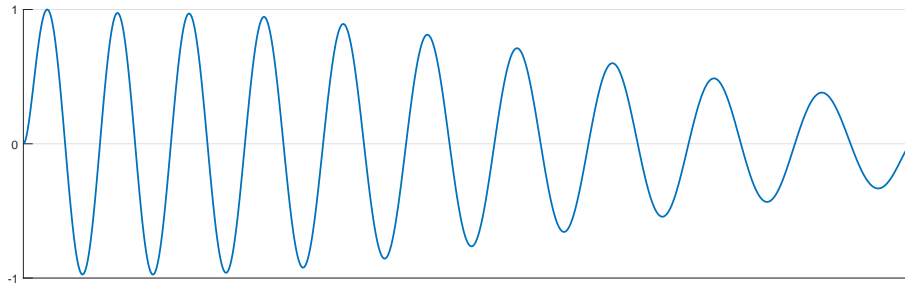


Figure 4.4: 20th mode shape in 2-D view

4

in Fig.4.4. This phenomenon appears due to the influence of increasing tension in the pipeline. Here in the beam model, larger tension leads to increasing stability which explains the phenomenon.

4.4. NUMERICAL RESULTS

From the above-mentioned model building information, a separate simulation model for the VIV of suspended pipeline can be developed step by step with suitable inputs. Here in the following, numerical results for such simulation model will be analysed.

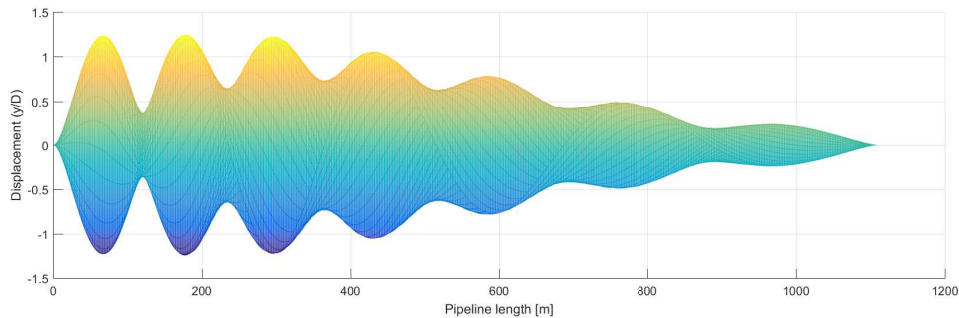


Figure 4.5: Envelope curve for lateral vibration ($U = 0.1952\text{ m/s}$)

For the input of current flow with speed of $U = 0.1952\text{ m/s}$, resulting in an initial length of 1109 m for the suspended pipeline, and the simulation has been performed with time length of 300 seconds. In order to acquire the overall motion information of the beam model, an envelope figure depicting the displacement throughout the simulation time of the whole beam model is shown as Fig.4.5. As can be seen, there are in total 7 peaks and troughs in the envelope curve, which means the beam model is excited 7th mode of vibration. The reason laid behind is that the current speed chosen has resulted in a shedding frequency of 0.857 rad/s calculated by the Strouhal formula in Eq.2.6, which is corresponding to the 7th

eigen-frequency of the suspended pipeline. Moreover, the maximum amplitude of the lateral vibration can be up to 1.2 times of outer diameter of the simulation.

To be more specific, a node is chosen from the beam model at the elevation length of 500 m, from seabed to sea level along the pipeline. For this node, the lateral vibration curve against time is illustrated. With the vibration information in time domain known, the motion can be analysed in frequency domain accordingly by the method of Fourier Transform. This is to verify clearly that at which frequency is that node vibrates.

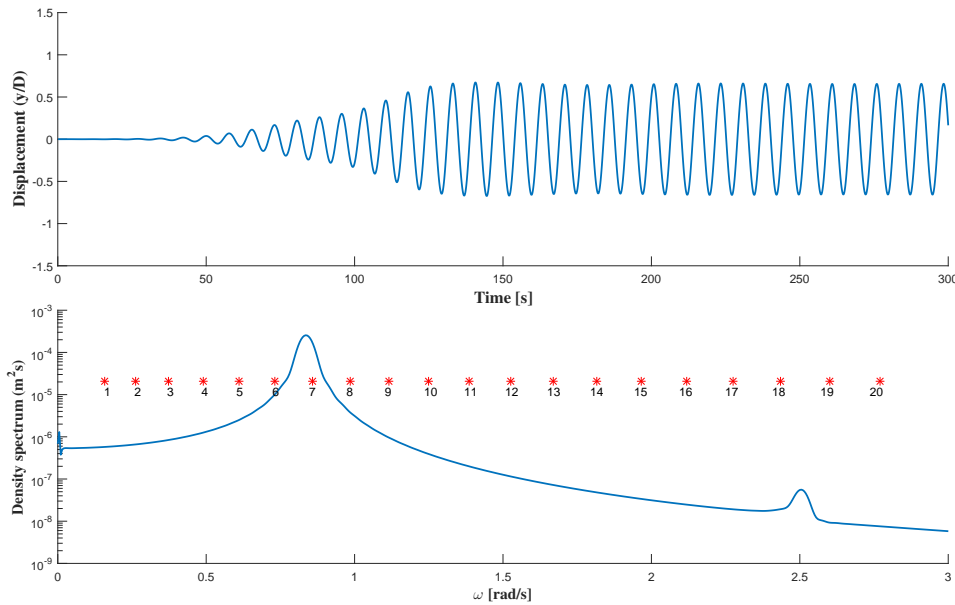


Figure 4.6: Displacement and spectra for lateral vibration (500 m)

As shown in Fig.4.6, the displacement is drawn and the amplitude of which has been normalised into the ratio of outer diameter for the pipeline. In the illustration of the spectra of the lateral vibration, the red star and corresponding numbers represent the order of modes for natural frequencies of pipeline. It can also be clearly seen that the main vibration frequencies of this node have explicit peaks at the region of 7th eigen-frequencies, which is the dominant frequency. This situation also occurs to other nodes in the beam model.

Furthermore, another current speed $U = 0.2560$ m/s has been input into the simulation model for double check. This current speed is for the lateral vibration of the suspended pipeline due which refers to 9th eigen-frequency of the suspended pipeline now. With the same process as that in the above contents,

the envelope curve is shown as Fig.4.7, there exists 9 peaks and troughs now.

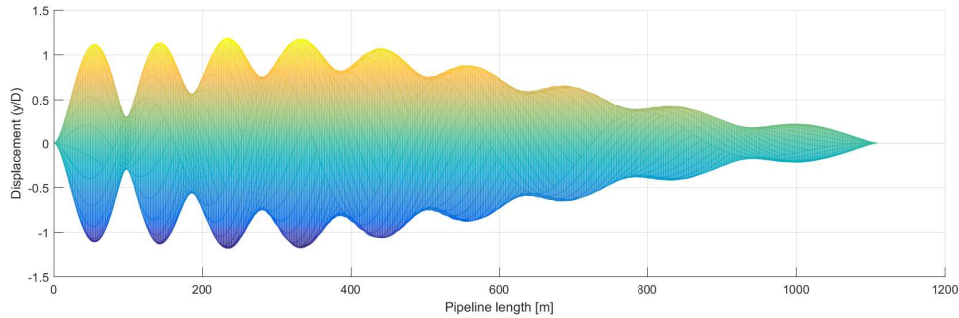


Figure 4.7: Envelope curve for lateral vibration ($U = 0.1952\text{ m/s}$)

After further check, the node at length of 500 m is again chosen to be analysed through Fourier Transform. The results is shown as Fig.4.8, where the 9th eigen-frequency is the dominant vibration frequency. Thus the simulation model is considered to be valid and effective. This separate model will be coupled to the seabed pipeline beam model in further study.

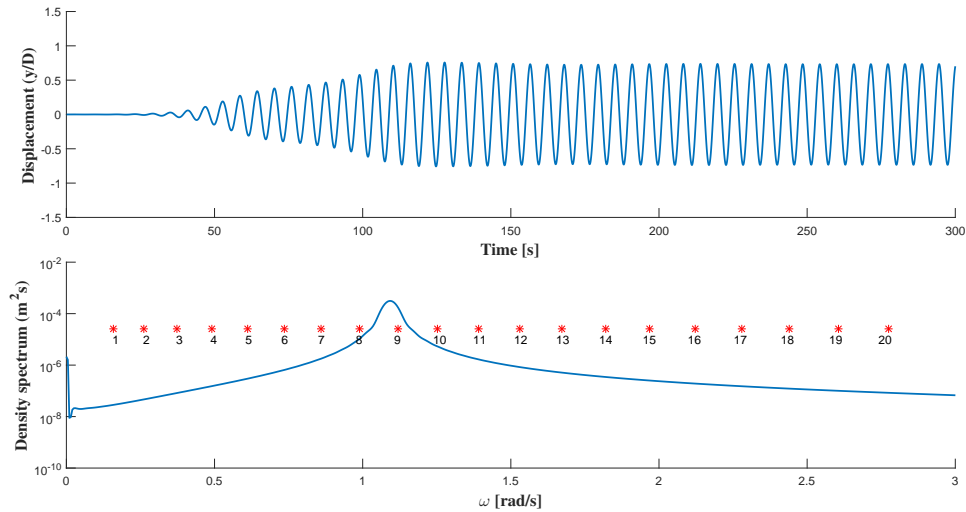


Figure 4.8: Displacement and spectra for lateral vibration (500 m)

As an appendix, here are also some chosen 3 dimensional modal shapes for the beam model ($U = 0.1952\text{ m/s}$) corresponding to the relevant frequency orders depicted in Fig.4.9.

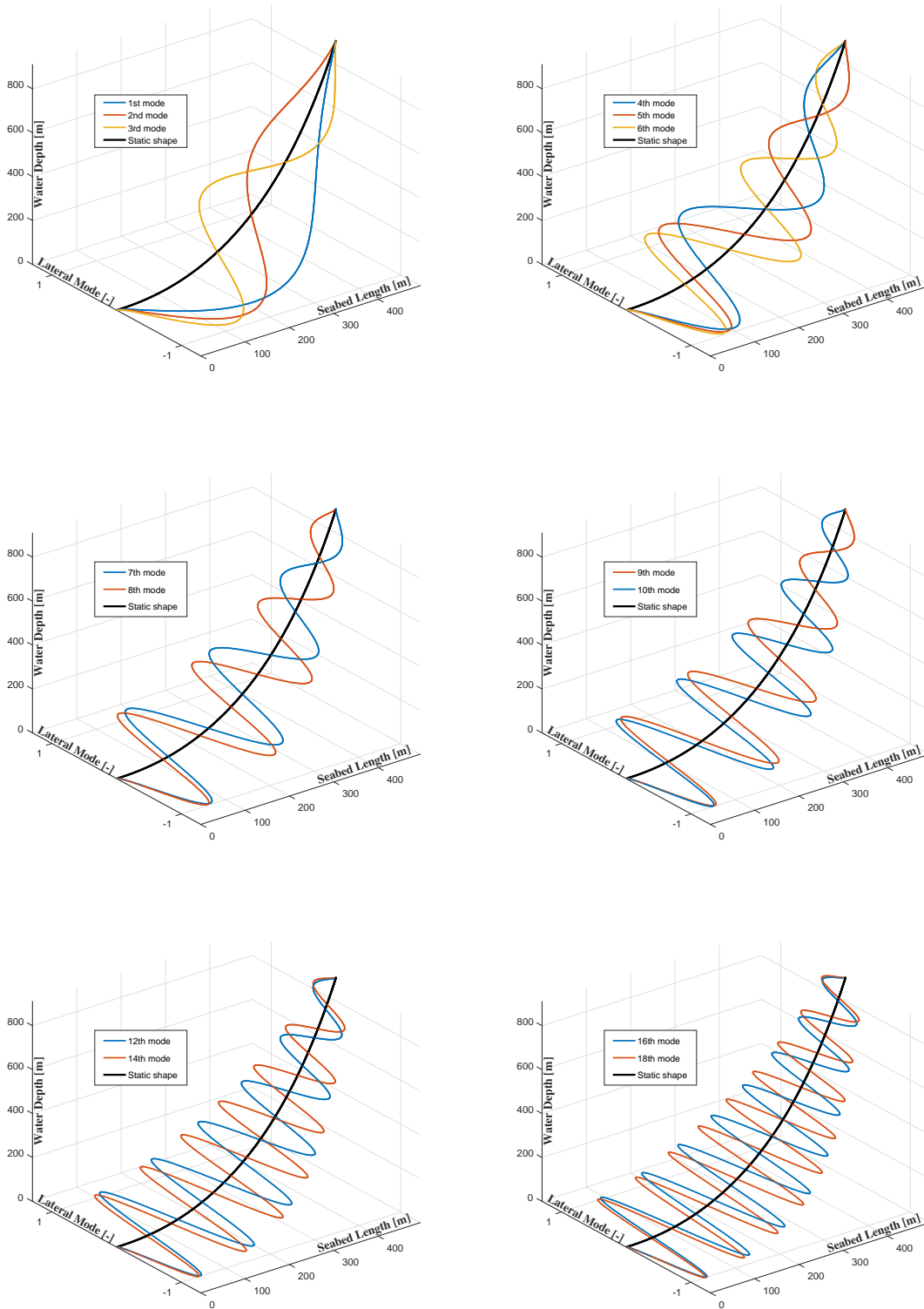


Figure 4.9: Modal shape examples

5

COUPLED PIPELINE MODEL

The characteristics for seabed pipeline motion and suspended pipeline motion has been stated already in Chapter 3 and Chapter 4 separately. The motion of pipelines has been analysed under the main influence of soil force and VIV separately in these two chapters. As stated before, the influence of VIV in suspended pipeline on the seabed pipeline yet experiencing with soil resistance, must be clarified. Thus, this chapter will focus on the vibration of overall pipeline model considering the coupling effects by combining these two independent analysing models together. Again in Sec.5.1, the general necessary supporting materials are stated here. After solid theories basis is laid in this section, the equations of motion for the overall pipeline model is proposed and deduced thoroughly in Sec.5.2. At last, the verification and results have been analysed in the Sec.5.4.

5.1. MODEL INFORMATION

The coupling model of suspended pipeline and seabed pipeline are connected at the TDP, in this research, namely the right boundary end of the seabed pipeline model as illustrated in Fig.3.7 and the lower boundary end of the suspended pipeline depicted in Fig.4.2. Thus the interface conditions for the connection point is rather a determinative to be established for the motion of the overall pipeline. The interface condition will be elaborated in the following part. Besides, the other model information of these separate parts are the same as that already have been explained in Sec.3.1 and Sec.4.1.

To summarize here, seabed pipeline in this part will be treated as an Euler-Bernoulli beam with reasonable length. Based on this point, the left boundary of seabed pipeline model is still considered as clamped. The tension distribution from TDP point, which is connected to the suspended pipeline, to the left clamped boundary end, remains the same as that in Chapter.3.7. The tension in TDP is noted to be continuous for these two parts. It is also considered as the same for the vertical penetration and

the material damping of seabed pipeline in overall model. The soil resistance loading and the hydrodynamic loading for this part takes the same procedure. The pipe-soil interaction will take effects only for the seabed pipeline part.

Moreover, for the suspended pipeline in this overall model, the Euler-Bernoulli beam assumption are adopted here. The initial configuration of suspended pipeline remains its shape and are connected to seabed pipeline. This is acceptable since the initial configuration is acquired together with the consideration for seabed pipeline as deduced in Appendix.A. The interface condition will be discussed as the following and the vessel connection end point will be treated as clamped. The coupling Van der Pol type wake oscillator will be kept the same and only be exerted at the suspended pipeline part. The same procedure will also occurs to the hydrodynamic loading pattern and the utilization of independence principle as stated in the Sec.4.1.

Boundary conditions and Interface conditions

For the overall pipeline model, the seabed pipeline is considered as a straight beam here and the suspended pipeline with in-plane bending is also considered as a straight beam model for out-of-plane motions, which has been investigated and verified in the Chapter.4. Accordingly the overall pipeline is also considered as a straight beam, note that the assumption is only effective while focusing on the out-of-plane vibration for the pipeline. The overall beam model is illustrated as Fig.5.1. In the illustration, the left end is the origin point and the length for seabed pipeline and suspended pipeline are L_b and L_s separately.

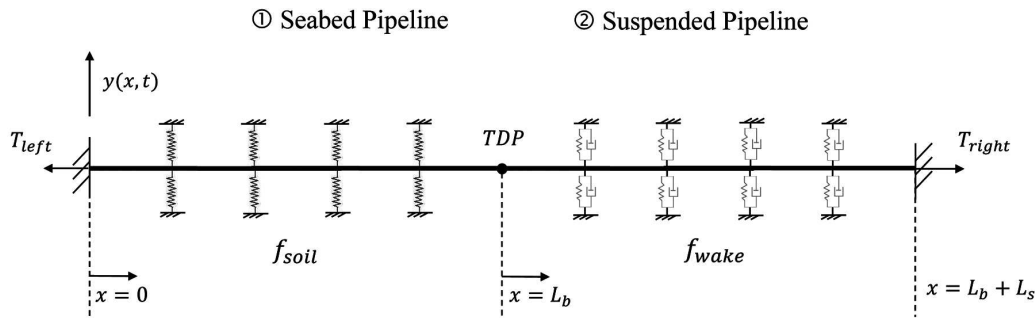


Figure 5.1: Coupled beam model illustration

For the far away left end of the seabed pipeline during J-lay process, the boundary end of which is considered as clamped. Thus according to the coordinates defined in the illustration, the boundary con-

ditions are given by:

$$y(-0, t) = 0 \quad (5.1a)$$

$$y'(-0, t) = 0 \quad (5.1b)$$

The boundary conditions for the vessel connection point of the suspended pipeline remains the same as that in Chapter.4, thus here comes the boundary conditions as:

$$y(L_b + L_s, t) = 0 \quad (5.2a)$$

$$y'(L_b + L_s, t) = 0 \quad (5.2b)$$

The interface conditions are the focus of this section. TDP point here plays the role of connection point between the seabed pipeline and suspended pipeline. The overall model here is intrinsically continuous results in the continuity of the interface conditions at the TDP in order to correctly modelling the behaviour of the overall pipelines. Thus the interface conditions are given as:

$$y_b(L_b, t) = y_s(L_b, t) \quad (5.3a)$$

$$y'_b(L_b, t) = y'_s(L_b, t) \quad (5.3b)$$

$$EI(y''_b(L_b, t) + a_1 \dot{y}''_b(L_b, t)) = EI(y''_s(L_b, t) + a_1 \dot{y}''_s(L_b, t)) \quad (5.3c)$$

$$EI(y'''_b(L_b, t) + a_1 \dot{y}'''_b(L_b, t)) = EI(y'''_s(L_b, t) + a_1 \dot{y}'''_s(L_b, t)) \quad (5.3d)$$

As shown in Eq.5.3, the displacements, slope angle, moments and shear force for both sides of TDP in suspended pipeline and seabed pipeline are continuous. Where y_b , y_s are the lateral displacement motion for seabed pipeline and suspended pipeline respectively.

The data used in this overall model also remains the same as that in separate model given by Tab.3.1 and Tab.4.1.

5.2. MODEL DESCRIPTION

After the necessary information and some simplifications provided in Sec.5.1, the problem for lateral vibration of this overall pipeline model in J-lay process can be illustrated as Fig.5.1. The overall model is connected by suspended pipeline and seabed pipeline at the TDP, which is also the origin point of the local coordinates defined in the illustration. Suspended pipeline are considered as a straight beam here and the length is defined as L_s . Seabed pipelines on bottom has the length of L_b . The total length equals to the summation of these two parts.

Now the equations of motion for the overall pipeline model can be derived considering the coupling of separate models as shown in Eq.5.4.

$$EI \frac{\partial^4 y_b}{\partial x^4} + a_1 EI \frac{\partial^5 y_b(x, t)}{\partial x^4 \partial t} - \frac{\partial}{\partial x} \left(T_b(x) \frac{\partial y_b(x, t)}{\partial x} \right) + (m + m_a) \frac{\partial^2 y_b(x, t)}{\partial t^2} = f_{ext} \quad 0 \leq x \leq L_b \quad (5.4)$$

$$EI \frac{\partial^4 y_s}{\partial x^4} + a_1 EI \frac{\partial^5 y_s(x, t)}{\partial x^4 \partial t} - \frac{\partial}{\partial x} \left(T_s(x) \frac{\partial y_s(x, t)}{\partial x} \right) + (m + m_a) \frac{\partial^2 y_s(x, t)}{\partial t^2} = f_q \quad L_b < x \leq L_b + L_s \quad (5.5)$$

$$\frac{\partial^2 q(x, t)}{\partial t^2} + \epsilon \omega_s(x) (q^2(x, t) - 1) \frac{\partial q(x, t)}{\partial t} + \omega_s^2(x) q(x, t) = \frac{A}{D} \left(\frac{\partial^2 y(x, t)}{\partial t^2} \right) \quad L_b < x \leq L_b + L_s \quad (5.6)$$

Where f_{ext} , f_q are already defined in the previous chapter representing the effects of external force in seabed pipeline and the influence of VIV in suspended pipeline separately. In addition, all the other variables used here have been given already. After the equations of motion are settled for the overall pipeline model, Again, the same procedures are followed in order to solve the coupling equations.

In Eq.5.4, there are generally two variables, namely the displacement y of overall pipeline and the wake parameter q in suspended pipeline only. The displacement variable are included in the form of partial derivative for time and space, while the wake variable are only the derivative of time. Central difference method is used to transform the continuous problem into a discrete one as far as derivative of space is concerned. After which the coupling partial differential equations with variable of time and space has turned into the ordinary differential equations which is only the function of time. Then the equations can be solved together using Newmark's method step by step in time sequence. The displacement information and wake variable value of each time step are recorded and analysed at last.

With the previous simplification work done in Chapter.3 and Chapter.4, the necessary work need to be done in this chapter is to reasonably combine the equivalent mass, stiffness, damping matrix in both seabed pipeline and suspended pipeline, correctly taking the TDP interface conditions into consideration. It has already been elaborated in Chapter 3 that the seabed pipeline on bottom has the length of L_b , divided to N_b elements. The division results in a model of $N_b + 1$ nodes. The boundary condition for displacements of end nodes are given in Eq.3.21 and Eq.3.22, thus the motion for 1st nodes, namely the infinite end, and the last nodes, namely the boundary condition, has already been included. This has results in a $N_b - 1 \times N_b - 1$ matrix in order to solve the displacements for the other nodes. The process reveals that the displacement for TDP in the overall model is not included in the seabed pipeline model, since it has been previously defined according to the boundary condition.

The same situation happens to the building process of the suspended pipeline beam model, which has a length of L_s and $N_s + 1$ nodes. Although the only difference is that the first node in suspended pipeline model is the TDP point. Thus the problem need to be solved since the movements of the TDP is both previously defined in separate models. While the movements of TDP plays an important role for the connection of separate models. Hence the node in TDP and the influence to surrounding nodes must be considered correctly into the overall model through the deduce of interface conditions. The process is illustrated in Fig.5.2.

Surrounding nodes around the TDP is shown in Fig.5.2. The deriving process for the interface condi-

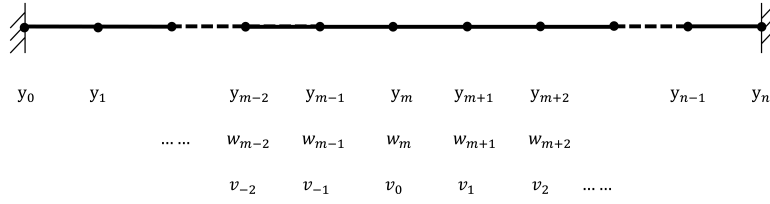


Figure 5.2: Nodes division for overall model

tion and consequent relation between nodes are as the following.

$$\begin{aligned} y_b(0, t) &= y_s(0, t) \\ w_m &= v_0 \end{aligned} \quad (5.7)$$

$$\begin{aligned} y'_b(L_b, t) &= y'_s(L_b, t) \\ \frac{w_{m+1} - w_{m-1}}{2h} &= \frac{v_1 - v_{-1}}{2h} \end{aligned} \quad (5.8)$$

$$\begin{aligned} EI y''_b(L_b, t) + a_1 EI \dot{y}''_b(L_b, t) &= EI y''_s(L_b, t) + a_1 EI \dot{y}''_s(L_b, t) \\ \frac{w_{m+1} - 2w_m + w_{m-1}}{h^2} + a_1 \frac{\dot{w}_{m+1} - 2\dot{w}_m + \dot{w}_{m-1}}{h^2} &= \frac{v_1 - 2v_0 + v_{-1}}{h^2} + a_1 \frac{\dot{v}_1 - 2\dot{v}_0 + \dot{v}_{-1}}{h^2} \end{aligned} \quad (5.9)$$

Substituting the Eq.5.7 into the Eq.5.9 and using Eq.5.8, the following simplified relation can be found.

$$\begin{aligned} (w_{m+1} - v_1) + a_1 \frac{\partial}{\partial t} (w_{m+1} - v_1) &= 0 \\ (w_{m-1} - v_{-1}) + a_1 \frac{\partial}{\partial t} (w_{m-1} - v_{-1}) &= 0 \end{aligned} \quad (5.10)$$

Number of solutions for Eq.5.10 can be unlimited. The solutions can be in the form of either Eq.5.11, Eq.5.12 or in the form of Eq.5.13 and Eq.5.14.

$$w_{m+1} = v_1 \quad (5.11)$$

$$w_{m-1} = v_{-1} \quad (5.12)$$

$$w_{m+1} - v_1 = X e^{-t} \quad (5.13)$$

$$w_{m-1} - v_{-1} = X e^{-t} \quad (5.14)$$

In Eq.5.13 and Eq.5.14, X means any real number and t is time. In this research, the solution in Eq.5.11 and Eq.5.12 has actual physical meaning. While for the solution that is a function of time in Eq.5.13 and Eq.5.14, it only has mathematical meaning. When the value of time increases to a very large number, these two equations are the same. Thus in this research, the first set of solution are adopted. Subse-

quently, fictitious nodes of w_{m+1} and v_{-1} are substituted by the real nodes v_1 and w_{m-1} . Moreover, the last interface condition can be written as Eq.5.15.

$$\begin{aligned} EI(y_b''''(L_b, t) + a_1 \dot{y}_b''''(L_b, t)) &= EI(y_s''''(L_b, t) + a_1 \dot{y}_s''''(L_b, t)) \\ \frac{w_{m+2} - 2w_{m+1} + 2w_{m-1} - w_{m-2}}{2h^3} + a_1 \frac{\dot{w}_{m+2} - 2\dot{w}_{m+1} + 2\dot{w}_{m-1} - \dot{w}_{m-2}}{2h^3} &= \frac{v_2 - 2v_1 + 2v_{-1} - v_{-2}}{2h^3} + a_1 \frac{\dot{v}_2 - 2\dot{v}_1 + 2\dot{v}_{-1} - \dot{v}_{-2}}{2h^3} \\ (w_{m+2} - w_{m-2}) + a_1 \frac{\partial}{\partial t} (w_{m+2} - w_{m-2}) &= (v_2 - v_{-2}) + a_1 \frac{\partial}{\partial t} (v_2 - v_{-2}) \end{aligned} \quad (5.15)$$

For the relation between w_{m+2} and w_{m-2} , together with v_2 and v_{-2} , the Eq.5.15 only is not enough. Consequently, the EOM was introduced in both nodes w_m and v_0 .

$$\begin{aligned} (m + m_a) \ddot{w}_m &= \frac{-EI}{h^4} (w_{m+2} - 4w_{m+1} + 6w_m - 4w_{m-1} + w_{m-2}) \\ &\quad - \frac{a_1 EI}{h^4} (\dot{w}_{m+2} - 4\dot{w}_{m+1} + 6\dot{w}_m - 4\dot{w}_{m-1} + \dot{w}_{m-2}) \\ &\quad + T_b(w_m) \frac{w_1 - 2w_0 + w_{-1}}{h^2} + T'_b(w_m) \frac{w_{m+1} - w_{m-1}}{2h} \end{aligned} \quad (5.16)$$

$$\begin{aligned} (m + m_a) \ddot{v}_0 &= \frac{-EI}{h^4} (v_2 - 4v_1 + 6v_0 - 4v_{-1} + v_{-2}) \\ &\quad - \frac{a_1 EI}{h^4} (\dot{v}_2 - 4\dot{v}_1 + 6\dot{v}_0 - 4\dot{v}_{-1} + \dot{v}_{-2}) \\ &\quad + T_s(v_0) \frac{v_1 - 2v_0 + v_{-1}}{h^2} + T'_s(v_0) \frac{v_1 - v_{-1}}{2h} \end{aligned} \quad (5.17)$$

Note that w_m and v_0 has the same motions as derived before. Thus Eq.5.16 and Eq.5.17 are equal to each other. The tension force is the same in nodes w_m and v_0 from both parts. The soil force and wake oscillation force are not written in this equation for the reason of high nonlinearity and also time dependent. These terms are treated as external force and applied to nodes directly. After simplification, the following equation is derived:

$$(w_{m+2} + w_{m-2}) + a_1 \frac{\partial}{\partial t} (w_{m+2} + w_{m-2}) = (v_2 + v_{-2}) + a_1 \frac{\partial}{\partial t} (v_2 + v_{-2}) \quad (5.18)$$

Following the same procedures for the derivation of Eq.5.10, the equation above can be simplified while solved together with Eq.5.15. The final solution is given by:

$$w_{m+2} = v_2 \quad (5.19)$$

$$w_{m-2} = v_{-2} \quad (5.20)$$

From the above deduce process, the motion of fictitious nodes are transformed to real existing nodes.

Thus the equations of motion for the interface nodes can be written as:

$$(m + m_a) \ddot{y}_{n_b} + \left(A_k y_{n_b+2} - B_{k_{n_b}} y_{n_b+1} + C_{k_{n_b}} y_{n_b} - D_{k_{n_b}} k y_{n_b-1} + A_k y_{n_b-2} \right) + \left(A_c \dot{y}_{n_b+2} - B_c \dot{y}_{n_b+1} + C_c \dot{y}_{n_b} - B_c \dot{y}_{n_b-1} + A_c \dot{y}_{n_b-2} \right) = f_{drag} + f_{soil} \quad (5.21)$$

The deduce process of the boundary conditions are not elaborated here any more for the sake of simplicity as which is already deduced already in previous chapters. The EOM for the boundary end node in seabed pipeline are written as Eq.3.33. The boundary end in suspended pipeline are written as Eq.4.15.

To make it clear from an overall view, the matrix for this coupled model is written as:

$$M \cdot \ddot{Y} + C \cdot \dot{Y} + K \cdot Y = F \quad (5.22)$$

Where terms Y , \dot{Y} and \ddot{Y} are the displacement, velocity and the acceleration for the nodes on this overall beam model respectively. Detailed composition is shown as Eq.5.23.

$$Y = \begin{bmatrix} y_1 \\ y_2 \\ \vdots \\ y_{m-1} \\ y_m \\ y_{m+1} \\ \vdots \\ y_{n-2} \\ y_{n-1} \end{bmatrix} \quad \dot{Y} = \begin{bmatrix} \dot{y}_1 \\ \dot{y}_2 \\ \vdots \\ \dot{y}_{m-1} \\ \dot{y}_m \\ \dot{y}_{m+1} \\ \vdots \\ \dot{y}_{n-2} \\ \dot{y}_{n-1} \end{bmatrix} \quad \ddot{Y} = \begin{bmatrix} \ddot{y}_1 \\ \ddot{y}_2 \\ \vdots \\ \ddot{y}_{m-1} \\ \ddot{y}_m \\ \ddot{y}_{m+1} \\ \vdots \\ \ddot{y}_{n-2} \\ \ddot{y}_{n-1} \end{bmatrix} \quad (5.23)$$

Where term F represents external load that the coupling beam model has experienced and is shown as the following. In which, the force matrix F consists of seabed pipeline part and the suspended pipeline part. The force composition for both parts has already been stated in previous chapters.

$$F = \begin{bmatrix} -\frac{1}{2} \rho C_d D_0 \dot{y}_1 |\dot{y}_1| - f_{ext_1} \\ -\frac{1}{2} \rho C_d D_0 \dot{y}_2 |\dot{y}_2| - f_{ext_2} \\ \vdots \\ -\frac{1}{2} \rho C_d D_0 \dot{y}_{m-1} |\dot{y}_{m-1}| - f_{ext_{m-1}} \\ -\frac{1}{2} \rho C_d D_0 \dot{y}_m |\dot{y}_m| - f_{ext_m} \\ \frac{1}{2} \rho D V_{m+1}^2 C_{VY_{m+1}} \\ \vdots \\ \frac{1}{2} \rho D V_{n-2}^2 C_{VY_{n-2}} \\ \frac{1}{2} \rho D V_{n-1}^2 C_{VY_{n-1}} \end{bmatrix} \quad (5.24)$$

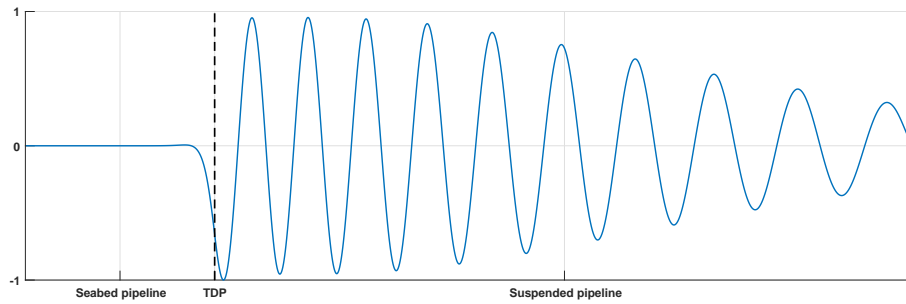


Figure 5.3: 20th mode shape in 2-D view

seabed pipeline part, most part of which are kept straight until its approaching the connection region with the suspended part. This is under the effects of large soil resistance simulated as a distributed spring with reasonable value in modal analysis for simplicity.

5

5.4. NUMERICAL RESULTS

In this section, the simulation results are demonstrated for coupled pipeline system comprising both seabed pipeline and suspended pipeline. It should be noticed that the simulation model does not include the influence of the dynamic laying process yet, which can be seen as a full cornerstone for the following works. However, this model can still be used to model the lateral walking of seabed part for a steel catenary riser due to the large VIV motion in suspended part resulted from current flow.

In the input variables for simulation test, the seabed pipeline has a length of 1000 m, to guarantee that the seabed part is long enough that the left end is unaffected. Suspended pipeline again has a total length of 1109 m under the uniform distributed current flow from seabed to sea level at the speed of $U = 0.1952$ m/s, the speed of which corresponds to the 7th eigen-frequency of the suspended pipeline. Total simulation time is 500 s by Newmark- β method. After the necessary information provided, the envelope curve of the lateral vibration for the beam model can be shown in Fig.5.4, which is a holistic view.

As can be seen from Fig.5.4, the seabed pipeline should have had the length of 1000 m as described above, while there is only 200 m in the picture. This is because under such conditions of input, large part of seabed pipelines are not influenced due to large resistance. Main influence part is in the length of rough 50 m next to the TDP. Thus for the convenience of illustration, only limited part of seabed pipeline are shown. The maximum amplitude for the lateral vibration in suspended part due to effects of VIV is 0.283 m, which equals to 1.04 time of outer diameter of the pipeline. Maximum amplitude happens at the pipeline length of 1287 m. The maximum amplitude in seabed pipeline happens around the TDP with the value of 0.036 m, which is 0.13 time of outer diameter.

Afterwards, four representative locations on the beam model are chosen to gain increasing compre-

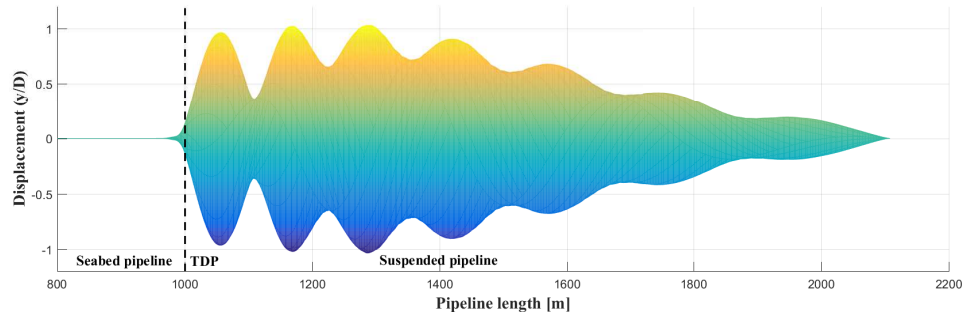


Figure 5.4: Envelope curve for coupled pipeline ($U = 0.1952$ m/s)

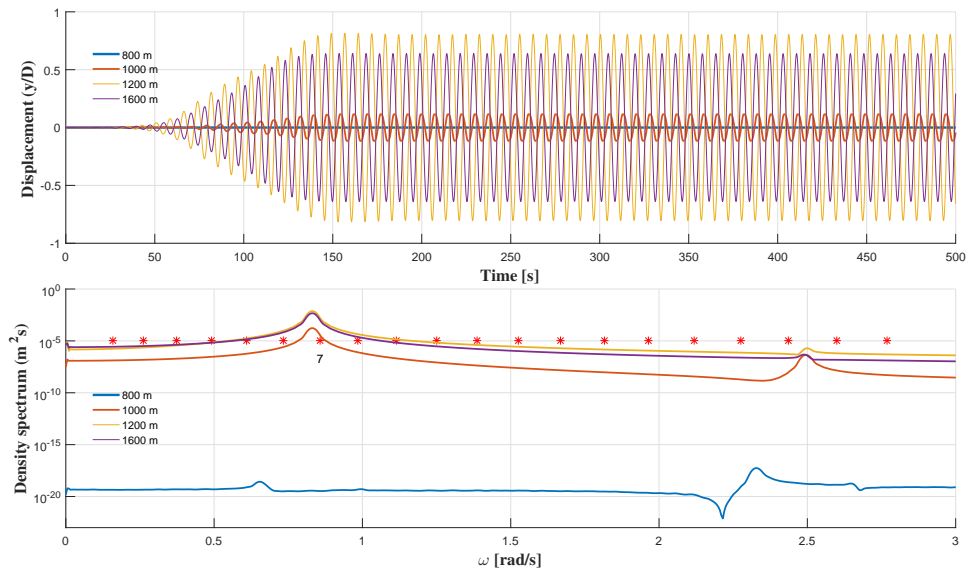


Figure 5.5: Displacement and spectra for lateral vibration of nodes

hending into the lateral vibration process of the pipeline system. The lateral displacement and vibration spectra in frequency domain of nodes in these locations are depicted in Fig.5.5. From the lateral displacement illustration, the displacement at the length of 800 m is nearly stationary throughout the simulation, the spectral analysis is also very small compared that to the nodes in suspended part, there are almost 15 orders of magnitudes. Thus at this place, the soil part can be seen as unaffected from the VIV. Moreover, the amplitude at the seabed part is relatively small even in the TDP compared to that in the suspended part, without considering the dynamic effects of laying in this region.

For the nodes at suspended part, though the amplitudes for lateral displacement varies a lot while the density spectral of which has shown similarity to a great extent. So is the spectral density curve trend of node at 1000m, though the amplitude is smaller, this is because of the soil resistance in this node. Furthermore, the spectral density mainly locates at the frequency region around the 7th eigen frequency of the suspended pipeline, not the natural frequency of coupled pipeline, which has corresponds to the Strouhal frequency of the current flow. It can be noticed that the peak in spectral figure is deviating from the 7th eigen-frequency marked in Fig.5.5, compared to Fig.4.6. Such phenomenon may results from the coupling effects of seabed pipeline and suspended pipeline, in which the soil resistance in seabed pipeline dissipate the energy transmitted from the suspended pipeline.

The above process are the modelling for situation that VIV happens throughout the simulation period, though the lateral amplitude for the vibration of seabed pipeline is relatively small, the seabed pipeline can also keep its location. To dig it further, a model when VIV is removed by setting current speed equalling to zero from half simulation time, the pipeline will finally becomes static with energy dissipation in from hydrodynamic resistance and soil resistance. The phenomenon that seabed can keep its bending shape when the coupled pipeline becomes still at last.

It is also found out that the soil stiffness may influence the amplitude for lateral vibration of seabed pipelines largely, the value for soil stiffness depends mainly on the soil types. Fig.5.6 has shown the envelope curve for a simulation with a 10 times smaller value of soil stiffness compared to the results in Fig.5.4.

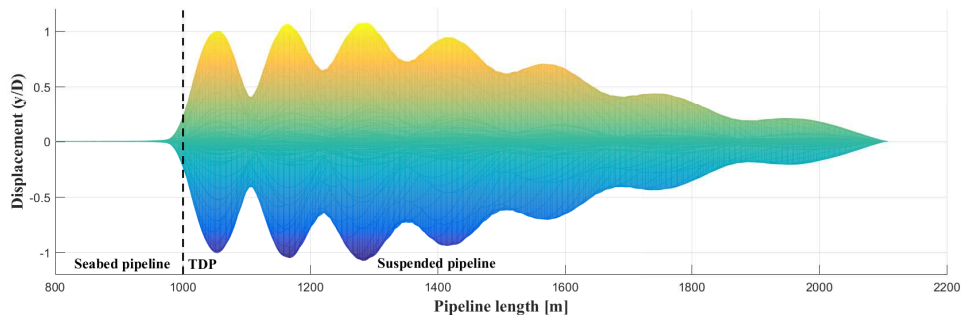


Figure 5.6: Envelope curve for coupled pipeline ($k_s = 6.95 \times 10^4 \text{ N/m}^2$)

When the other variables are kept the same, the maximum amplitude for lateral vibration in seabed pipeline has the value of 0.063 m, which is 0.23 time of outer diameter. Which is nearly two times as a comparison for the results in Fig.5.4. Here are also some chosen 3-D modal shapes corresponding to the relevant frequency orders depicted in Fig.5.7 as an appendix.

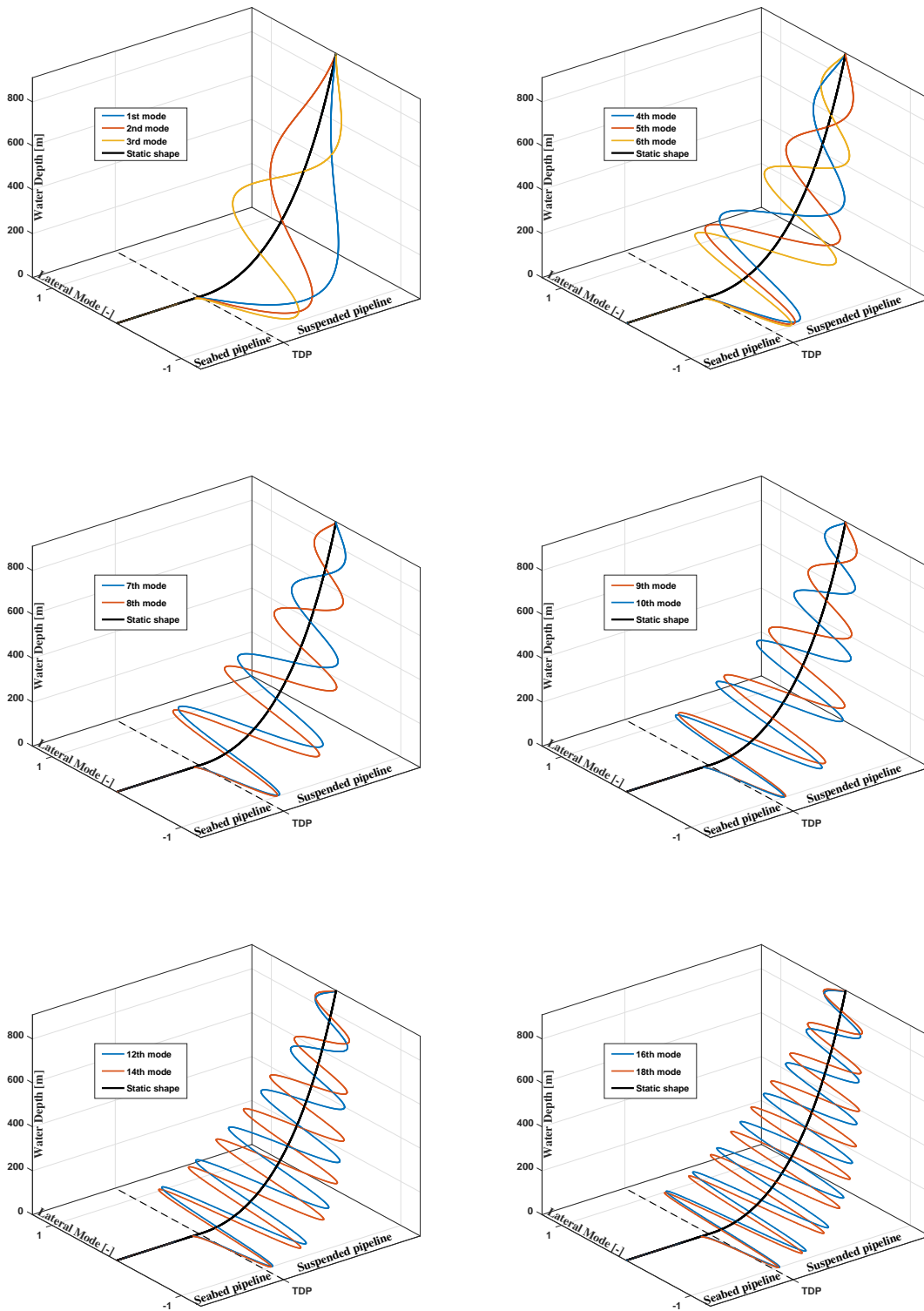


Figure 5.7: Modal shape examples

6

INFLUENCE OF TDZ

Previous chapters have described in detail the modelling process for the lateral vibration of pipelines during J-lay, yet without considering the influence of laying process. During the laying operation, the connection part of seabed pipeline and suspended pipeline are highly affected by the random vessel motions and all kinds of hydrodynamic forces. A probable result may occur that TDP is moving in laying process. Thus in this chapter, the influence on the lateral vibration due to this phenomenon is investigated.

6.1. MODEL INFORMATION

During laying process, sometimes the as-laid pipeline on seabed can not keep a straight laying route yet would presents the bending shape like snake, which is not expected by the engineer. In order to find out possible cases for this phenomenon, the dynamic laying process is analysed and modelled. When pipeline is being laid down, pipelines are undergoing cyclic motions due to diversified sea state and resulting unpredictable vessel motions. These unexpected factors may result in more stress concentration and force amplification in the touchdown zone around where the laying pipeline touches the seabed.

TDP movement

The influence for the dynamic laying effects can be divided into vertical pipeline oscillation case and the lateral pipeline oscillation case. The vertical oscillation of pipeline in the touchdown zone may lead to the detachment of seabed and pipelines, which means that there is no pipe and soil contact. Thus the pipeline experiences no soil resistance in this region. Moreover, the soil properties in this region varies a lot due to dynamic pipeline movement. Soil in this region is usually softened and remoulded, but is difficult to be quantified here.

Speculations have been made here that the existence of touchdown zone would exert influence on the magnitude of lateral vibration of the pipelines and lateral bending shape will be magnified here. In order

to simulate the mechanism for of touchdown zone effects, some modification should be made based on the previously defined coupling model. Since the essence of the touchdown zone is random detachment of pipelines from the seabed, resulting less soil force at these pipeline segment. Hence, the basic idea to incorporate this mechanism is that (i) the in-plane initial configuration remains the same as that in static situation and (ii) a touchdown zone is isolated in seabed part of the coupling pipelines.

After a specific zone has been isolated simulating the movement of touchdown point, an acceptable description of that should be elaborated in the next. Throughout the laying process, the dynamic behaviour of pipelines in touchdown zone can be very complex and difficult to be reproduced. It may be influenced by estimated stress concentration in the touchdown zone due to a catenary shape of the whole pipeline. This has resulted in a changing vertical load on the soil varying along the pipeline length, which is also higher than the as-laid pipeline weight at a certain locations of this region. This can be estimated through structural analysis of suspended pipelines with the laying angles known and axial tension calculated. The soil properties at the touchdown region can also be influenced by the horizontal and vertical oscillations of the pipelines due to the vessel motions. The oscillations of which can be estimated from the analysis of vessel motions taking into consideration of wave motions.

Since the essence for this research is to investigate the influence of varying range of soil force results from the movements of touchdown point at existing touchdown zone. Thus the above mentioned factors will not be included here which is beyond the scope of this research. The most characteristic for the phenomenon that the soil force becomes zero due to the detachment of pipelines from soil at seabed in the touchdown zone is captured. This kind of detachment is oscillating along with time. Here is an illustration for the movement of touchdown point in this research. As can be seen from Fig.6.1, the touchdown

6

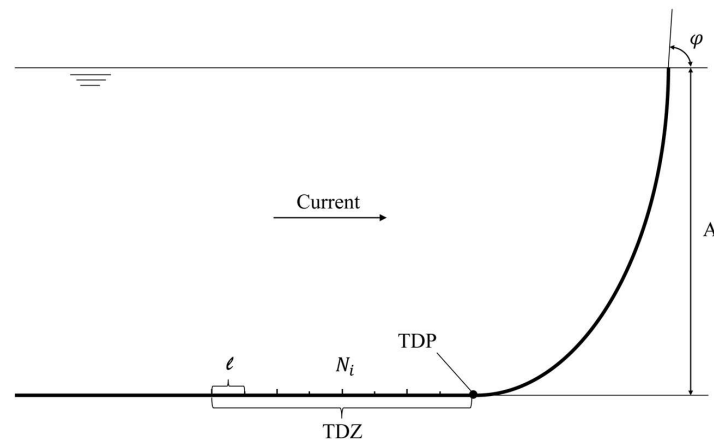


Figure 6.1: Illustration for TDP movement at TDZ

zone is specified in the seabed pipeline part and the initial touchdown point is marked as the connection point between suspended pipeline and the seabed pipeline. The movement of touchdown point is given

by a harmonic function as Eq.6.1. The reason for the adjustment in Eq.6.1 is to simulate the movement of touchdown point to the left from initial touchdown point as marked in the Fig.6.1.

$$L_{TDP} = A_{TDP}(1 - \cos(\omega_{TDP}t)) \quad (6.1)$$

There are two influential factors describing the characteristics of touchdown point movement at the touchdown zone. The first important determinative factor is A_{TDP} , controlling the magnitude of the length of the touchdown zone. The second influential factor is the ω_{TDP} , controlling the frequency of the touchdown point movement as elaborated later. The value of which should be investigated into to guarantee an effective results from the simulation.

For pipelines with various characteristics under different environmental loading, the magnitude for the length of touchdown zone may change a lot. Especially for the situation of a storm when laying process is done, and when the risers suspended from a platform are concerned. There are some relatively reasonable values for the range of touchdown region in practice. From the guidance manual about geotechnical and foundation design considerations released by American Petroleum Institute (API) [18], the typical length of touchdown region, in an engineering case similar to our research, ranges within about ± 15 m, namely with the length of roughly 30 m. This is the case corresponding to the influence of daily wave loading. Moreover, for a the situation of a storm, the distance can be extended into ± 25 m, namely 50 m for the length of touchdown zone. There is another field studies [19] has shown that the touchdown zone length of such scale is very realistic value for these kinds of specific seabed, pipe properties and laying geometry. In this research, the value for length of touchdown zone is determined as 40 m, which has made the value of A_{TDP} equal to 20 m.

The frequency for TDP movements, namely ω_{TDP} , is concerned largely with the actual horizontal and vertical oscillation of the laying vessel and the random hydrodynamic forces. This can be estimated by the analysis of the vessel motions under the influence of environmental loading, which has beyond the scope of this research. Moreover, the importance of the frequency is less than that of the magnitude of the touchdown zone. In order to carry on with the research, an estimation value is given here. The period of the touchdown point movements is 25 seconds. For a simulation time of 500 seconds, there will be 20 cycles for the movement of touchdown point, thus the influence of the movement can be observed in detail.

The above-mentioned model information are the new changes for the future simulation of touchdown point movement. The other information about the model comprising seabed pipelines model information, the suspended pipelines model information and the coupled pipeline model information is the same as already stated in Chapter 5. After the necessary information preparation work above, next section is the building up process for the simulation model of the moving touchdown point.

6.2. MODEL DESCRIPTION

The theoretical foundation has been laid for the simulation model of additional touchdown point movement with the information provided above. Except for the only difference stated above, the building up process for the simulation model are the same as that of static laying process model defined in previous chapters for coupled pipeline system. The model is illustrated in Fig.6.2. Here in Fig.6.2, the only differ-

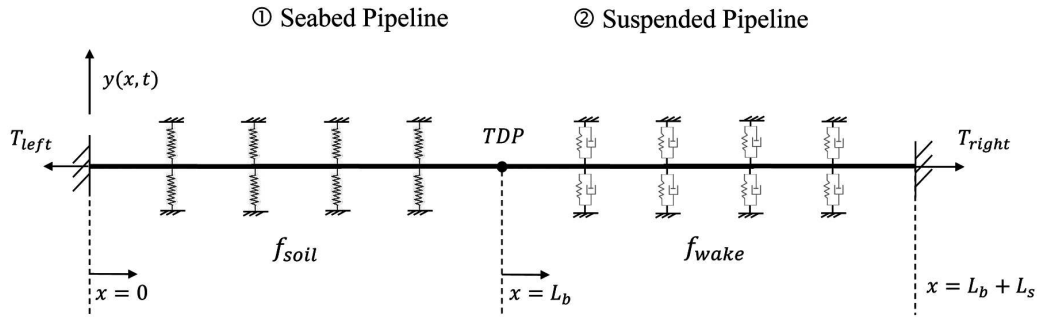


Figure 6.2: Beam model illustration

ence is shown in the seabed pipeline part that there contains a touchdown zone on the left of connection point, namely the touchdown point. The movement of touchdown point will change the soil force distribution in the seabed pipelines and this will be elaborated later.

The equations of motion for the beam model is the same as that shown in the Eq.5.4 to Eq.5.6. After which, the continuous beam model is transformed into discrete nodes. Central difference method is used here for the simplification of turning partial differential equations with high order derivative of time and space variables into ordinary equations only with high order derivative of time. Besides, the determination of boundary and interface conditions are the same in these two parts. At last, the modified ordinary differential equations are solved by Newmark- β method. The deduce process for the calculation matrix used in the calculation will not be elaborated any more as this is the same as that in the previous chapter.

What should be emphasized here is that the gradual change of soil force distribution due to the appearance of touchdown point movements. After the beam model is discretized into nodes with the same manners in Chapter 5, the magnifying illustration for the touchdown movement in a certain moment is shown as the following Fig.6.3. Where the L_{TDP} represents the travelling distance of touchdown point as time is going on, which has already been defined in Eq.6.1. The distance between two continuous node is marked by l . In a certain moment, the touch down point has moved into the location between node N_i and N_{i+1} and the length between node N_i and the touchdown point is defined by l^* , which is a continuous changing value as a function of time. In addition, the value for l^* ranges from 0 to l .

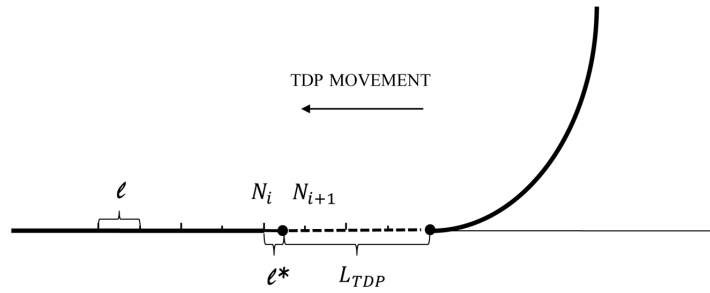


Figure 6.3: Magnifying illustration for TDP movement

Since the touchdown point moves and the moving distance has already been defined by L_{TDP} , the numerical sequence number of node N_i can be determined once the initial nodes partition is known. For the sequence number of nodes larger than N_{i+1} , the soil force becomes zero. There is only hydrodynamic force in this part. But for the soil force applied into node N_i and N_{i+1} , special care should be taken together with the changing value of l^* . Since finite difference method is used here, while the essence of which is to discretize the continuous model into discrete elements, and the distributed force in one element is also applied together into a node representing the force of element. According to this idea, the soil force for node N_i and N_{i+1} is determined through the following process as shown in Fig.6.4.

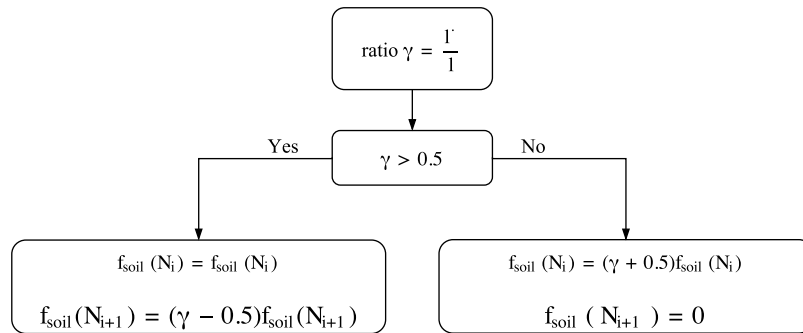


Figure 6.4: Soil force for adjacent nodes containing TDP

The soil force distribution for the nodes containing touchdown point should be modified as shown above at every time step. Where the ratio γ represents the proportion of real length l^* of element experiencing soil force over the whole length of single element l . Initially, when the value of ratio smaller than

0.5, namely the touchdown point is within the element range represented by node N_i , the soil force is the sum of soil force at half element length (0.5) on the left of the node N_i and at the real element length γ on the right of the node N_i . While there is no soil force for the node N_{i+1} . When the value of ratio γ is bigger than 0.5, namely the touchdown point begin to locate at the range of soil element representing by node N_{i+1} . Thus the soil force for node N_i remain as the same as the whole element length which does not need to be adjusted. While for the node N_{i+1} , the ratio of element length undergoing soil force is over the whole element length is $\gamma - 0.5$. The soil force for node N_{i+1} need to be adjusted.

The direct results for the movement of touchdown point is the change of soil force distribution as time going on. This description process is defined above for the calculation of soil force in this research. Since the soil force in this model is the only alteration part compared to the static laying process model defined in Chapter 5, which plays the role of external forces in the simulation model. The other parts in this simulation model remains the same as that in static laying process model, thus the main structure of the simulation model remains the same. Furthermore, the verification step is skipped due to the similarity with previous model. To continue, the simulation results can be concluded in next section.

6.3. NUMERICAL RESULTS

From the above information provided, the new simulation lateral vibration model including the influence of TDZ during the dynamic laying process is presented in this section.

The simulation test is based on the current speed of $U = 0.1952$ m/s, as the same as that in Chapter 5 for the convenience of comparison. The total simulation time is 600 s, during which the current flow is distributed uniformly throughout the simulation. The movement of touchdown point will begin from the beginning to check the influence on lateral vibration of seabed pipeline and will stop at the time of 500 s to see the difference. First of all, the envelope curve is illustrated for the whole pipeline part as Fig.6.5.

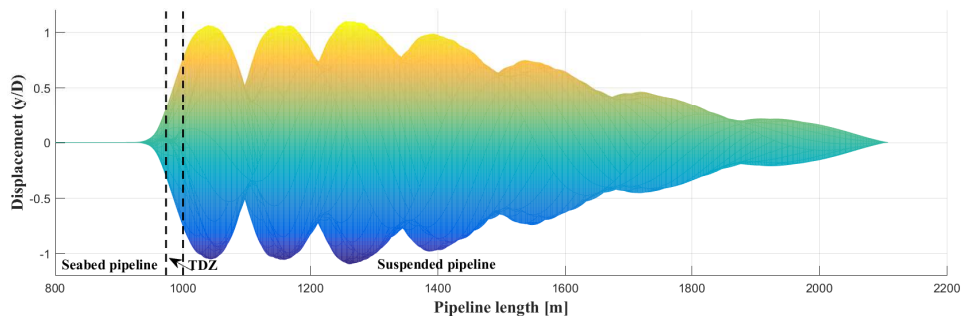


Figure 6.5: Envelope curve for coupled pipeline (With TDZ)

From Fig.6.5, the conclusion can be drawn that the amplitudes for lateral vibration in the TDZ is magnified largely due to the movement of TDP when compared to Fig.5.4. After analysing the data acquired in this simulation, the maximum lateral displacement is 0.21 m, about 0.76 time of the outer diameter

for the pipeline. This is a much larger value as expected than the value acquired without the influence of TDZ in Chapter 5. Moreover, the detailed vibration information of seabed part is depicted in Fig.6.6 by selecting a representative node at the middle location in TDZ, which has a length of 980 m from the left boundary end in the beam model .

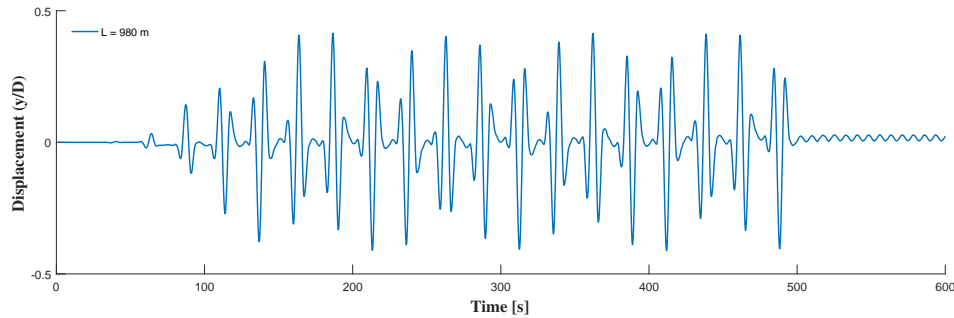


Figure 6.6: Lateral vibration of $L = 980\text{m}$

As shown in Fig.6.6, the lateral vibration of which before 500 s has turned into a bit of periodically chaotic status compared to the displacement plot in Fig.5.5. While after the time 500 s, the vibration becomes a regular one. The reason for such phenomenon is due to the movement of TDP as time goes on, which resulting in a changing distribution of soil resistance force. At the moment that node 980 has a relatively lower amplitude, it is applied with soil resistance force, and vice versa for the higher amplitudes situations.

Further more, another simulation has been exerted, in which the current speed is set to be zero during half of the simulation time, there also appears the results the seabed pipeline in TDZ region can keeps a bending shape after reaching a static state due to energy dissipation. When comparing the results with that in Chapter 5, the maximum lateral displacement is also larger.

7

INFLUENCE OF PIPELINE LAYING

Dynamic laying process will influence the lateral vibration of pipelines definitely. The influence of which comes from various factors, this research mainly focuses on two aspects due to the limited scope of this research. First influential factor is the existence of touchdown zone, which has already been expatiated in Chapter 6. The simulation model of which are based on the model for static laying process, thus it has played the role of a connecting link between simulation models for pure static laying process and for the dynamic laying process separately. The second influential factor of the lateral vibration of the pipelines, the dynamic laying process to be exact, will be further investigated in this chapter.

7.1. MODEL INFORMATION

For the purpose of taking dynamic laying process into account, the intrinsic characteristics of the process should be clearly analysed beforehand. When the laying vessels is in operation, pipelines are constantly laid at a certain speed, the laying speed in other words. The speed of which can vary a lot for different type of laying vessels, typically S-lay, J-lay and reel lay approaches. For the J-lay method in this research, pipelines are released at a certain speed from the laying vessel continuously, at the same time, the seabed pipelines is increasing its length as the laying operation goes on. Moreover in this research, assumption comes that the laying configuration of the pipeline system is kept the same as that calculated for initial static configuration when focusing on the lateral vibration of the pipeline system. Thus the configuration of suspended pipelines remains the same and the total length of which does not change.

With the appearance of current flows, the suspended pipeline in sea water may undergo vortex induced vibration which is the main source of the lateral vibration for the pipeline system. This kind of lateral vibration in suspended pipelines will definitely results in the vibration of seabed pipelines, which may jeopardize the straight configuration of as-laid pipelines thorough the hinderance of soil. Conse-

quently, as the laying process goes on, seabed pipelines gain its length gradually, which may deviate from the pre-set straight laying route continuously. Therefore the influence of dynamic laying process should be investigated and analysed so as to describe the influence qualitatively. With the intention of modelling the dynamic laying process, additional modification on the simulation model for static laying process should be done, as will be explained in detail in following contents.

Introduction of fictitious pipeline

Lots of work has been done for the numerical model of static laying process which is assembled from the separate part of seabed pipelines and suspended pipelines. These two part of pipelines have been defined with a finite length as it is given beforehand. The length of suspended pipelines is calculated through the initial static configuration of the J-lay pipeline under a given current situation. While the length of seabed pipelines is defined with enough length to guarantee that the faraway end from the laying direction is not concerned with the laying operation. It is clear that the length of both parts are pre-defined with a constant value through the simulation of static laying process. Compared to the situation above, one of the most apparent change for the dynamic laying process modelling is that the length of the pipeline system is increasing as the laying process is operated. The difficulty of this simulation model also lays here. To simplify the problem, the problem of touchdown zone is not considered here. There consequently comes the assumption of initial laying configuration is kept constant as defined in static laying process model, the only difference is actual movement of pipelines through the route of static configuration. In other words, the only difference is the increasing length of seabed pipelines due to the pipe laying process.

Taken the length change of the model into account, a relatively simple and precise solution must be reasonably proposed considering the calculation speed of numerical simulation. If the length is increased in every time step of the simulation process, the whole calculation structure of the pipeline model need also to be changed in every time step since the element division of the pipeline need also to be adjusted with increasing length. The number of whole calculation steps can be very large to guarantee an acceptable resolution in Newmark- β method, thus if this idea is adopted the calculation will be tremendously time-consuming. A substitution solution is proposed as an alternation that the length of pipelines need to be laid is pre-defined in the whole coupling pipeline system. Here, the concept of fictitious pipelines part is introduced which is named compared to seabed pipelines and suspended pipelines. Based on this idea, if the simulation time and the laying speed is given, the length of fictitious pipelines is known by simple calculation. Thus the coupling pipeline system comprises the seabed part, suspended part and fictitious part now. The whole length of the pipeline system is known also. The calculation structure of whole pipeline system is carried out throughout the simulation since the element division of the model is constant from start to end.

To continue, the fictitious pipeline is released into the water during laying process as time goes on. Namely the released part of which begins to experience the vortex induced vibration under the influence of current flows, which has become part of the suspended pipeline around the beam region of vessel. Simultaneously, an equivalent length of suspended pipeline initially locating around the seabed becomes

the seabed pipelines and start to undergo soil resistance. Although the whole pipeline system is calculated together, remaining part in fictitious pipelines should be kept still until it is released. Furthermore, the remaining part cannot affect the calculation results in the already laid part. During the dynamic laying modelling process, the interface between the already laid part in fictitious pipeline and the remaining part in fictitious part should remain the function of fixed boundary as defined in static laying process. Only this requirement is satisfied, the remaining part in fictitious part can be kept still and will not affect the calculation results for this dynamic process.

Essentially, the lateral vibration in beams is transmitted in the form of waves as shown in numerical solutions. When the wave in structure runs into a fixed boundary, the transmitted wave will be reflected. The magnitude of the wave will not be altered after the reflection while the original shape of which is kept reversely. After recalling the knowledge from structural dynamics, a dashpot with infinitely large damping coefficients plays the same role as a fixed boundary. Based on the idea above, distributed dashpot with infinitely large damping coefficients can be applied to the remaining part of the fictitious part. In addition, the distributed dashpot is eliminated gradually along with the pipe laying process. The detail will be further elaborated after the finite difference method is used for the discreteness of the beam model in Sec. 7.2.

Information gather

The introduction of fictitious pipeline into the pipeline system has been already elaborated in the above section. Which is the main change for the simulation model of dynamic laying process compared to that in static laying process. Besides the model information for fictitious part described above, the other simulation model information is summarised together in the following for the reason that the dynamic laying process model is still based on the static laying process simulation model and thus there will be some overlap part for both models, only the difference will be contained here.

With the intention to organise the general layout for the details of the model, the following contents are concluded. The coupling pipeline system here used to simulate the dynamic laying process comprises three part, namely seabed pipelines, suspended pipelines and fictitious pipelines as given before. The initial configuration of the coupling pipeline system are pre-defined as that in the static laying configuration. The seabed pipelines will experience vertical penetration at first, which will also be assumed as a constant value due to its self submerged weight as has already been stated in Chapter 3. This is because the vertical vibration is beyond the scope of this research and the coupling effects between vertical and lateral vibration is relatively small. The suspended pipeline behaves more like stiffened catenary since the water depth is large enough that most portions of suspended pipelines can be considered as catenary cables solely, except for the region near the seabed where the bending stiffness of suspended pipelines can not be neglected due to the boundary layer phenomenon and thus is treated as a beam. The stiffened catenary is considered as a combination of beam and cable part. The static shape of which under the effects of currents can be analysed through the combination of numerical and analytical method together as elaborated in Appendix A. The static initial configuration acquired is used when dynamic laying process simulation is carried out. For the lateral vibration of the coupling pipelines is relatively small, which

is moving around the initial static configuration of the coupling system. The fictitious part is released gradually as the laying operation going on. The information about initial configuration will be used in the tension calculation in the beam model and the vortex induced vibration of suspended pipeline in the future. The coupling pipeline system is considered as a straight beam since the focus of this research is on the lateral vibration, namely the out-of-plane vibration for the pipeline. The in-plane configuration of the pipeline can be seen as independent from lateral vibration of the pipeline system again.

During laying process, main environmental load on the pipeline system is again considered here. There is no external load for the fictitious part, that is also applied with distributed dashpot with extremely large damping coefficient. The suspended pipeline undergoes the hydrodynamic forces under the influence of current flow and surround sea water. The in-line drag force is concerned with the initial configuration of the pipelines and the out-of-plane lift force is modelled by wake oscillator model. The inertia force is considered as added mass into the structure. Seabed pipelines here is undergoing both hydrodynamic forces and the nonlinear soil force as defined before. The only difference and difficulty here is that the length of pipeline movements as the laying process going on. Consequently, the external force distribution has changed.

The internal damping in pipeline system here is also represented by the material damping, the idea of which has already been stated in Chapter 3. Besides, the coupling pipeline system comprises three parts, the left and right boundary end are both clamped, where the displacement and slope are both zero. There are two interface conditions also in this beam model, the first one locates at the touchdown point between seabed pipeline and suspended pipeline, the second one locates at the the connection point between the suspended pipeline and fictitious pipeline. Interface conditions at both point are continuous as the pipeline characteristics for different parts are the same, the difference is influence the external environmental loading. The continuity is guaranteed by the equivalence of displacement, slope angle, bending moment and the shear force at the both side of the interfaces.

It is also worth mentioning that the tension throughout the pipelines are the most changeable variable in the calculation process. Where the idea of tension calculation in seabed pipelines is the same as that in Chapter 3. But as the laying process goes on, the length of seabed pipeline is increasing, thus the tension along the length of which change with time as well. This will be included into the calculation process. The suspended pipeline will remain its length in a dynamic process. The increasing length from fictitious part is the same as the decreasing length into the seabed pipelines. The tension in a certain location of the suspended pipeline remain the same. While for the dynamic laying process, the space coordinates for a certain element is changing as time goes, thus the tension for it is changing too. For the remaining part in fictitious pipeline, there is no need to consider the tension since results will not be influenced for its role of clamped boundary with extremely large dashpot. This will be elaborated in next section.

7.2. MODEL DESCRIPTION

With theoretical expound provided above, the simplified model for dynamic laying process can be illustrated as Fig.7.1 by combining the fictitious part, for the convenience of facilitating understanding.

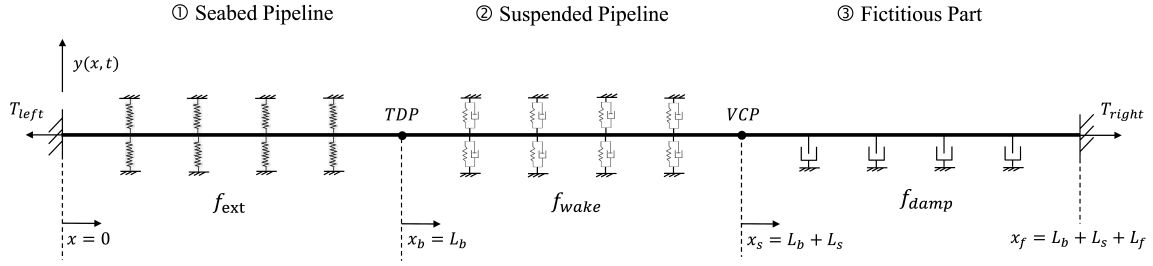


Figure 7.1: Beam model illustration including fictitious part (Top view)

Where x indicates the local coordinates along the pipeline length and $y(x, t)$ represents the lateral vibration of the pipeline as a function of time and pipeline length. Tension in the beam model varies through the beam model indicated by T_{left} and T_{right} . The length L_b , L_s , L_f refer to the length of seabed pipeline, suspended pipeline and fictitious part separately. The f_{soil} represents external loading in the seabed pipelines including the most characteristic loading of soil, f_{wake} represents the vortex induced vibration for the suspended pipeline and $f_{damping}$ is the represents the distributed extremely large damping in this fictitious part which plays the role of fixed boundary in the calculation process.

Now the equations of motion for the overall pipeline model can be derived considering the coupling of separate models as shown in Eq.7.1 to Eq.7.4.

$$EI \left(\frac{\partial^4 y_b(x, t)}{\partial x^4} + a_1 \frac{\partial^5 y_b(x, t)}{\partial x^4 \partial t} \right) - \frac{\partial}{\partial x} \left(T_b(x) \frac{\partial y_b(x, t)}{\partial x} \right) + (m + m_a) \frac{\partial^2 y_b(x, t)}{\partial t^2} = f_{ext} \quad 0 \leq x \leq x_b \quad (7.1)$$

$$EI \left(\frac{\partial^4 y_s(x, t)}{\partial x^4} + a_1 \frac{\partial^5 y_s(x, t)}{\partial x^4 \partial t} \right) - \frac{\partial}{\partial x} \left(T_s(x) \frac{\partial y_s(x, t)}{\partial x} \right) + (m + m_a) \frac{\partial^2 y_s(x, t)}{\partial t^2} = f_q \quad x_b < x \leq x_s \quad (7.2)$$

$$EI \left(\frac{\partial^4 y_f(x, t)}{\partial x^4} + a_1 \frac{\partial^5 y_f(x, t)}{\partial x^4 \partial t} \right) - \frac{\partial}{\partial x} \left(T_f(x) \frac{\partial y_f(x, t)}{\partial x} \right) + (m + m_a) \frac{\partial^2 y_f(x, t)}{\partial t^2} = f_{damp} \quad x_s < x \leq x_f \quad (7.3)$$

$$\frac{\partial^2 q(x, t)}{\partial t^2} + \epsilon \omega_s(x) (q^2(x, t) - 1) \frac{\partial q(x, t)}{\partial t} + \omega_s^2(x) q(x, t) = \frac{A}{D} \left(\frac{\partial^2 y(x, t)}{\partial t^2} \right) \quad x_b < x \leq x_s \quad (7.4)$$

Where f_{ext} , f_q are already defined in the previous chapter representing the effects of pipe-soil interaction together with the hydrodynamic force in seabed pipeline and the influence of VIV in suspended pipeline separately. Moreover, the detailed expression of f_{ext} and f_q has already been defined in previous chapters and will not be expanded again. Furthermore, f_{damp} means the damping force in the fictitious part. The value for which can be clearly expressed as

$$f_{damp} = -c_{dpf} \cdot \dot{y}_f \quad (7.5)$$

In Eq.7.5, c_{dpf} means the damping coefficients of the dashpot, the value of which is set as a very large

number as 1×10^{32} here. Since the damping coefficient of the dashpot is set as infinitely large, thus the damping force is extremely large accordingly. After the equations of motion are settled for the overall pipeline model, again, the numerical methods are followed in order to seek solutions for the coupling equations. The numerical solution process has large similarity as that in previous chapters. But after the introduction of dynamic laying process due to the gradual change of length in diverse pipeline parts, the process will certainly becomes much more different in detailed solution process.

For the intention of acquiring the motion information, controlling equations in Eq.7.1 to Eq.7.4 must be resolved. Similarly, the equations turn into solving the partial derivative equations as the precious models. Using central difference method afterwards, the partial differential equations of the beam model containing both partial derivatives of time and displacement has turned into the ordinary differential equations with only partial derivative of time in second order. Next, these equations can be solved by together using the Newmark- β method in steps with given time period. During solving process, the value for displacement, velocity and acceleration of the beam model in nodes is recorded and can be analysed later. And so is the value for wake variable. Such process will be elaborated in the next.

The nodes division of the beam model are shown as Fig.7.2 in the following. This is the initial nodes division without considering the dynamic laying, namely there is no length changing yet as will be explained in the following.

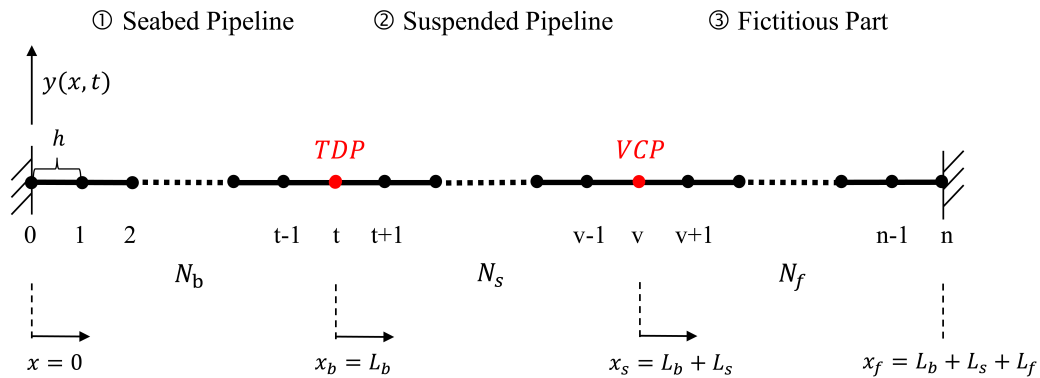


Figure 7.2: Nodes division for beam model illustration including fictitious part (Top view)

It is shown in this nodes division picture that the continuous beam model is divided into discrete nodes. Three pipeline parts in the beam with length of L_b , L_s , L_f separately are divided into nodes with the value of N_b , N_s , N_f correspondingly. Since the boundary conditions for this model is fixed, thus motions for the first node and last node are already known, which will not be included into the calculation process accordingly. The sequence number of first node before touchdown point (as the touchdown point may move) or the node at the touchdown point is marked as t , so is the vessel connection point marked

as ν . The value of t and ν may change as the movement of these two points in pipe laying process. The distance between two contiguous nodes has constant values h , regardless of the different pipeline parts. Initially, the touchdown point and vessel connection point are in the place of nodes, while in the moving process for the pipe laying, these two points will change the relative position in the beam model as will be shown later in Fig.7.3.

During the simplification process, it should be noted that the structural properties of the three pipeline parts remains the same, bending moment EI and cross section for example. While the tension in the suspended part and seabed pipeline marked by $T(s)$ and $T(b)$ varies according to the relative location in space, namely in the beam model. The same situation occurs to the derivative of tension in this two parts, $T'(s)$ and $T'(b)$. However, the tension and its derivative, $T(f)$ and $T'(f)$ in fictitious part has no influence to the results, thus $T(f)$ is set as constant equalling to the tension of connection point with the suspended pipeline, $T'(f)$ is zero accordingly. The tension and its derivative at different nodes is interpolated from the continuous model. After the simplification process, the equation in every node can be written as:

For seabed pipelines:

$$(m + m_a) \ddot{y}_{bi} + EI \left(\frac{y_{bi+2} - 4y_{bi+1} + 6y_{bi} - 4y_{bi-1} + y_{bi-2}}{h^4} \right) - T_b(i) \left(\frac{y_{bi+1} - 2y_{bi} + y_{bi-1}}{h^2} \right) + a_1 EI \left(\frac{\dot{y}_{bi+2} - 4\dot{y}_{bi+1} + 6\dot{y}_{bi} - 4\dot{y}_{bi-1} + \dot{y}_{bi-2}}{h^4} \right) - T'_b(i) \frac{y_{bi+1} - y_{bi-1}}{2h} = f_{ext} \quad 1 \leq i \leq t \quad (7.6)$$

For suspended pipelines:

$$(m + m_a) \ddot{y}_{si} + EI \left(\frac{y_{si+2} - 4y_{si+1} + 6y_{si} - 4y_{si-1} + y_{si-2}}{h^4} \right) - T_s(i) \left(\frac{y_{si+1} - 2y_{si} + y_{si-1}}{h^2} \right) + a_1 EI \left(\frac{\dot{y}_{si+2} - 4\dot{y}_{si+1} + 6\dot{y}_{si} - 4\dot{y}_{si-1} + \dot{y}_{si-2}}{h^4} \right) - T'_s(i) \frac{y_{si+1} - y_{si-1}}{2h} = f_q \quad t+1 \leq i \leq \nu \quad (7.7)$$

For fictitious pipelines:

$$(m + m_a) \ddot{y}_{fi} + EI \left(\frac{y_{fi+2} - 4y_{fi+1} + 6y_{fi} - 4y_{fi-1} + y_{fi-2}}{h^4} \right) - T_f(i) \left(\frac{y_{fi+1} - 2y_{fi} + y_{fi-1}}{h^2} \right) + a_1 EI \left(\frac{\dot{y}_{fi+2} - 4\dot{y}_{fi+1} + 6\dot{y}_{fi} - 4\dot{y}_{fi-1} + \dot{y}_{fi-2}}{h^4} \right) - T'_f(i) \frac{y_{fi+1} - y_{fi-1}}{2h} = f_{damp} \quad \nu+1 \leq i \leq n-1 \quad (7.8)$$

Along with the vortex induced vibration in suspended part, the equation is simplified as:

$$\ddot{q}_i + \epsilon_i \omega_{s_i} (q_i^2 - 1) \dot{q}_i + \omega_{s_i}^2 q_i = \frac{A_i}{D} \ddot{y}_i \quad t+1 \leq i \leq \nu \quad (7.9)$$

After the equations are simplified, a second step should also be taken as considering the boundary conditions and the interface conditions in the beam model, which is for the intention of guaranteeing the continuity of the nodes in these equations. Deduce process for the interface conditions at the touchdown point and the vessel connection point is the same as that in Chapter 5 Fig.5.2. For a specific part, there

remains the fictitious nodes beyond the part for boundary nodes around the interface nodes. Through the same deduce process, these fictitious nodes are related to the existing nodes in adjacent parts just as the way in Chapter 5. For simplicity, this will not be elaborated again here. Due to the continuity of nodes in the motions for beam model, Eq.7.6 to Eq.7.8 can be combined together as Eq.7.10, in which the external force for separate parts has been also be combined together.

For overall pipelines:

$$(m + m_a) \ddot{y}_i + EI \left(\frac{y_{i+2} - 4y_{i+1} + 6y_i - 4y_{i-1} + y_{i-2}}{h^4} \right) - T(i) \left(\frac{y_{i+1} - 2y_i + y_{i-1}}{h^2} \right) + a_1 EI \left(\frac{\dot{y}_{i+2} - 4\dot{y}_{i+1} + 6\dot{y}_i - 4\dot{y}_{i-1} + \dot{y}_{i-2}}{h^4} \right) - T'(i) \frac{y_{i+1} - y_{i-1}}{2h} = f_{total} \quad 1 \leq i \leq n-1 \quad (7.10)$$

The above equations can be further explicitly shown as:

$$(m + m_a) \ddot{y}_i + (A_k y_{i+2} - B_{ki} y_{i+1} + C_{ki} y_i - D_{ki} y_{i-1} + A_k y_{i-2}) + (A_c \dot{y}_{i+2} - B_c \dot{y}_{i+1} + C_c \dot{y}_i - B_c \dot{y}_{i-1} + A_c \dot{y}_{i-2}) = f_{total} \quad (7.11)$$

Where the coefficients in Eq.7.11 is expanded here.

$$A_k = \frac{EI}{h^4} \quad B_{ki} = \frac{4EI}{h^4} + \frac{T_i}{h^2} + \frac{T'_i}{2h} \quad C_{ki} = \frac{6EI}{h^4} + \frac{2T_i}{h^2} \quad D_{ki} = \frac{4EI}{h^4} + \frac{T_i}{h^2} - \frac{T'_i}{2h} \quad (7.12)$$

$$A_c = \frac{a_1 EI}{h^4} \quad B_c = \frac{4a_1 EI}{h^4} \quad C_c = \frac{6a_1 EI}{h^4}$$

It should also be stressed in Eq.7.12 that, coefficients B_{ki} , C_{ki} and D_{ki} are not only changing with nodes, but will also varying with time as per the laying process in introduced next, while the other coefficients are constant values. The value of these tension term in nodes are acquired in the Appendix A. As the nodes change its position in laying process model, the tension and its derivative in corresponding node will also change its value as time going on. The value of which is interpolated from the initial tension force distribution for static laying process analysis. Thus for each time step, these coefficients will change their values accordingly. The phenomenon for varying tension will not influence the material damping term, which according to the definition is only concerned with the displacement term.

Next, the clamped boundary conditions at both end of the beam model are introduced. Since the deduce process is same as that in precious chapters, thus again the conclusion will be given directly. For node $i = 1$:

$$(m + m_a) \ddot{y}_1 + ((A_k + C_{k1}) y_1 - B_{k1} y_2 + A_k y_3) + ((A_c + C_c) \dot{y}_1 - B_c \dot{y}_2 + A_c \dot{y}_3) = f_{total_1} \quad (7.13)$$

For node $i = n - 1$:

$$(m + m_a) \ddot{y}_1 + ((A_k + C_{k_{n-1}}) y_{n-1} - D_{k_{n-1}} y_{n-2} + A_k y_{n-3}) + ((A_c + C_c) \dot{y}_{n-1} - B_c \dot{y}_{n-2} + A_c \dot{y}_{n-3}) = f_{total_{n-1}} \quad (7.14)$$

Now, all the differential equations as per nodes have been explained and given, the calculation of the partial differential equations can be thus continued with Newmark- β methods. Before carrying on, the ordinary differential equations need to solve can be concluded together clearly in matrix form again as Eq.7.15.

$$M \cdot \ddot{Y} + C \cdot \dot{Y} + K \cdot Y = F \quad (7.15)$$

Where the variables Y , \dot{Y} and \ddot{Y} are the displacement, velocity and the acceleration for nodes on discrete beam model accordingly. M here is the equivalent mass matrix of the beam model, K is the equivalent stiffness matrix, C is the equivalent damping matrix and F is the equivalent external force matrix of the beam model. Detailed composition for the overall pipeline model comprising three separate part is shown as Eq.7.16.

$$Y = \begin{bmatrix} y_1 \\ y_2 \\ \vdots \\ y_{t-1} \\ y_t \\ y_{t+1} \\ \vdots \\ y_{v-1} \\ y_v \\ y_{v+1} \\ \vdots \\ y_{n-2} \\ y_{n-1} \end{bmatrix} \quad \dot{Y} = \begin{bmatrix} \dot{y}_1 \\ \dot{y}_2 \\ \vdots \\ \dot{y}_{t-1} \\ \dot{y}_t \\ \dot{y}_{t+1} \\ \vdots \\ \dot{y}_{v-1} \\ \dot{y}_v \\ \dot{y}_{v+1} \\ \vdots \\ \dot{y}_{n-2} \\ \dot{y}_{n-1} \end{bmatrix} \quad \ddot{Y} = \begin{bmatrix} \ddot{y}_1 \\ \ddot{y}_2 \\ \vdots \\ \ddot{y}_{t-1} \\ \ddot{y}_t \\ \ddot{y}_{t+1} \\ \vdots \\ \ddot{y}_{v-1} \\ \ddot{y}_v \\ \ddot{y}_{v+1} \\ \vdots \\ \ddot{y}_{n-2} \\ \ddot{y}_{n-1} \end{bmatrix} \quad (7.16)$$

Where the term F is the combination of different pipeline parts, including the seabed pipelines, suspended pipeline and the fictitious part. Interfaces of these three parts are the touchdown point and the

vessel connection point. The external forces for these separate parts have already been stated as previous.

$$F = \begin{bmatrix} -\frac{1}{2}\rho C_d D_0 \dot{y}_1 |\dot{y}_1| - f_{soil_1} \\ -\frac{1}{2}\rho C_d D_0 \dot{y}_2 |\dot{y}_2| - f_{soil_2} \\ \vdots \\ -\frac{1}{2}\rho C_d D_0 \dot{y}_{t-1} |\dot{y}_{t-1}| - f_{soil_{t-1}} \\ -\frac{1}{2}\rho C_d D_0 \dot{y}_t |\dot{y}_t| - f_{soil_t} \\ \frac{1}{2}\rho D V_{t+1}^2 C_{VY_{t+1}} \\ \vdots \\ \frac{1}{2}\rho D V_{v-1}^2 C_{VY_{v-1}} \\ \frac{1}{2}\rho D V_v^2 C_{VY_v} \\ -c_{dp_f} \cdot \dot{y}_{v+1} \\ \vdots \\ -c_{dp_f} \cdot \dot{y}_{n-2} \\ -c_{dp_f} \cdot \dot{y}_{n-1} \end{bmatrix} \quad (7.17)$$

For the equivalent matrix of K , C and M in this beam model, the form of which are the same as that in the Eq.3.40, Eq.3.41 and Eq.3.39 separately. The difference is the dimension of the matrix has changed with the value of node number and the dimension of which are all in the form of $(n-1) \times (n-1)$ matrix. It also should be paid additional attention that the tension part in Eq.7.11 has changed while the intrinsic characteristic structural components in which remains the same.

7

The above mentioned process are the calculation model for static laying process with the fictitious part pipeline. Taking the simulation further that the dynamic laying process is considered, length of pipeline model in seabed and fictitious part will certainly change, the nodes divided initially as shown in Fig.7.2 will consequently moves as the space location of pipelines also moves. This will be very complicated if the nodes division changes as time goes by, which has certainly increase the complexity of the simulation. Thus another way of thinking is adopted by keeping the nodes division form as constant, while the force distribution has been changed according to the laying process. In other words, a specific nodes is attached to a fixed location in the pipeline, thus the recorded motion information for the node represents the motions of corresponding space location of the pipeline. During pipe laying process, nodes division illustration is shown as Fig.7.3. Where L_{lay} is the length of laying from initial position at a certain moment. N_{lay} is the integer value of nodes number contained in the laying length. l^* is the length between touchdown point and the adjacent node belonging to the seabed pipeline. Compared the nodes division for dynamic laying process in Fig.7.3 with the illustration for that before dynamic laying process in Fig.7.2, the touchdown point and the vessel connection point has changed their positions. Where the part before the TDP is seabed pipeline, the fictitious part locates after VCP and the suspended pipeline part is in-between. As also can be seen, the seabed pipeline is gradually increasing its length while the fictitious part is decreasing its length accordingly. The suspended pipeline remains its length as a constant

With the above mentioned model building process, every variable in the partial differential equations for the overall beam model has been explained and the transformed ordinary differential equations will be solved by using Newmark's method once the initial conditions of the beam model are given. Then the results are given as per time step. During solving process, the Jacobian matrix for this modified simulation model for dynamic laying process is given again in the Appendix C.

7.3. NUMERICAL RESULTS

Whether the dynamic laying process will influence the lateral bending shape of laid pipelines and how much the influence can be are the main research interests of this thesis, based on the foundation laid in previous chapters, results for the simulation model of it is shown in this section.

Here in the simulation example, length for seabed pipeline, suspended pipeline and the fictitious part are 500 m, 1109 m and 1000 m separately. The laying speed is assumed to be 1 m/s in this simulation, referring to the modelling time of 960 s here, the laying distance will be 960 m in this simulation. With these parameters defined and following the above mentioned procedures, lateral vibration can be solved and recorded as time goes on for the dynamic laying process.

The results for dynamic laying process is better to be seen in the simulation video, while for the thesis, 4 consecutive time moment during the simulation are chosen at which time the lateral vibration of the pipeline system are drawn. In Fig.7.4, time moments are chosen at 50 s, 300 s, 600 s and 960 s separately.

As can be seen in Fig.7.4, the dynamic laying process is well simulated from the very beginning at time 50 s to the simulation end. The length of suspended pipeline is constant. Seabed pipeline has an increasing length equalling to the decreasing length of fictitious part. At the mean time, TDP and VCP are used to differentiate the connection point among these three pipeline parts. As expected, the suspended pipeline are experiencing VIV throughout the modelling, the maximum amplitude of the lateral vibration in this region is about one diameter. The fictitious part is stationary before the the nodes in this part are released into the region of suspended pipeline, the process of which is elaborated in previous sections. The focus is the seabed pipelines, as more and more pipeline are laid onto the seabed, thus the as-laid pipeline are experiencing with more and more soil resistance. The already laid part, namely faraway from the TDP, may not be able to keep straight due to soil hinderance, thus a laying route deviating from the initial straight line may happens. This phenomenon has been captured by the model in Fig.7.4, where shows a trend that the the seabed pipeline is deviating from the straight configuration.

When the simulating process is done, at the time moment of 960 s, the maximum displacement for the seabed pipeline now is 0.04m, equalling to 0.15 time of outer diameter of the pipeline. This value is slightly larger than that in the static laying process as shown in Chapter 5. Further research are still needed to identify the major influential factors on the amplitude of maximum lateral vibration in dynamic laying process.

To continue, some representative nodes on the coupled pipeline system will be selected and the lateral vibration in time domain of which is illustrated here for the intention of gain further insights.

For the suspended pipeline, two nodes located at the length of 800 m and 1200 m have been selected

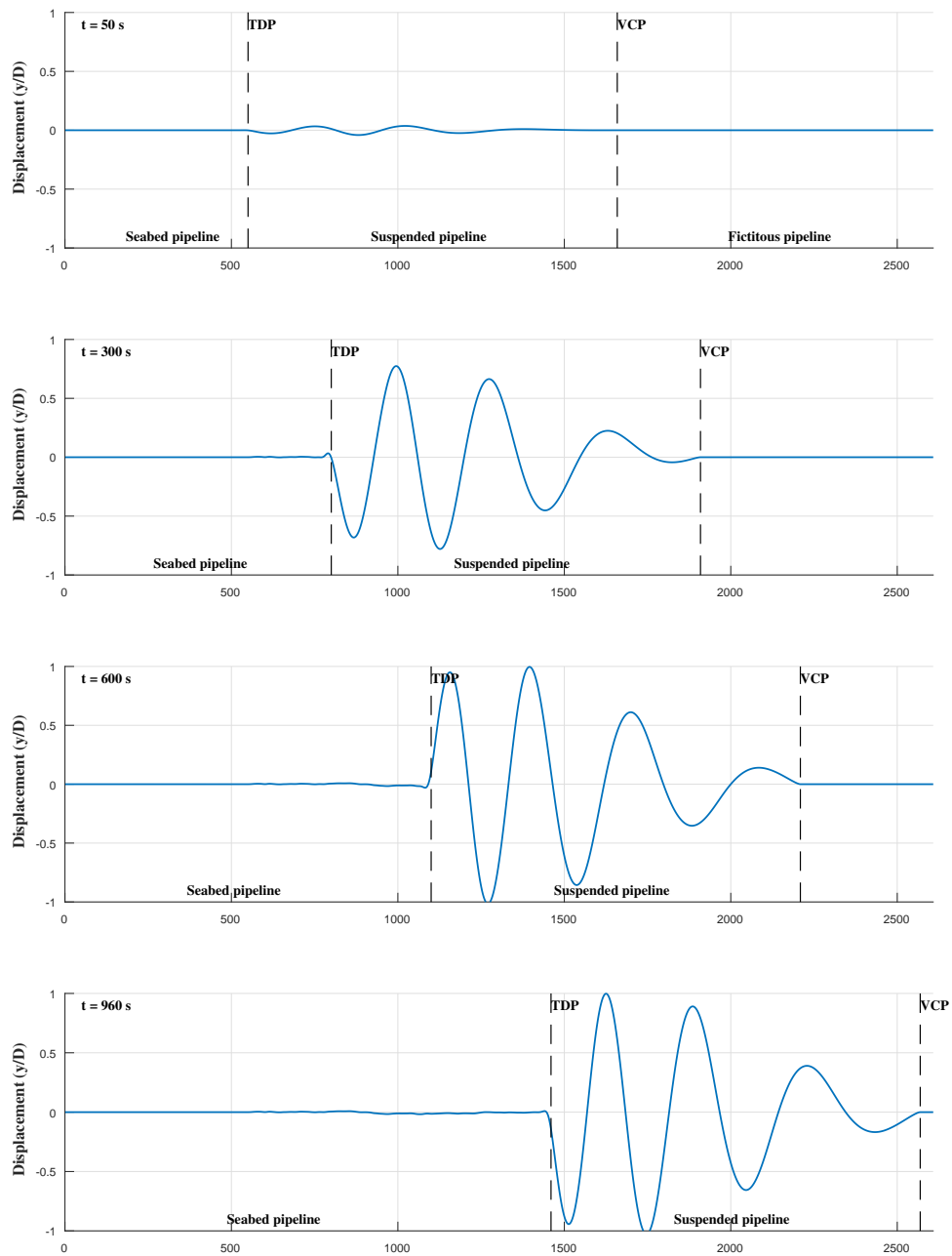


Figure 7.4: Laying process illustration at varying time moments

according to the coordinates in Fig.7.3. The lateral vibration of which through out the simulation is depicted in Fig.7.5.

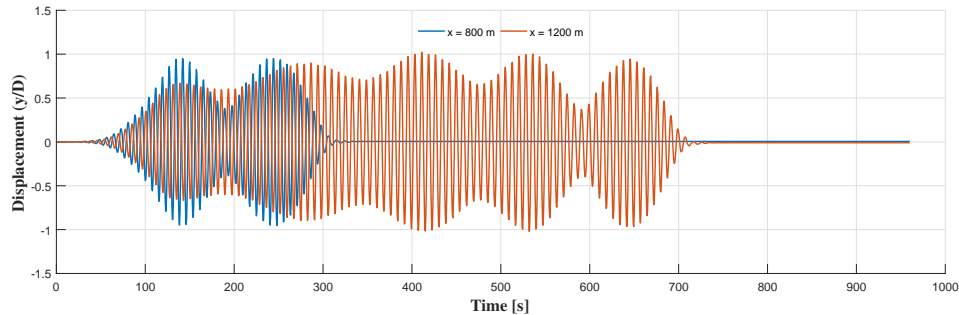


Figure 7.5: Lateral displacement for nodes on suspended pipeline

As can be seen from the above picture that, the node located at $x = 800\text{m}$ is relatively close to the seabed. When $x = 300\text{m}$, the nodes begin to touch the seabed and consequently undergoes the soil resistance, thus the amplitude of its vibration decreases very quickly and stop to vibrate with displacement of about 1.5 mm. While for comparison, the node at $x = 1200\text{m}$ undergoes the same process but at the time 400 s later. Finally it has a lateral displacement of about 3 mm. During the simulation process, it has mainly vibrated under the influence of VIV. When compared to Fig.4.6, the lateral vibration plot does not have the steady state yet with changing amplitudes. The reason for this may lay behind the redistribution of the VIV energy in the pipeline due to the relative alternation for the space positions of the nodes.

For the fictitious pipeline, two nodes located at the length of 1700 m and 2100 m have been selected, the lateral vibration of which is depicted in Fig.7.6.

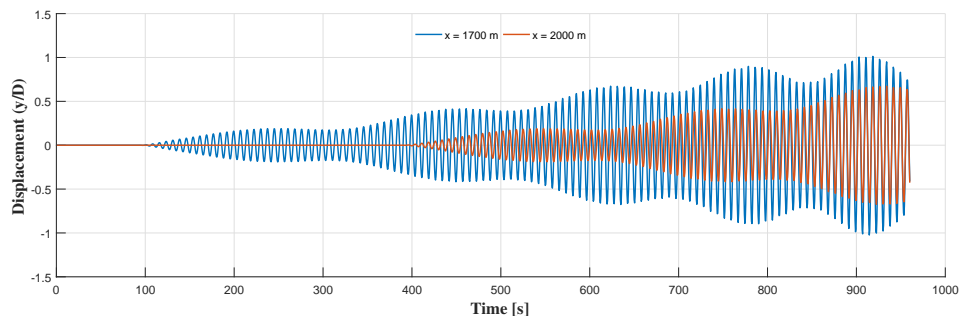


Figure 7.6: Lateral displacement for nodes on fictitious pipeline

The lateral vibration for fictitious nodes varies from that in the suspended part. As shown in Fig.7.6, the node at $x = 1700\text{m}$ only begins to vibrate at the time of about 100s after the node is released from

the fictitious part into the suspended pipeline at that time. The reason for this is due to the extremely large damping dashpot applied in the fictitious part before the nodes are released. The same situation occurs to node located at $x = 2100\text{m}$ later. After the nodes comes into the region of suspended pipeline, the VIV will plays the major role and the amplitude of which will increase as it was laid lower and lower approaching the seabed.

8

CONCLUSION

In this thesis, the numerical calculation models simulating the lateral vibration of pipeline system during J-lay process have been established step by step. Separate models for simulating pipe-soil interaction in seabed pipeline and VIV in suspended pipeline are proved to function well and coupled models for both pipeline part are further modified to incorporate the main features for the dynamic analysis with or without involvement of laying operations.

8.1. CONCLUSION

There are in total 5 simulation models for the lateral vibration of pipelines that have been built up from Chapter 3 to Chapter 7. They are summarized here as listed below:

- Seabed pipeline model focuses on the pipe-soil interaction.
- Suspended pipeline model includes the VIV mechanism.
- Coupled pipeline model analysis without considering the dynamic laying operation. This can be used to simulate the seabed walking for Steel Catenary Riser (SCR) due to VIV.
- Coupled pipeline model incorporates the influence of Touch Down Zone (TDZ).
- Coupled pipeline model considered the dynamic laying operations.

After the model verification process and simulation results analysis, several conclusions can be drawn here.

- The soil resistance is highly nonlinear and may present stick-slip phenomenon. It can holds the seabed pipeline in a bending shape.

- Creative methods have been developed in this thesis which helps solving static initial configuration of suspended pipeline considering boundary layer phenomenon (Stiffened Catenary) under effects of current flow.
- VIV in suspended pipeline is able to causing the bending shape of seabed pipeline around the connection location with soil resistance.
- The existence of **TDZ** magnifies the amplitude of bending shape in seabed pipeline.
- Dynamic laying operations leads the seabed pipeline to deviating from its straight configuration.

8.2. FURTHER STUDY

Apart from the researches have been done in this thesis, some future study can be propose here.

- The numerical models already acquired can be improved and recalibrated with comparison to suitable experimental results in practice.
- The coupling effects of **TDZ** and the pipe laying operations can be further coupled together in one simulation model for the purpose of acquiring more accurate results, though with plenty of work.
- Parameters study can be implemented for the influential factors contributing to the amplitude of lateral vibration, the effects of current speed and soil properties for example.

A

STATIC LAYING CONFIGURATION

Calculation for initial static configuration of suspended pipeline is an essential procedure, which needs to solve in advance of many other problems. In this research, the in-plane vibration of the pipeline system is not concerned. The pipeline system will be considered as keeping its static configuration in-plane.

The initial configuration of suspended pipeline directly decides the value for axial tension throughout the overall pipeline system including on-bottom pipelines. The tension is horizontal while changing its value for on-bottom pipeline as stated in Chapter 3. Moreover the axial tension for suspended pipeline is increasing from seabed to sea surface with cumulative weight of the pipeline. Besides, this research focuses on the out-of plane vibration of the pipeline and the initial in-plane configuration is a required reference. For the VIV of suspended pipeline, the information of initial static laying configuration is also required when the uniform current flows across the suspended pipeline.

The uniform flows will not only arouse large VIV in suspended pipeline but also will influence the initial configuration of that due to large accumulative in-plane drag force. Although the static initial configuration of coupling pipeline system is considered as consistent throughout the dynamic analysis process of lateral vibration for the pipeline system, the influence of current flow in-plane should be investigated into. The first part is the main deduction process for the static initial configuration without the effects of current flows, which is solved by analytical solution. The second part is the investigation of static initial configuration considering current flows, which is solved by numerical solution since the analytical solution is not applicable any more due to the complexity of current flow normalization on bending suspended pipeline. After that, some parameters study has also been conducted concerned with current flow properties.

A

A.1. STATIC INITIAL CONFIGURATION WITHOUT CURRENT

Solutions for the suspended pipeline during J-lay have been developed both analytically, yet with some approximations, and numerically. These analytical solutions vary from simple catenary shape to more precise model includes boundary layer assumption. In the boundary layer approach, the main parts of the suspended pipeline is considered as catenary. While for the boundary region for the suspended pipeline close to the seabed, the bending stiffness of the pipeline becomes dominant and the boundary layer is considered as a beam here. In the essay of Lenci, the influence of boundary layer phenomenon is of great important while the seabed stiffness only has scarce influence. Thus in the process for determining the laying configuration, the seabed stiffness is considered as infinite. The analytical calculation process below is mainly based on the previous work from Lenci 2005.

For the configuration of pipeline during deep sea laying process, the most simplest model for describing the initial shape is the catenary assumption. In which, the bending stiffness of the pipeline is neglected and the pipeline is seen as a cable model only loaded with tension instead of a beam model. While taking the boundary layer phenomenon into consideration, the problem can be solved through singular perturbation theory, which is thorough yet very exhaustive. The solution provided here is proposed based on the observation that in the suspended part, just ahead of the touch down point (TDP), the vertical displacement is small at a certain interval of unknown length L_1 , where the boundary phenomenon is going to occur. Thus the first part of the suspended pipeline is seen as a linear beam considering the bending stiffness. The model can be seen a combination of beam and cable as illustrated in Fig.A.1.

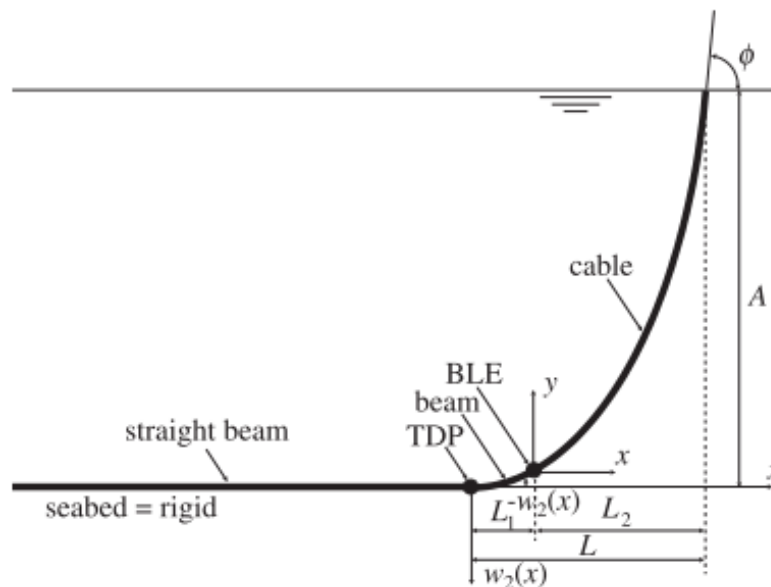


Figure A.1: Illustration for beam & cable model (Copyright from Lenci)

The governing equation for the beam part of the pipeline is written as

$$EIw_2''''(x) - Tw_2''(x) = p \quad (\text{A.1})$$

Where $w_2(x)$ is the deformed shape in the local coordinates system, the origin of which locates at the touch down point (TDP). The y-axis is upward vertical and x increases from the boundary layer end (BLE) points to the vessel. P is the constant submerged weight of the beam in unit length and T is the tension in the beam which is seen as also constant here. The related bending moment and shear force here are given by $M_2(x) = EIw_2''(x)$, $S_2(x) = -EIw_2'''(x)$ separately.

The general solution for Eq.A.1 is solved as Eq.A.2.

$$w_2(x) = -\frac{p}{2T}x^2 + c_3 + c_4x + c_5\sinh(\gamma x) + c_6\cosh(\gamma x), \quad 0 \leq x \leq L_1, \quad \left(\gamma = \sqrt{\frac{T}{EI}} \right) \quad (\text{A.2})$$

In the remaining part of the suspended pipeline, the assumption of simple cable catenary is used, namely in the range of $0 \leq x \leq L_2 = (L - L_1)$. It becomes apparent that the governing equation for this simple cable catenary is written as A.3. The interface condition for the connecting node of these two part at the boundary layer end point (BLE) would be given properly next.

$$y'' = \delta \sqrt{1 + [y'(x)]^2} \quad (\text{A.3})$$

The general solution for A.3 is the classical catenary equation.

$$y(x) = c_7 + \frac{1}{\delta} \cosh(\delta x + c_8), \quad L_1 \leq x \leq L \quad (\text{A.4})$$

Where $y(x)$ is the shape function for the cable part in the previous defined coordinate system. Here $\delta = p/H$, again p is the submerged weight in vertical direction and H is the constant horizontal tension. With reference to Eq.A.4, the slope angle can be easily understand given the first derivative of displacement equation, namely $\theta(x) = \arctan[y'(x)]$. The tension in the cable catenary can be derived as the following with reference to A.3.

$$\begin{aligned} \tilde{T} &= \sqrt{H^2 + (H \cdot y'(x))^2} \\ &= H \cdot \sqrt{1 + y'(x)^2} \\ &= \frac{p}{\delta^2} y''(x). \end{aligned} \quad (\text{A.5})$$

Here although the cable assumption does not include the meaning of bending, an approximation is derived here by the multiplication for bending stiffness and the curvature of the cable.

$$\tilde{M}(x) = EI \frac{d\theta}{ds} = EI \frac{d\theta}{dx} \frac{dx}{ds} = \frac{\delta^3}{[y''(x)]^2}$$

A

The approximated shear is also derived as the following equation after the bending moment is derived above.

$$\tilde{S}(x) = \frac{dM}{ds} = \frac{dM}{dx} \frac{dx}{ds} = -2EI\delta^6 \frac{y'(x)}{[y''(x)]^4}$$

. After all the variables defined for both beam part and cable part, the interface condition for these two parts and boundary conditions at both ends is written as Eq.A.6.

$$\text{TDP} \begin{cases} w_2(0) = 0, \\ w_2'(0) = 0, \\ M_2(0) = 0. \end{cases} \quad \text{BLE} \begin{cases} -w_2(L_1) = y(0), \\ -w_2'(L_1) = y'(0), \\ T = \tilde{T}(0), \\ M_2(L_1) = \tilde{M}(0), \\ S_2(L_1) = \tilde{S}(0). \end{cases} \quad \text{Vessel} \begin{cases} y(L_2) = A, \\ y'(L_2) = \tan \phi. \end{cases} \quad (\text{A.6})$$

To conclude, there are ten unknowns in the previous beam and cable equations including c_3 , c_4 , c_5 , c_6 , c_7 , c_8 , T , L_1 , L_2 , and δ . While the variables EI , p , A , and ϕ are given in this process. Since there are also ten boundary conditions and interface conditions in Eq.A.6. Thus the variables can be solved. It is worth mentioning that the solution process here is a little bit difficult since the equation group is highly non-linear. Before solving the equations, a few steps of deduce is performed first. The following part is to find the relations between these ten variables so as to simplify the calculation process. After the deduce, the conclusion comes that there are two variables T and L_1 which are the determinative. Once the value of these two variables are known, the other eight variables can be derived from these two clearly. Substituting the given variables into boundary condition at TDP in Eq.A.6, the following relations can be derived.

$$c_3 = -\frac{pEI}{T^2}, \quad (\text{A.7})$$

$$c_6 = \frac{pEI}{T^2}, \quad (\text{A.8})$$

$$c_4 = -\gamma c_5. \quad (\text{A.9})$$

To continue, when deal with the interface conditions for Boundary layer end (BLE), the following equations can be derived.

$$c_7 = -w_2(L_1) - \frac{1}{\delta} \cosh(c_8), \quad (\text{A.10})$$

$$\sinh(c_8) = -w_2'(L_1), \quad (\text{A.11})$$

$$w_2''(L_1) = -\frac{\delta}{\cosh^2(c_8)}, \quad (\text{A.12})$$

$$w_2'''(L_1) = 2\delta^2 \frac{\sinh(c_8)}{\cosh^4(c_8)}, \quad (\text{A.13})$$

$$\delta = \frac{p}{T} \cosh(c_8). \quad (\text{A.14})$$

At last, the boundary conditions at the vessel gives that

$$c_7 = A - \frac{1}{\delta \cos \phi}, \quad (\text{A.15})$$

$$\tanh(\delta L_2) = \frac{-\sinh(c_8) + \cosh(c_8) \sin \phi}{\cosh(c_8) - \sinh(c_8) \sin \phi}. \quad (\text{A.16})$$

$$(\text{A.17})$$

These equations are highly non-linear, thus some simplification should be made here in order to get trustful results. Some variables are strongly related to other variables and can be expressed using other variables. The simplified solution for this algebraic system can be derived by eliminating the variable c_7 in Eq.A.10 and Eq.A.15 and eliminating the variable δ in Eq.A.12 and Eq.A.13 by the expression of δ in Eq.A.14.

$$A - \frac{1}{\cos \phi} \frac{T}{p \cosh(c_8)} = -w_2(L_1) - \frac{T}{p}, \quad (\text{A.18})$$

$$w_2''(L_1) = -\frac{p}{T \cosh(c_8)}, \quad (\text{A.19})$$

$$w_2'''(L_1) = 2 \frac{p^2 \sinh(c_8)}{T^2 \cosh^2(c_8)}. \quad (\text{A.20})$$

To continue simplifying the equation in Eq.A.18, the expression for $\cosh(c_8)$ in Eq.A.19 can be substituted into Eq.A.18.

$$w_2(L_1) + \frac{T^2}{p^2 \cos \phi} w_2''(L_1) + A + \frac{T}{p} = 0, \quad (\text{A.21})$$

Eq.A.21 is intrinsically an equation of T and L_1 for the solution of c_5 . Thus after the above steps of simplification, the final solution of the algebraic system depends on the determination of T and L_1 . After solving these two variables, the other variables can be solved in sequence. From Eq.A.11, the expression for $\cosh(c_8)$ is written as $\cosh(c_8) = \sqrt{1 + [w_2'(L_1)]^2}$. While substituting this equation into Eq.A.19 and Eq.A.20, the final core algebraic system for T and L_1 only can be derived.

$$f_1(T, L_1) = w_2''(L_1) \sqrt{1 + [w_2'(L_1)]^2} + \frac{T}{L_1} = 0, \quad (\text{A.22})$$

$$f_2(T, L_1) = w_2'''(L_1) + 2w_2'(L_1) [w_2'(L_1)]^2 = 0. \quad (\text{A.23})$$

The equations above is the highly non-linear source of the whole algebraic system, and can be solved with classical methods such as Newton-Raphson method or other improved algorithms. Here in this research the non-linear equations are solved in Matlab, which accept the trust-region dogleg algorithm by default. The final answer is also verified through another solution method using Maple. There will appears many solutions and it is necessary to choose the answer with meaning and neglect the others.

After the variables are solved, the descriptive functions for the beam and cable part of the pipeline in

A

J-lay have been determined. With the given statistics in Tab.3.1 for this research, the final results for the initial configuration can be illustrated as Fig.A.2.

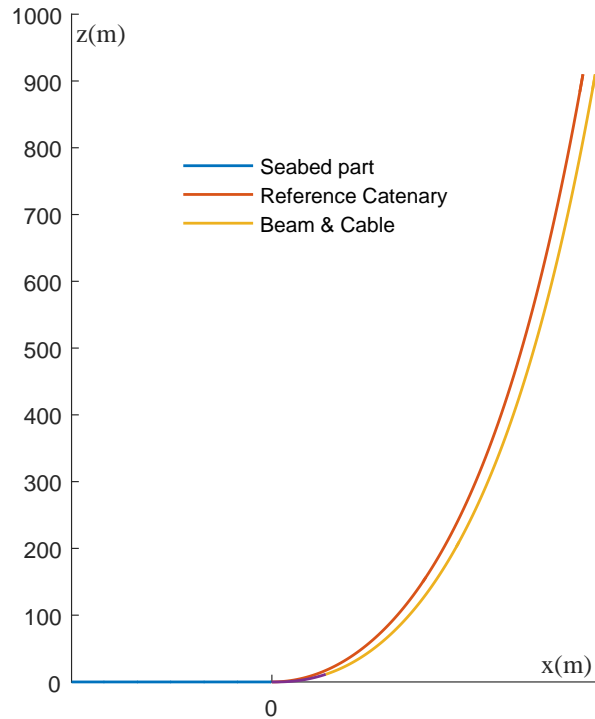


Figure A.2: Laying configuration for beam & cable model

A.2. STATIC INITIAL CONFIGURATION WITH CURRENT

The analysing procedures for initial static configuration of pipeline system has laid a strong foundation for the further research about extra effects of current flows. In Sec.A.1, the analytical solutions have been extracted by reasonable beam and cable assumption. The general solutions for the equations of equilibrium in both beam and cable part can be written out clearly since there is no current force appears, which is a highly non-linear external force due to the bending shape of the suspended pipeline. Thus in order to research into the effects of currents flow, numerical integration methods are adopted here.

Still taking boundary layer into consideration, the suspended pipeline is again considered as a combination of beam part and cable part as shown in Fig.A.1. The only difference is the appearance of current

flow as shown in Fig.A.3. Another reason adopting the same model is that the results acquired through different calculation methods can be compared and checked. Through the literature study work for such questions, there are no direct solutions found for considering boundary layer in current flow conditions. In Wang's thesis for the J-lay configuration problem, hydrodynamic force is taken into account while the suspended part pipeline is treated as cable in the whole part without considering the boundary layer. Thus improvement has been made in this research that both hydrodynamic forces and the boundary layer effects in J-lay problems. Several innovation points in this process have been developed. The boundary

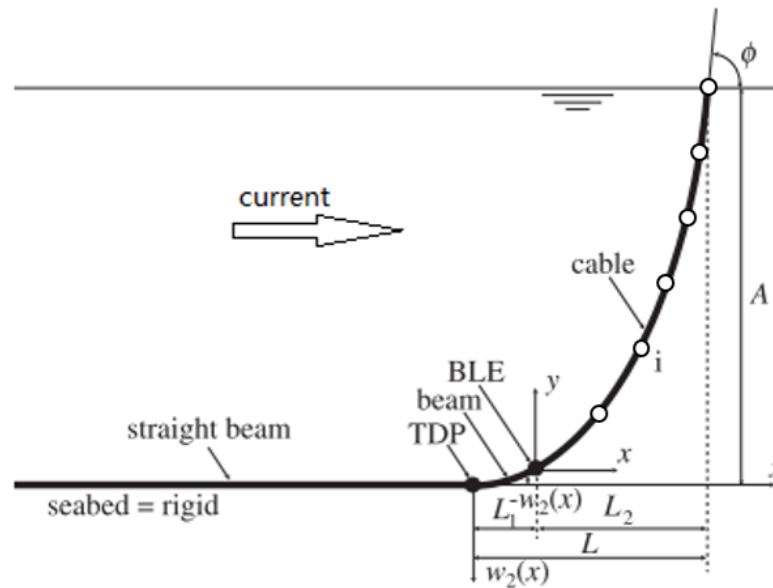


Figure A.3: Illustration for beam & cable model under currents

conditions in TDP and top end point of this model and the interface conditions in BLE remain the same as that in Sec.A.1 to guarantee the continuity of the model as. While there is no analytical solution for cable parts subjected to non-linear hydrodynamic force any more, and a numerical iteration process for the cable configuration in future will be exerted in the following process, thus the core problems here is to find a most suitable BLE point under a most appropriate top tension that can guarantee the continuity in TDP and BLE point as numerically given in Eq.A.6. Because there is no direct analytical solution, thus the position of BLE should be predefined here, with the horizontal length of L_1 and vertical height of h from the TDP. These two variables together with the top tension is core variables for the iteration as will be explained thoroughly in the following part.

Since the beam part is only a small portion of total suspended pipeline length, and locates around the TDP with deep depth where the current speed is usually small compared to that in large cable part, thus the beam part is under little influence of the current and the general solutions for this part is the same as

already stated in Sec.A.1. Again, the general solution for the beam part is given as:

$$w_2(x) = -\frac{p}{2T}x^2 + c_3 + c_4x + c_5\sinh(\gamma x) + c_6\cosh(\gamma x), \quad 0 \leq x \leq L_1, \quad \left(\gamma = \sqrt{\frac{T}{EI}}\right) \quad (\text{A.24})$$

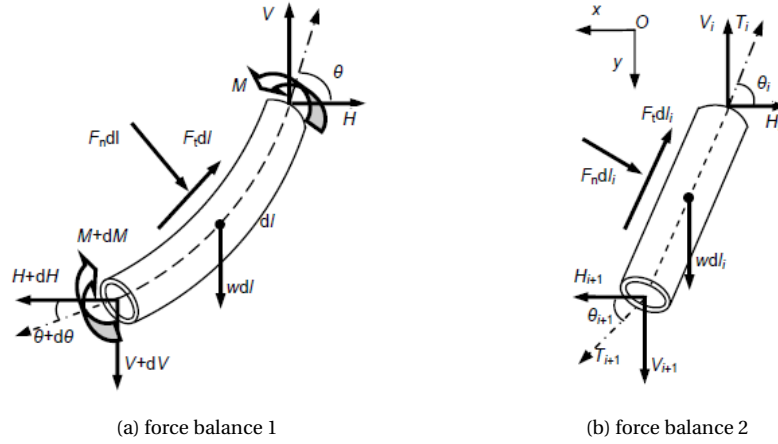


Figure A.4: Force balance of suspended pipeline segment (Copyright from Wang Lizhong)

While for cable part of suspended pipeline, the force balance has to be analysed with hydrodynamic force before continuing the numerical calculation. Now a small segment of suspended pipeline is considered as shown in Fig.A.4a. The pipe segment has a length of dl undergoing hydrodynamic loading, gravity and the internal forces. Taking the balance equilibrium of pipe segment in vertical direction, horizontal direction and the bending moment, one may get the following three equations,

$$dV = F_t dl \sin \theta - F_n dl \cos \theta - wdl, \quad (\text{A.25})$$

$$dH = F_n dl \sin \theta - F_t dl \cos \theta, \quad (\text{A.26})$$

$$dM = V dl \cos \theta - H dl \sin \theta. \quad (\text{A.27})$$

Where θ refers to the inclination slope of the suspended pipeline, w is the submerged weight for unit length of the suspended pipeline. The hydrodynamic forces here is calculated by the classical Morison's equation. The force can be divided into normal and tangential direction, F_n and F_t , as per the pipeline segment. These two equations are expressed by,

$$F_n = \frac{1}{2} \rho_{sea} C_n D (v \sin \theta)^2, \quad (\text{A.28})$$

$$F_t = \frac{1}{2} \rho_{sea} C_t D (v \cos \theta)^2. \quad (\text{A.29})$$

Where, the coefficients C_n and C_t are the drag force coefficients in normal and tangential direction separately. In this research, C_n is chosen at the value of 1.25 as the previously chosen value and C_t is 0.024 as recommended in Wilson's thesis. It should also be noticed that the direction of hydrodynamic force is related to that of current flow. When the current flow changes its direction, so is the hydrodynamic force.

The previous analysis are based on the pipeline segment subjected to bending moment, but for the suspended pipeline with sufficient length in sea water, it can be assumed as cable by neglecting the bending moment as already done in Sec.A.1. Thus for simplicity, the force balance illustrated in Fig.A.4a turns into the illustration in Fig.A.4b by neglecting bending moment. The balance equation for bending moment in Eq.A.27 has been simplified into

$$\frac{V}{H} = \tan\theta \quad (\text{A.30})$$

Where V and H are components of axial tension decomposed into vertical and horizontal direction separately. The axial strain and shear strain in suspended pipeline is neglected again, thus the following relations in Fig.A.4b can be derived as

$$dx = dl \cos\theta, \quad (\text{A.31})$$

$$dy = dl \sin\theta. \quad (\text{A.32})$$

Though the cable assumption of suspended pipeline here does not provide flexure, the bending moment value need to be solved in order to verify the continuity of bending moment in the BLE point between the beam and cable part. An approximation solution has been acquired here by multiplying the bending stiffness EI of the pipeline and the curvature at a certain point:

$$M(l) = EI\kappa(l) = EI \frac{\partial\theta}{\partial l} \quad (\text{A.33})$$

After the theoretical background are prepared above, the numerical iteration process can be continued for the configuration of cable part, given an initial tension T_1 at the VCP and the height h of BLE point. Now, the vertical length of cable part pipeline is $A - h$, which can be divided into n elements. Each element has the vertical length of dy and are numbered increasingly from top end to the BLE point as shown in Fig.A.3. For an element i in the cable part, the iteration process can be concluded as:

$$x_{i+1} = x_i + \frac{dy}{\tan\theta_i}, \quad (\text{A.34})$$

$$y_{i+1} = y_i + dy, \quad (\text{A.35})$$

$$dl_i = \frac{dy}{\sin\theta_i}, \quad (\text{A.36})$$

$$V_{i+1} = V_i + F_{ti}dl_i \sin\theta_i - F_{ni}dl_i \cos\theta_i - wdl_i, \quad (\text{A.37})$$

$$H_{i+1} = H_i + F_i dl_i \cos\theta_i + F_{ni} dl_i \sin\theta_i, \quad (\text{A.38})$$

$$\theta_{i+1} = \arctan \frac{V}{H}, \quad (\text{A.39})$$

A

Note that the boundary conditions at the VCP is intrinsically satisfied as the starting point during the iteration process. Through the iteration process of cable part, the configuration of cable can be built up from the vessel connection point ($i = 1$) to the boundary layer end point ($i = n + 1$). The information of all the nodes in cable part including the x , y , dl , V , H , θ are solved in cascade. In order to guarantee the continuity of beam and cable part pipeline at BLE point, the first two interface conditions in Eq.A.6 are used here, which ensure the displacement and slope continuity of these two parts. Substituting Eq.A.24 into these two interface conditions, the following equations can be acquired,

$$-\frac{p}{2T_{n+1}}L_1^2 + c_3 + c_4L_1 + c_5\sinh(\gamma L_1) + c_6\cosh(\gamma L_1) = A - y_{n+1} = h, \quad (\text{A.40})$$

$$-\frac{p}{T_{n+1}}L_1 + c_3 + c_4 + \gamma c_5\cosh(\gamma L_1) + \gamma c_6\sinh(\gamma L_1) = \tan(\theta_{n+1}), \quad (\text{A.41})$$

Moreover, the first two boundary conditions at TDP in Eq.A.6 can be derived as the following equations with general solution of the beam part.

$$C_3 + C_6 = 0, \quad (\text{A.42})$$

$$C_4 + \gamma C_5 = 0, \quad (\text{A.43})$$

The four unknowns C_3 , C_4 , C_5 and C_6 control the shape of beam part pipeline and can be solved through Eq.A.40 Eq.A.43 if the value of variable L_1 is given. L_1 here is the variable for identifying the magnitude of boundary layer horizontal length, the value of which usually varies within a certain range. Thus the initial tension T_1 , BLE height h , boundary layer length L_1 are the core variables for the iteration process. If these three variables are given, the configuration for both beam part pipeline and the cable part pipeline can be settled through the above deduction process. The next step is to check the validity of the given value for T_1 , h and L_1 . The criterion is the other unused boundary conditions and interface conditions must be satisfied within an acceptable predefined small number. To elaborate, the continuity of bending moment and shear force at the BLE point and the bending moment in TDP should be close to zero in accord with the assumption that the soil stiffness is infinite as per the initial configuration problem.

It is also worth mentioning here that backward difference method is used for the curvature derivation at BLE point. Before which, the necessary information of slope angle θ_i at each node in cable part are known through iteration process. It should be noted here, the writer had also checked the method of curve fitting for calculation of curvature at BLE point in cable part, but the results has large deviation, which is not to be recommended here. The other necessary information is the variable of dl_i is also recorded in the same process. Calculation of curvature at BLE point in beam part becomes easier since the analytical equation of beam is already derived with all unknown coefficients solved. The results can be compared then. For the curvature at TDP, it is calculated through the same process with analytical solution, the value of which is compared with zero according to the assumption. Only if all the conditions are satisfied, the given combination value for the T_1 , h and L_1 are adoptable, which means that the initial configuration of the suspended pipeline are solved.

Furthermore, the range of predefined value for the three core variables are discussed here. For the initial tension given in at the VCP, the value of which is initially set as $T_1 = 1.1 wA$. After the above process are conducted, the vertical force in each node of the cable part should be checked to guarantee that value of vertical force at any nodes of the cable part is bigger than zero ($V_i \geq 0$), which means that the tension at the VCP is large enough to support the pipeline. If there appears any vertical force ($V_i < 0$), the initial tension must be subsequently increased unless the criterion is satisfied. After which the iteration process can be continued, T_{n+1} and θ_{n+1} in Eq.A.41 can be thus used. Here the value of L_1 and h are predefined within a reasonable range around the exact value calculated in the analytical solutions by Lenci's method in Sec.A.1.

The whole calculation process is illustrated in the flow chart as Fig.A.5. It is clearly shown that the possible value for L_1 and h are distributed in the space range, represented by $L_{1lower} \leq L_1 \leq L_{1upper}$ and $h_{lower} \leq h \leq h_{upper}$. The range used here is calculated based on the solution from Lenci's method, the typical searching range for both variables L_1 and h used here are $\pm 20\text{m}$ and $\pm 10\text{m}$ separately. Notice that larger searching range often means the increasing demand for computational time. Thus for improvement, the solution can also be sought step by step. In the first step, a relatively larger mesh grid can be divided in order to find a solution with less accuracy but the calculation process of which can be rather quick. Then the next step is to have the mesh grid around the preliminary solution divided finer, the solution can be derived with more and more accuracy. It is also should be noted here that this is a highly non-linear problem, many answers may appear if a relatively large ϵ is accepted. Thus extra efforts must be paid here in the selection process. The acceptable value of ϵ is set as 1×10^{-5} here in this research.

With the above calculation process done, the initial configuration of suspended pipeline is acquired under the effects of currents. Some comparison work will be done in the following.

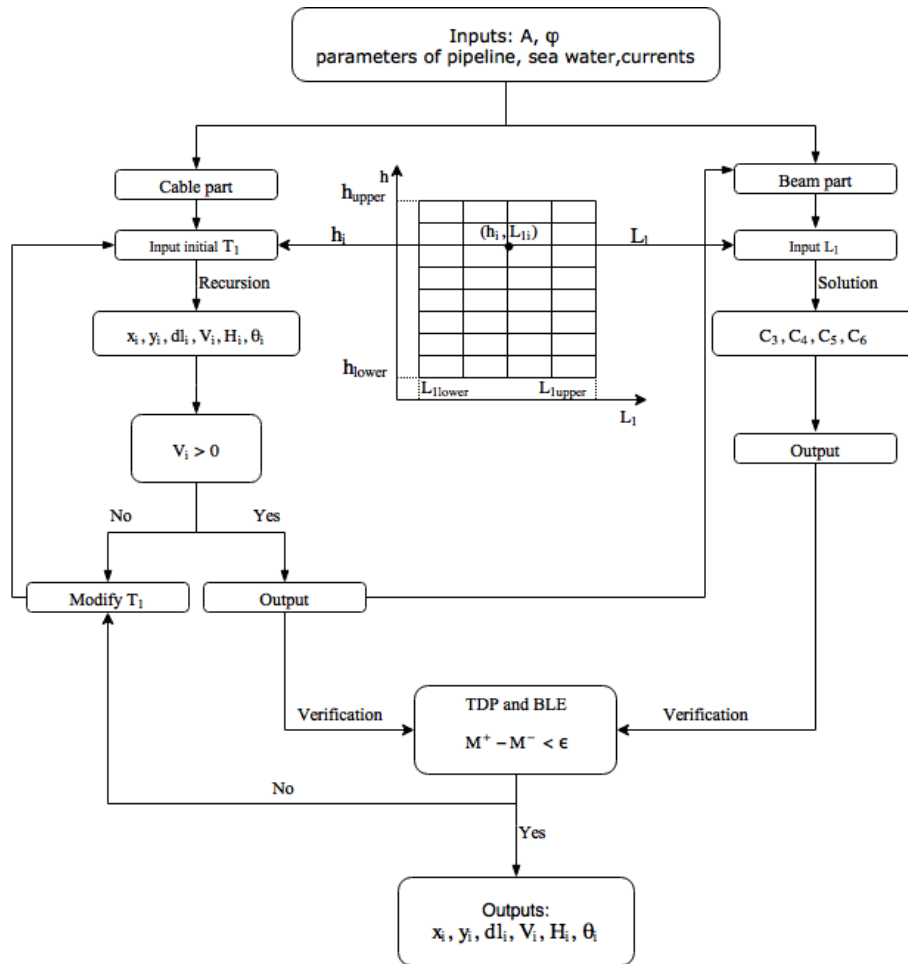


Figure A.5: Calculation process illustration

Verification for the model

After the calculation model is set up, verification work must be conducted before carrying on. The current speed is set as zero in the calculation model, such problem solved by the new model becomes the same as that in typical Lenci's thesis. Comparison between these two model has been checked after the results is calculated out. The comparison results is shown in Fig.A.6. As can be shown clearly in Fig.A.6, the reference results from Sec.A.1, are depicted in solid lines. Reference catenary line here is the results for considering the whole pipeline as a cable without boundary layer. While taking boundary layer into consideration, the beam and cable part in Lenci's method are depicted separately, namely the reference beam and reference cable. Results from new models are illustrated here by the dash line, once again, there are two parts including beam and cable part for the suspended pipeline considering the boundary layer.

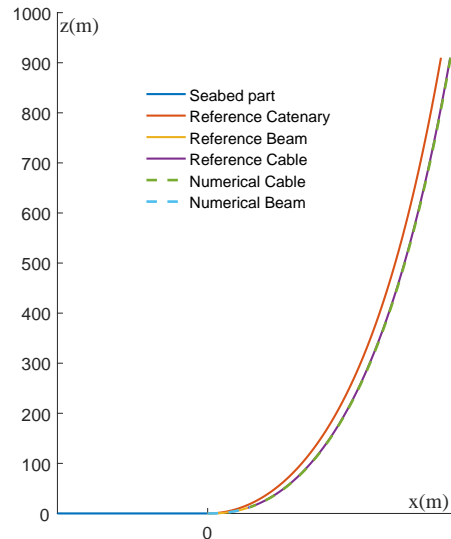


Figure A.6: Comparison between Lenci's model and the new model

From the picture, one may find that the difference between these two models are acceptable and nearly the same for the situation of no current flow involved. Conclusion can be drawn that this new model here is a success and is also trustful here.

Influence from different current speed

After the verification work done in last part, the new model is used for the calculation of initial configuration under the influence of varying current speed, which has been set here as $-1, -0.5, 0, 0.5, 1, 1.5$ m/s. Note that the positive current direction is the same as the horizontal axis in the figure. As per the negative direction for current, the model can only work in a certain range. It has already been checked that for negative current speed up to nearly -1.2 m/s together with other parameters in this research, the pipeline will not keep its shape as a similar catenary shape and become nearly straight or has a inverse bending shape. This calculation model will not be available again, which has also beyond our scope of research.

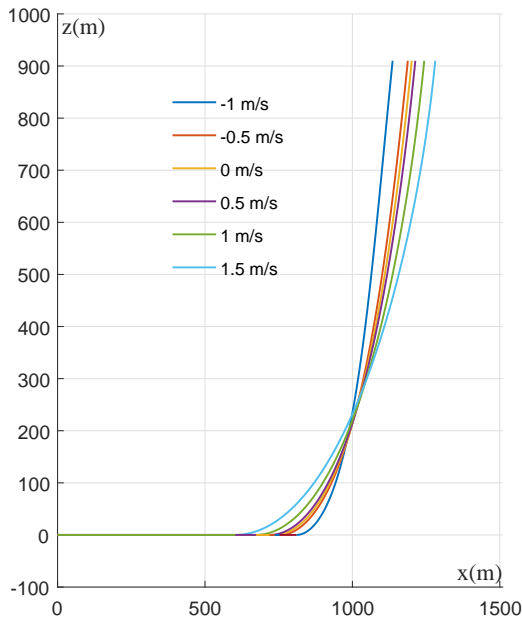
Fig.A.7a has been a reference for the situation that the whole suspended pipeline is seen as pure catenary. While Fig.A.7b is the illustration of results for beam and cable model. Fig. A.7c is the comparison of this two results. Dashed line here represents beam & cable model, solid line is the results for cable part. These two results has large similarity as per the bending shape. The main difference mainly exists in the boundary layer region when the figure is zoomed in around the TDP. While for the large cable part of suspended pipeline, the difference is small. The boundary layer phenomenon becomes more and more important with increasing negative current speed value and vice versa.

A

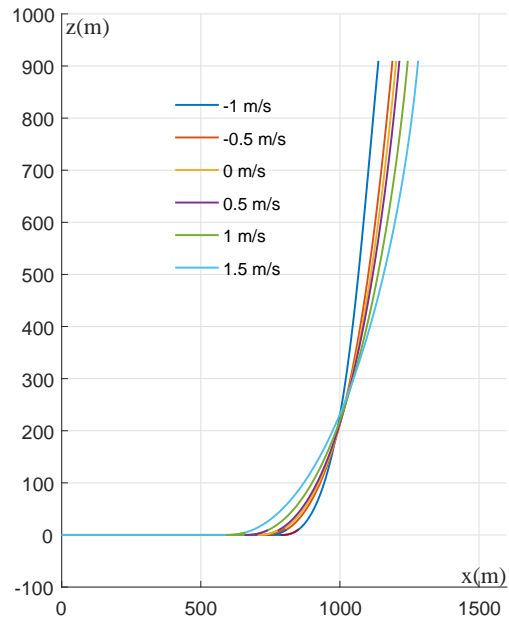
Influence of current profile

All the above mentioned results are based on the linearly distributed current speed. Current speed at the sea level has maximum value and the speed of which becomes zero at the seabed. Here in this part, another constant current profile from the sea level to the seabed level is used, in which the current speed are considered constant throughout the water depth.

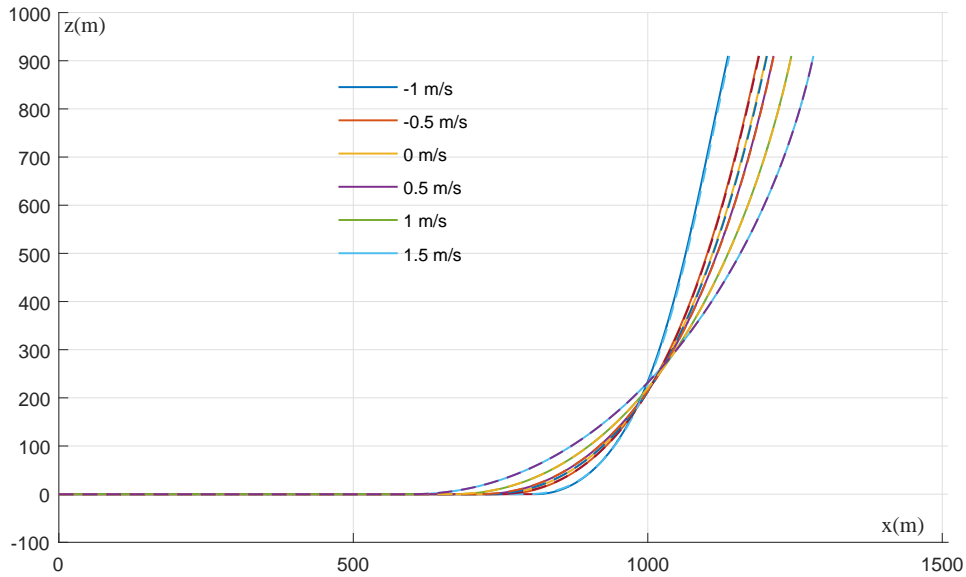
The results is shown in Fig.A.8, solid lines represent the outcomes from shear current settings and dashed lines refer to results from constant current profiles. With larger hydrodynamic forces results from different current speed setting, the bending shape becomes more and more explicit.



(a) Cantenary



(b) Beam & Cable



(c) Comparison

Figure A.7: Results for difference currents speed

A

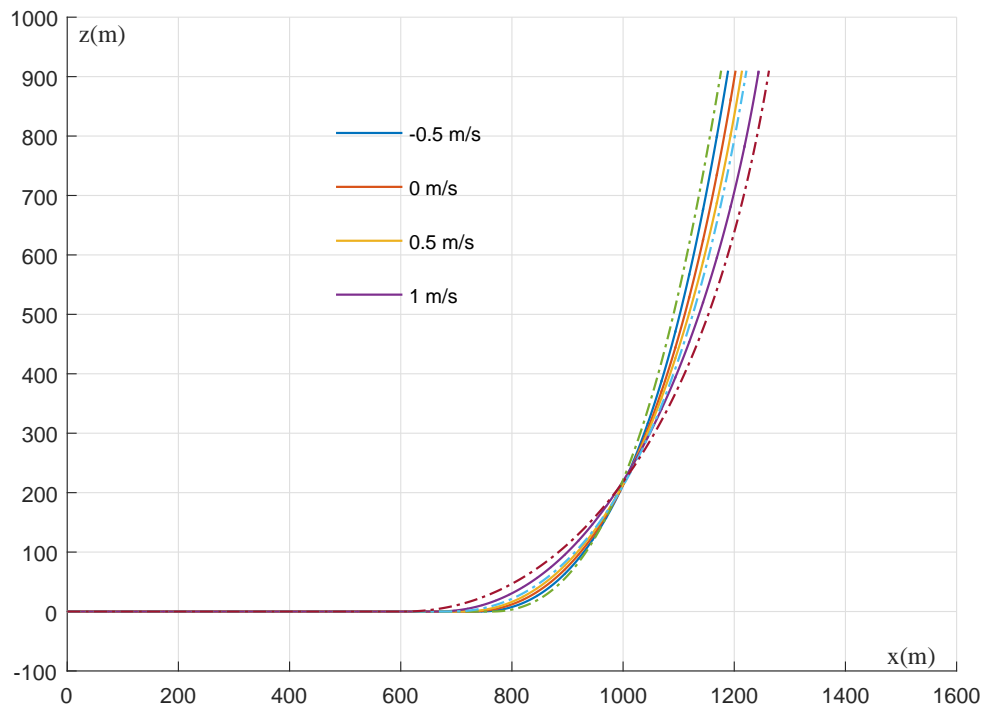


Figure A.8: Different current profile comparison

B

VIV DEDUCE

As stated in Chapter 4, the coupling mechanism of VIV for cylinders have been modelled in many ways. The Van der Pol type wake oscillator model is used in this research, which is based on the thesis of Facchinetti. The coupling mechanism for flow past pipeline has been already elaborated both in Sec.2.2 and Sec.4.2. In this appendix, some supplementary deduce will be stated here.

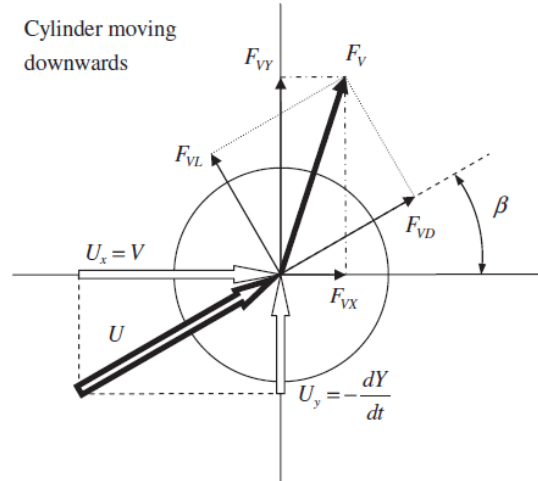


Figure B.1: Fluid force for the pipeline segment (Copyright from Ogink)

The illustration for the flow past cylinder is like Fig.B.1, where the incident current is in the x direction and the cylinder is moving in the y direction. As in this research, only the cross-flow vibration of the

pipeline is focused, namely the y direction in Fig.B.1. Motion in the in-line flow direction are insignificant and thus neglected.

As shown in Fig.B.1, the cylinder is experiencing a vibration velocity of $\frac{dY}{dt}$, and the incident current has the velocity of V . Thus the relative velocity between current and cylinder in this case is:

$$U = \sqrt{U_x^2 + U_y^2} = \sqrt{V^2 + \left(\frac{dY}{dt}\right)^2} \quad (\text{B.1})$$

Here also comes the meaning for angle β , which is the angle between relative velocity U and the x axis. The definition is given as:

$$\sin \beta = \frac{U_y}{U} \quad \text{and} \quad \cos \beta = \frac{U_x}{U} \quad (\text{B.2})$$

Moreover, the force between cylinder and the current are the most important components for the following analysis. The total hydrodynamic force is F_V and can be decomposed into F_{VX} of in-line direction, and F_{VY} of cross-flow direction. Another way of decomposition is F_{VD} , and F_{VL} , which are the drag and lift force separately with respect to the relative velocity U . For the convenience of following calculation, decomposition of fluid force into x and y direction is selected. While the value of drag and lift force are investigated and can be expressed by drag and lift coefficients based on many studies. From Fig.B.1, the relation between F_{VX} , F_{VY} and F_{VD} , F_{VL} are deduced as the following:

$$F_{VY} = F_{VD} \sin \beta + F_{VL} \cos \beta \quad (\text{B.3})$$

Introducing the dimensionless coefficients for the force term, the above equation can be transformed into:

$$\frac{1}{2} \rho D L V^2 C_{VY} = \frac{1}{2} \rho D L U^2 C_{VD} \sin \beta + \frac{1}{2} \rho D L U^2 C_{VL} \cos \beta \quad (\text{B.4})$$

To make it clear, the above equations can be further simplified into :

$$C_{VY} = (C_{VD} \sin \beta + C_{VL} \cos \beta) \frac{U^2}{V^2} \quad (\text{B.5})$$

Where C_{VL} is defined as linearly proportional to wake variable q as $C_{VL} = \frac{C_{L0} q}{2}$, which is based on the analysis of Faccinetti et al. C_{VD} is defined as $C_{VD} = C_{D0}$. The value of C_{L0} and C_{D0} are experienced value acquired from experiments. With the equation for C_{VY} established, the following numerical calculation can be continued. The same deduce process can be conducted if the in-line force components are considered.

C

NUMERICAL SOLUTION

The equations of motion for the beam model are simplified from partial differential equations to ordinary differential equations of time, the process of which has already been deduced in detail. The next task is to seek solutions for these differential equations as a function of derivative of time. Analytical solution can not be acquired due to the high complexity of the beam model loading terms. Instead, the numerical approximation to the exact solutions are adopted in practical engineering use. Several numerical methods for the differential equations are developed based on the idea of numerical integration. Among these numerical methods, Euler method, Newmark-beta method, Wilson- θ method, Runge-Kutta methods and some commercial softwares are the mostly used. These methods are based on time-domain analysis of the system.

C.1. NEWMARK- β METHOD

In this research, the simplified ordinary differential equations contains highly nonlinear terms for soil force and wake lift force. Thus Newmark-beta method are adopted due to its convenience for the numerical estimation of the dynamic response of structures. This method is first suggested by Professor Nathan Newmark in 1959.

For a given problem in time domain as defined in Eq.C.1 for time step j , the essence of this method is to seek solutions for the governing equations in next time step $j + 1$ as given in Eq.C.2.

$$M\ddot{y}_j + C\dot{y}_j + Ky_j = f_j \quad (C.1)$$

\Downarrow

$$M\ddot{y}_{j+1} + C\dot{y}_{j+1} + Ky_{j+1} = f_{j+1} \quad (C.2)$$

For the relation of acceleration, velocity and displacement between two time steps, the following de-

duce process are shown as below. The extended mean value theorem are used in Newmark- β method, thus the velocity and displacement for time step $j + 1$ are given as:

$$\dot{y}_{j+1} = \dot{y}_j + \Delta t \ddot{y}_\gamma \quad (\text{C.3a})$$

$$y_{j+1} = y_j + \Delta t \dot{y}_j + \frac{1}{2} \Delta t^2 \ddot{y}_\beta \quad (\text{C.3b})$$

Where the expression \ddot{y}_γ and \ddot{y}_β are defined as the following:

$$\ddot{y}_\gamma = (1 - \gamma) \ddot{y}_j + \gamma \ddot{y}_{n+1} \quad 0 \leq \gamma \leq 1 \quad (\text{C.4a})$$

$$\ddot{y}_\beta = (1 - 2\beta) \ddot{y}_j + 2\gamma \ddot{y}_{n+1} \quad 0 \leq 2\beta \leq 1 \quad (\text{C.4b})$$

Substitute the Eq.C.4 into Eq.C.3 separately, the expression can be further derived as:

$$\dot{y}_{j+1} = \dot{y}_j + (1 - \gamma) \Delta t \ddot{y}_j + \gamma \Delta t \ddot{y}_{j+1} \quad (\text{C.5a})$$

$$y_{j+1} = y_j + \Delta t \dot{y}_j + \frac{1 - 2\beta}{2} \Delta t^2 \ddot{y}_j + \beta \Delta t^2 \ddot{y}_{j+1} \quad (\text{C.5b})$$

The above are core relations for the displacement, velocity, and acceleration between time steps in Newmark method. Also in the deduce process, parameter γ and β are used to control the variation of acceleration between the time step. Different values will definitely influence the stability and accuracy of the method in solve actual problems. Reasonable value of γ is equal to 0.5 here and the value of β are chosen as 0.25 here, which is the special case for constant average acceleration and the method becomes unconditionally stable as checked through Eq.C.6. The judgement for the stability of Newmark- β method are:

$$\frac{\Delta t}{T_j} \leq \frac{1}{\pi\sqrt{2}} \frac{1}{\sqrt{\gamma - 2\beta}} \quad (\text{C.6})$$

In Newmark- β method, the solution at time step $j + 1$ is directly concerned with the equation of motion at time $j + 1$, which means this method belongs to the implicit method. Generally, iterations would have been required to reach the solution especially for nonlinear systems. But for linear systems, it was shown that iteration were avoided. To continue the deduce process, acceleration \ddot{y}_{j+1} can be acquired from Eq.C.5b.

$$\ddot{y}_{j+1} = \frac{1}{\beta(\Delta t)^2} (y_{j+1} - y_j) - \frac{1}{\beta\Delta t} \dot{y}_j - \left(\frac{1}{2\beta} - 1\right) \ddot{y}_j \quad (\text{C.7})$$

Then substitute \ddot{y}_{j+1} derived into Eq.C.5a, the expression for velocity \dot{y}_{j+1} is as:

$$\dot{y}_{j+1} = \frac{\gamma}{\beta\Delta t} (y_{j+1} - y_j) - \left(1 - \frac{\gamma}{\beta}\right) \dot{y}_j + \Delta t \left(1 - \frac{\gamma}{2\beta}\right) \ddot{y}_j \quad (\text{C.8})$$

Substituting Eq.C.8 and Eq.C.7 into the equations of motions for time step $j + 1$, the following expression

is given by:

$$\hat{K}y_{j+1} = \hat{f}_{j+1} \quad (\text{C.9})$$

Where in Eq.C.9,

$$\hat{K} = K + \frac{\gamma}{\beta\Delta t}C + \frac{1}{\beta(\Delta t)^2}M \quad (\text{C.10a})$$

$$\hat{f}_{j+1} = f_{j+1} + \left(\frac{1}{\beta(\Delta t)^2}M + \frac{\gamma}{\beta\Delta t}C\right)y_j + \left(\frac{1}{\beta\Delta t}M + \left(\frac{\gamma}{\beta} - 1\right)C\right)\dot{y}_j + \left(\left(\frac{1}{2\beta} - 1\right) + \Delta t\left(\frac{\gamma}{2\beta} - 1\right)C\right)\ddot{y}_j \quad (\text{C.10b})$$

For a linear system, the only unknown y_{j+1} can be solved directly by Eq.C.11 with the other variables known or expressed by y_{j+1} . After the solution of y_{j+1} , velocity and acceleration can be calculated by Eq.C.7 and Eq.C.8.

$$y_{j+1} = \hat{f}_{j+1} / \hat{K} \quad (\text{C.11})$$

While for a nonlinear system in this research, the external force f_{j+1} in the right-hand side of Eq.C.10b is also related to the unknown variable y_{j+1} in an implicit nonlinear manner. Thus in the solving process of the variable f_{j+1} , iteration method must be used. Generally, iterative methods like the basic Newton-Raphson method can be used in this situation. In this research, the nonlinear equations are solved by MATLAB for convenience. After the solution for y_{j+1} is acquired after iteration. Again, the velocity and acceleration for time step $(j + 1)$ can be computed through Eq.C.7 and Eq.C.8. Then the above mentioned process is repeated for the next time step.

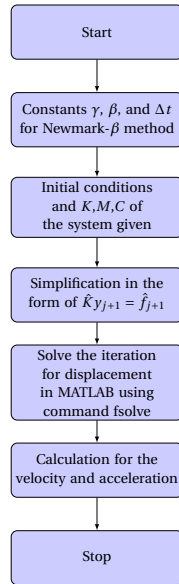


Figure C.1: Illustration for Newmark- β method

C.2. JACOBIAN MATRIX

While the Newmark- β method mentioned above are used for nonlinear system in this research, the iteration procedure must be taken into consideration. In this research, the iteration process are conducted by MATLAB using the built-in program of 'fsolve', which is based on the nonlinear least-squares algorithms. During the solving process, built-in program in 'fsolve' will approximate the Jacobian matrix for the nonlinear equations system need to be solved. Such approximation is applied by finite differencing method, which is rather time-consuming. Thus in order to improve the calculation speed for this large groups of nonlinear equations, Jacobian matrix for which should be provided beforehand.

The beam models in this research is divided into n element with $n + 1$ nodes. Moreover, the equations of motions for this beam model has the number of $n - 1$ due to the simplification of boundary conditions, which is written explicitly as Eq.C.12. These equations are further expressed in detail as shown in the equations of motion in Chapter 3, Chapter 4, Chapter 5 for the beam models.

$$\begin{cases} F_1 = f_1(y_1, \dots, y_{n-1}) \\ \vdots \\ F_{n-1} = f_{n-1}(y_1, \dots, y_{n-1}). \end{cases} \quad (\text{C.12})$$

Thus the mathematical models for the first order partial derivatives of these equations are referred to Jacobian as the following:

$$J(y_1, \dots, y_{n-1}) = \begin{bmatrix} \frac{\partial F_1}{\partial y_1} & \dots & \frac{\partial F_1}{\partial y_{n-1}} \\ \vdots & \ddots & \vdots \\ \frac{\partial F_{n-1}}{\partial y_1} & \dots & \frac{\partial F_{n-1}}{\partial y_{n-1}} \end{bmatrix} \quad (\text{C.13})$$

With the definition for the Jacobian matrix above, the specific Jacobian matrix for beam models can be deduced afterwards. For the beam models of seabed pipeline part, the equations of motion for which is shown as Eq.3.23. This can be further simplified into Eq.3.36. The first and second order time derivative of unknown y_n can be substituted through Newmark- β method as in Eq.C.7 and Eq.C.8. Then the Jacobian matrix for this soil model can be written as

$$\begin{aligned} J_b &= M_b \cdot \frac{\partial \ddot{y}_i}{\partial y_i} + C_b \cdot \frac{\partial \dot{y}_i}{\partial y_i} + K_b - \frac{\partial f_{drag}}{\partial y_i} - \frac{\partial f_{soil}}{\partial y_i} \\ &= \frac{1}{\beta(\Delta t)^2} \cdot M_b + \frac{\gamma}{\beta \Delta t} \cdot C_b + K_b + \frac{\gamma}{\beta \Delta t} \frac{1}{2} \rho C_d D (\text{sgn}(\dot{y}_i) \cdot \dot{y}_i + |\dot{y}_i|) \cdot E + k_s A' \cdot E' \end{aligned} \quad (\text{C.14})$$

Where the variables and matrix are all defined in the beam model for seabed pipeline, except E is the unit matrix has the same dimension as of M_b , C_b and K_b in the seabed pipeline beam model. Moreover, matrix E' has the same dimension as the above matrices while is only valid in elements through the judgements of the soil model as illustrated in Fig.3.6.

While for the Jacobian matrix in suspended pipeline beam model, there is a little difference. The

equations of motion have double number of divided nodes due to the coupling terms of wake variable for each node. Thus the Jacobian matrix for suspended beam model is also the coupling results of both displacement variable y_i and the wake variable q_i . The new Jacobian matrix are shown as the following according to the assembly method of the nonlinear equation group for solving the coupling equations.

$$J_s = \left[\begin{array}{c|c} J_s & J_{s-q} \\ \hline J_{q-s} & J_q \end{array} \right] = \left[\begin{array}{cc|cc} \frac{\partial F_{s_1}}{\partial y_1} & \dots & \frac{\partial F_{s_1}}{\partial y_{n-1}} & \frac{\partial F_{s_1}}{\partial q_1} & \dots & \frac{\partial F_{s_1}}{\partial q_{n-1}} \\ \vdots & \ddots & \vdots & \vdots & \ddots & \vdots \\ \frac{\partial F_{s_{n-1}}}{\partial y_1} & \dots & \frac{\partial F_{s_{n-1}}}{\partial y_{n-1}} & \frac{\partial F_{s_{n-1}}}{\partial q_1} & \dots & \frac{\partial F_{s_{n-1}}}{\partial q_{n-1}} \\ \frac{\partial F_{q_1}}{\partial y_1} & \dots & \frac{\partial F_{q_1}}{\partial y_{n-1}} & \frac{\partial F_{q_1}}{\partial q_1} & \dots & \frac{\partial F_{q_1}}{\partial q_{n-1}} \\ \vdots & \ddots & \vdots & \vdots & \ddots & \vdots \\ \frac{\partial F_{q_{n-1}}}{\partial y_1} & \dots & \frac{\partial F_{q_{n-1}}}{\partial y_{n-1}} & \frac{\partial F_{q_{n-1}}}{\partial q_1} & \dots & \frac{\partial F_{q_{n-1}}}{\partial q_{n-1}} \end{array} \right] \quad (C.15)$$

As shown in Eq.C.15, the Jacobian matrix for the suspended pipeline can be divided into four parts. The upper half part contains the first order derivative of displacement variable, while in the lower half part of the matrix comprises the first order derivatives of the wake variable. Notice that in the upper right part of the whole matrix in Eq.C.15, the first order derivatives of wake variables are acquired from coupling equations of motion of beam model displacements. While for the lower left part of the matrix, the first order derivatives of displacement variables are deduced from coupling terms in the equations of motion for the wake.

The components of J_y in the upper left corner is expressed by

$$\begin{aligned} J_y &= M_s \cdot \frac{\partial \ddot{y}_i}{\partial y_i} + C_s \cdot \frac{\partial \dot{y}_i}{\partial y_i} + K_s - \frac{\partial f_q}{\partial y_i} \\ &= \frac{1}{\beta(\Delta t)^2} \cdot M_s + \frac{\gamma}{\beta \Delta t} \cdot C_s + K_s + \frac{\gamma}{\beta \Delta t} \frac{1}{2} \rho D \left(C_{D0} \left(\sqrt{V_i^2 + \dot{y}_i^2} + \frac{\dot{y}_i^2}{\sqrt{V_i^2 + \dot{y}_i^2}} \right) - \frac{C_{L0} q_i}{2} V_i \frac{\dot{y}_i}{\sqrt{V_i^2 + \dot{y}_i^2}} \right) \cdot E \end{aligned} \quad (C.16)$$

Where E is the unit matrix with same dimension of the equivalent stiffness, mass and damping matrix. E matrix here is also used in the following equations.

The components of J_{y-q} in the upper right corner is expressed by

$$J_{y-q} = -\frac{\partial f_q}{\partial q_i} = -\frac{1}{4} \rho D C_{L0} V_i \sqrt{V_i^2 + \dot{y}_i^2} \cdot E \quad (C.17)$$

The components in the upper-right corner is also deduced with reference to Eq.4.23. The right-hand side of which is the coupling terms for displacement variable. Calculate the derivative and the following

equation can be derived.

$$J_{q-y} = \frac{1}{\beta(\Delta t)^2} \frac{A_i}{D} \cdot E \quad (\text{C.18})$$

Where A_i is the tuning coefficients for the wake oscillator model as stated in Sec.4.2. Similarly, after investigating into the left-hand side of the Eq.4.23, first order derivative of wake variable are deduced and written as

$$J_q = \frac{1}{\beta(\Delta t)^2} \cdot E + \epsilon_i \omega_{s_i} \left(2q_i \dot{q}_i + \frac{\gamma}{\beta \Delta t} q_i^2 - \frac{\gamma}{\beta \Delta t} \right) \cdot E + \omega_{s_i}^2 \cdot E \quad (\text{C.19})$$

Where ϵ_i and ω_{s_i} are the tuning coefficient and the shedding frequency elaborated in Sec.4.2.

The above-mentioned contents are the assembly method of Jacobian matrices for seabed pipeline beam model and suspended pipeline beam model separately. Then for the overall pipeline model, the Jacobian matrix is in essence a combination of separate pipeline model parts, which is given as Eq.C.20. The combination of J_b and J_s in interface are basically the same as the combination of equations of motions using the interface conditions as stated in Chapter.5 and thus will not be elaborated here. The critical point need to be aware is that the drag force and soil resistance inducing Jacobian matrix components only take effects at soil beam model part in the overall beam model part. The same situation occurs to the Jacobian matrix from the coupling wake term for the suspended pipeline part. The assembly of overall Jacobian matrix should be paid attention to.

$$J_s = \begin{bmatrix} J_b & & \\ & J_s & J_{s-q} \\ & J_{q-s} & J_q \end{bmatrix} \quad (\text{C.20})$$

Further more, the Jacobian matrix form for the dynamic laying process is shown as following Eq.C.21. The only difference is the augmented part of fictitious part in the matrix, which has also resulted in the relative location change of other parts inside the matrix.

$$J_s = \begin{bmatrix} J_b & & & \\ & J_s & & J_{s-q} \\ & & J_f & \\ & J_{q-s} & & J_q \end{bmatrix} \quad (\text{C.21})$$

The partial differential equations are already given in Eq.7.3, after the same simplification process as seabed pipeline part, thus the Jacobian matrix for this particular part is deduced and written as the fol-

lowing Eq.C.22. The other terms are remaining the same as that in the previous defined one.

$$\begin{aligned} J_f &= M_f \cdot \frac{\partial \ddot{y}_i}{\partial y_i} + C_f \cdot \frac{\partial \dot{y}_i}{\partial y_i} + K_f - \frac{\partial f_{damp}}{\partial y_i} \\ &= \frac{1}{\beta(\Delta t)^2} \cdot M_f + \frac{\gamma}{\beta \Delta t} \cdot C_f + K_f + \frac{\gamma}{\beta \Delta t} c_{dpf} \cdot E \end{aligned} \quad (C.22)$$

After supply the Jacobian matrix into the solver, the calculation speed is much quicker. The validity of the Jacobian matrix has been verified by comparing the results acquired from the solver with and without the Jacobian, the only difference for which is the calculation speed.

REFERENCES

- [1] Q. Bai and Y. Bai, *Subsea Pipeline Design, Analysis, and Installation* (Elsevier Science, 2014).
- [2] N. Willis, P. West, *et al.*, *Interaction between deepwater catenary risers and a soft seabed: large scale sea trials*, in *Offshore Technology Conference* (Offshore Technology Conference, 2001).
- [3] T. K. Sen, M. Hesar, *et al.*, *Riser soil interaction in soft clay near the touchdown zone*, in *Offshore Technology Conference* (Offshore Technology Conference, 2007).
- [4] I. Ojalvo, *Coupled twist-bending vibrations of incomplete elastic rings*, *International Journal of Mechanical Sciences* **4**, 53 (1962).
- [5] H. Elostalo, S. Huang, and A. Incecik, *Dynamic response of steel catenary riser using a seabed interaction under random loads*, *Ocean Engineering* **69**, 34 (2013).
- [6] D. Bruton, D. White, C. Cheuk, M. Bolton, M. Carr, *et al.*, *Pipe/soil interaction behavior during lateral buckling, including large-amplitude cyclic displacement tests by the safebuck jip*, in *Offshore Technology Conference* (Offshore Technology Conference, 2006).
- [7] D. N. Veritas, *Influence of Pressure in Pipeline Design: Effective Axial Force*, *Omae*, 1 (2005).
- [8] Dnv-Os-F101, *Submarine Pipeline Systems*, *Norsok Standard*, 367 (2012).
- [9] S. Lenci and M. Callegari, *Simple analytical models for the J-lay problem*, *Acta Mechanica* **178**, 23 (2005).
- [10] Y. Bai and Q. Bai, *Subsea Pipelines and Risers*, Elsevier ocean engineering book series (Elsevier Science, 2005).
- [11] R. Clough and J. Penzien, *Dynamics of structures*, Dynamics of Structures Ray W. Clough, Joseph Penzien (McGraw-Hill, 1975).
- [12] D. N. V. (Organization), *Dynamic Risers: DNV Offshore Standard Dnv-OS-F201, 2001*, Offshore standard (BDet Norske Veritas, 2001).
- [13] A. Bokaian, *Natural frequencies of beams under tensile axial loads*, *Journal of Sound and Vibration* **142**, 481 (1990).
- [14] L.-z. Wang, F. Yuan, Z. Guo, and L.-l. Li, *Numerical analysis of pipeline in j-lay problem*, *Journal of Zhejiang University-SCIENCE A* **11**, 908 (2010).
- [15] R. Ogink and A. Metrikine, *A wake oscillator with frequency dependent coupling for the modeling of vortex-induced vibration*, *Journal of Sound and Vibration* **329**, 5452 (2010).
- [16] M. Facchinetti, E. de Langre, and F. Biolley, *Coupling of structure and wake oscillators in vortex-induced vibrations*, *Journal of Fluids and Structures* **19**, 123 (2004).

-
- [17] Y. Qu and A. Metrikine, *Time domain simulation of vortex-induced vibration of a curved beam using a wake oscillator model*, .
- [18] A. P. Institute and A. N. S. Institute, *Geotechnical and Foundation Design Considerations: ANSI/API Recommended Practice 2GEO ; ISO 19901-4:2003 (modified), Petroleum and Natural Gas Industries - Specific Requirements for Offshore Structures, Part 4 - Geotechnical and Foundation Design Considerations*, API RP (API Publ. Services, 2014).
- [19] Z. Westgate, M. Randolph, D. White, and P. Brunning, *Theoretical, numerical and field studies of offshore pipeline sleeper crossings*, in *Proceedings of the 2nd International Symposium on Frontiers in Offshore Geotechnics*, Vol. CD (CRC Press/Balkema, 2011) pp. 845–850.